Sasol Advanced Fuels Laboratory

UNIVERSITY OF CAPE TOWN

Investigating the Feasibility of Characterising Gasoline Autoignition using a Motored Engine Apparatus

---

Author:

Simon Demnitz

Supervised by:

Adjunct Professor Andy Yates

A dissertation submitted to the Department of Mechanical Engineering, University of Cape Town, in partial fulfilment of the requirements for the degree of Master of Science in Engineering

Cape Town, South Africa
20 June 2007

Declaration

I know the meaning of plagiarism and declare that all the work in the document, save for that which is properly acknowledged, is my own.

I have used the Harvard convention for citation and referencing. Each significant contribution to, and quotation in this project from the works of other people has been attributed, and has been cited and referenced.

I have not allowed, and will not allow anyone to copy my work with the intention of passing it off as his or her own work.

Signature Signed by candidate

Acknowledgements

This project was initiated and sponsored by:

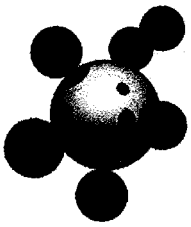

Sasol Technology Fuels Research funded this project and is gratefully acknowledged.

The writer wishes to thank the following people for their help in this project:

Dr Andy Yates – Project Supervisor

Mr Graham Smith – Consultation and Design of Electrical Components

Mr Aaron Wetzler – Design of Fuelling Control Unit

Mr Wayne Smith – Consultation with regard to Electrical Systems Management

Terms of reference

In March 2004, Dr Andy Yates of the Sasol Advanced Fuels Laboratory at UCT initiated this project. The Sasol research team has done extensive study in the area of chemical kinetics fuel combustion modelling and engine modelling applications. Much experimental work is required to confirm the results obtained from chemical kinetics based models. It was decided that a motored engine would be able to provide test conditions for autoignition of gasoline fuels in a suitable range in order to confirm a proposed autoignition model, developed as a result of Chemkin modelling. Modification of a test engine for these experimental applications were required as part of the thesis requirement. The fuel n-heptane was used for the commissioning of the device and justification of the experimental technique.

The specific instructions of the Sasol Advanced Fuels Laboratory were to:

1. Modify an existing single cylinder engine with the capabilities for heated inlet manifold air temperature to 600K and choked inlet air pressure to 0.4 bar. This would enable a wide enough range in terms of engine peak conditions to effectively explore the characteristic ignition delay curve.

2. Modify the engine inlet with a fuel injection system, in order for the device to have the potential of adjustability for different fuels and equivalence ratios. The injection map should be determined and tested over the experimental range of variable inlet air densities through inlet air heating, inlet air choking and engine speed variation.

3. Insert the relevant transducers and equipment for engine test data acquisition. A range of tests was required for a chosen fuel and compression ratio.

4. Build a dynamometer, consisting of a frame, driving element and load control system.

Abstract

Development of a predictive octane model is a potentially useful tool for designing fuel blends for meeting octane specifications. One of the approaches adopted is through chemical kinetic modelling of the autoignition properties of constituent compounds. The results obtained from models, however, are dependant on experimental data for validation. It was the intention of this thesis to provide empirical data that could be used confirm a recently proposed autoignition model based upon the results obtained from chemical kinetics modelling.

Motored engines have been used extensively for the investigation of autoignition properties of fuels. They are useful in interpreting results from conventional ignition delay measuring systems as well as giving practical insight into the process of autoignition in spark ignition engines. The conditions required for autoignition reactions to take place are easily produced in a motored engine with a suitable compression ratio.

A single cylinder engine was modified so that the inlet conditions could be adjusted and n-heptane was tested in the device. Fuelling was controlled with an injection system which was calibrated for n-heptane use in the engine. A range of inlet conditions were determined that would enable peak conditions in the engine to result in autoignition of the fuel. The autoignition data was then used in describing the ignition delay characteristics of the fuel and the range of interest, the so called negative temperature coefficient region.

Autoignition experiments were performed in the engine and the data was analysed by the comparison of measured autoignition reactions with predicted reaction times; the predictions were calculated using the new empirical autoignition model. Direct analysis of the model resulted in good correlation of measured and predicted overall autoignition reaction times, with improved correlation of cool flame reaction times with initial temperature adjustment. Modification of initial temperature values in the indirect model application (whereby traces were generated using an engine model with autoignition prediction capabilities) resulted in similar observances.

These initial results led to the conclusion that the temperature and Arrhenius parameter adjustments necessary to obtain a perfect fit in the autoignition model were indicative of errors involved in the temperature measurement or in the fuel metering. Recommendations for further work on the engine would be the investigation of a dynamometer system that would be free from noise transmission during operation and that would enable experimentation with lower engine speeds. Further work on the inlet system would be the installation of shielded thermocouples and

a quicker acting heater controller. A fundamental change in fuel metering calibration is required. A further recommendation is that a variable compression ratio engine should be used to enable the attainment of a wider range of readings for fuel characterisation and possibly eradicate the problems experienced with fuelling.

Table of contents

List of figures

List of tables

Nomenclature

TDC – Top dead centre

ATDC – After top dead centre

BMEP – Brake mean effective pressure

FMEP – Frictional mean effective pressure

IMEP – Indicated mean effective pressure

CAD – Crank angle degrees

CFR – Cooperative Fuels Research

CCR – Critical compression ratio

ON – Octane number

RON – Research octane number

MON – Motor octane number

RCM – Rapid compression machine

NTC – Negative temperature coefficient

PRF – Primary reference fuel

ECU – Electronic control unit

1 Introduction

A predictive octane model for gasoline fuel blends is a potentially useful tool in designing fuel blends so that they meet specifications in the ASTM octane rating test. Fuel blends are tested in a standardized CFR engine, the compression ratio being adjusted until a standard knock intensity is recorded. The octane rating is determined by blending two reference fuels to obtain the same knock intensity at the same engine conditions. Knock is believed to be the result of the autoignition of unburnt end-gas charge, which is subjected to compression via the piston motion and the propagating flame front in a spark ignition engine. Since the octane number of a gasoline blend is not equivalent to the proportional sum of the octane values of the individual constituents by volume, a fundamentally based approach in investigating autoignition reaction chemistry is necessary for the development of a predictive octane model.

One of the approaches taken is through chemical kinetic modelling of the autoignition chemistry of constituent compounds. A study was undertaken by Viljoen et al. (2005) whereby representative fuel compounds of a gasoline blend were modelled using reduced chemical kinetics in order to investigate their respective ignition delay characteristics. A correlative model for the fuel autoignition trends has been proposed by Yates et al. (2007), which can be used to develop a comprehensive predictive octane model.

Chemical kinetics results are dependant on experimental data for verification. Experimental devices for measuring ignition delay include: rapid compression machines, flow reactors and shock tubes. Although the primary reference fuels have been extensively investigated through various experimental and chemical modelling approaches, there remains a need for experimental validation of the data from other classes of fuels such as olefins, aromatics and alcohols.

1.1 Problem definition

The aim of this thesis was to confirm the validity of the chemical kinetic modelling results and fuel autoignition model through experimentation using a motored engine. The adopted approach was to induce autoignition in a modified engine, subjecting the charge to dynamic polytropic conditions under which knock occurs. Analysis of the data included the incorporation of an ignition delay model to obtain results which were intended to confirm the autoignition model parameters derived from the chemical kinetics study.

Included in the project requirements was the design, construction and commissioning of the device for the characterization of the ignition delay properties of a fuel over an extended pressure-temperature range. As a proof of concept for the technique, n-heptane was tested in the device.

1.2 Objectives

1. Modify an existing single cylinder engine with the capabilities for heated inlet manifold air temperature to 600 K and choked inlet air pressure to 0.4 bar. This would enable a wide enough range in terms of engine peak conditions to effectively explore the characteristic ignition delay curve.

2. Modify the inlet with a fuel injection system, in order for the device to have the potential of adjustability for different fuels and equivalence ratios. The injection map should be determined and tested over the experimental range of variable inlet air densities through inlet air heating, inlet air choking and engine speed variation.

3. Insert the relevant transducers and equipment for engine test data acquisition. A range of tests is required for a chosen fuel and compression ratio.

4. Build a dynamometer, consisting of a frame, driving element and load control system.

A comprehensive engine model including autoignition thermodynamics was required for the analysis of the data. Correlation of measured experimental results with the calculated values based on chemical kinetics derived Arrhenius parameters, was required as a proof of concept of the technique.

1.3 Layout of document

This document is structured as follows:

Chapter 2 is a review of the relevant literature and an introduction to the background theory of fuel ignition delay. A general introduction to the octane rating test, autoignition chemistry, autoignition modelling and experimental validation is given and then more specifically, the chosen method of validation via the motored engine technique is introduced with the relevant literature.

Chapter 3 discusses the experimental method for data analysis.

Chapter 4 covers the practical modifications necessary for the commissioning of the apparatus and the test procedure for data capture.

Chapter 5 gives the preliminary data correction methods required for further analysis.

Chapter 6 gives the results and discussion of data derived from testing.

Chapter 7 gives the conclusions of the study and recommendations for further work.

2 Theoretical Background

2.1 Octane characterisation

2.1.1 Definition of spark knock

From the beginning of the internal combustion engine era, audible knock has been detected in spark ignition engines, prohibiting power development and thermodynamic efficiency improvements and usually leading to severe engine damage. During the compression stroke in normal engine operation, the fuel-air mixture is compressed by the piston motion and is spark ignited a few crank angle degrees before top dead centre (TDC). The resulting flame front travels through the cylinder progressively, igniting the unburned gas and eventually becoming extinguished at the end of its travel. Work is transferred to the piston via the expanding hot gases, which are eventually expelled via the exhaust valve by the piston on its return stroke.

The occurrence of knock in abnormal engine operation is regarded to be the result of the autoignition of unburnt end-gas subjected to compression via the piston motion and the propagating flame front. The end gas, consisting of a fuel, air, and residual gas mixture ahead of the flame front, is compressed to pressures and temperatures that result in the initiation of a chemical reaction characterized by the rapid release of energy. Formation of high local pressures and the propagation of the ensuing pressure waves across the combustion chamber occurs, producing the characteristic noise attributed to knock. Severe knock can destroy the engine via erosion damage of the piston and cylinder head, as well as general overheating.

Thus the autoignition behaviour of a fuel, responsible for ignition in a diesel engine and knock in a spark ignition engine, is an important factor in engine design.

2.1.2 The octane rating method

Gasoline fuel is a blend of hundreds of organic species produced from oil refinery processes. As is shown later, this presents a problem for chemists involved in numerical reaction simulation studies for the purpose of characterizing fuels, since the complexity of the constituents of any practical gasoline fuel are not easily simplified for fundamental reaction modelling. Gasoline fuels are rated according to octane number (ON), which is a measure of their propensity to knock. In the 1930s the standardized knock test was developed in a Cooperative Fuels Research (CFR) engine in order to rate gasoline fuels. The CFR engine is a four-stroke, carburetted, single cylinder, variable compression ratio engine. The test is run at a constant

carburetted, single cylinder, variable compression ratio engine. The test is run at a constant speed with a fixed heated inlet air temperature according to the methods prescribed by the ASTM D2699 and D2700 method. The test mixture is introduced and the compression ratio increased until the engine knocks at a certain intensity measured by a pressure transducer, and signal conditioned by the knock meter. The compression ratio attained at knocking is termed the critical compression ratio (CCR). This measured compression ratio is then matched to the CCR obtained for a primary reference fuel blend, which knocks at the same intensity. The volumetric composition of the reference blend is used to give the octane value for the fuel. The primary reference fuels are iso-octane (2,2,4 tri-methyl-pentane), defined as 100 octane and n-heptane, defined with a zero octane value. These pure hydrocarbon fuels were originally chosen for the octane test as they exhibit similar evaporative and boiling qualities, as well as being relatively easily obtained at a high purity level.

ON = (vol%).iso-octane Equation 2-1

The original octane test research method, assigning a fuel a research octane number (RON), was found to be inadequate in describing a fuel's knock propensity in a practical engine. A more realistic test method was required. Thus the motor method was introduced, with test conditions of higher inlet manifold temperature and engine speed, as well as variable spark timing advancement and a shrouded valve for in-cylinder charge mixing. The RON was more often used in academic research while the motor octane number (MON) was intended as a better indication of a fuel's knock susceptibility in a practical engine, undergoing higher loads and speeds. However, a recent study by Yates et al. (2005) showed that for modern fuel injection vehicles (as opposed to carburetted ones), the RON number is a better indicator of the fuel's performance in the engine, This provides test conditions which result in a closer match of the autoignition range that a fuel undergoes in the pressure and temperature conditions in modern engines. The RON and MON engine test conditions are compared in Table 2-1.

As previously mentioned, a fuel's knock propensity may vary under different engine conditions. Fuel octane sensitivity is described as a measure of this difference and is defined as the arithmetic difference of a fuel's RON and MON value. Thus for the reference fuels it is zero by definition, resulting in most alkanes showing sensitivities close to zero (owing to their similarities to the reference fuels in chemical structure and hence autoignition chemistry). At low octane values, some alkanes reveal a lower RON than MON value, but for the range of octane numbers used for commercial purposes the MON is usually the lower value. The reason for high sensitivity values of some fuels is explored at a later stage in this chapter.

Table 2-1: RON and MON test conditions

Parameter	RON Test	MON Test
Engine Speed	600 rpm	900 rpm
Spark Timing	13^0 BTDC	19^0 - 26^0 BTDC (function of compression ratio)
Inlet Air Temperature	52^0C	38^0C
Inlet Mixture Temperature	Not controlled	149^0C
Air-fuel Ratio	Adjusted for maximum knock intensity	Adjusted for maximum knock intensity

2.1.3 Effect of fuel structure on knock tendency (Heywood, 1988)

2.1.3.1 Paraffins

1. Increased length of the carbon chain results in increased knock tendency.
2. Side chains from the basic chain molecule results in decreased knock tendency.
3. Methyl groups added onto the basic chain in certain positions results in decreased knock tendencies.

2.1.3.2 Olefins

1. Two or three double bonds decrease knock tendency in most cases. (Also exhibits higher RON-MON sensitivity.)

2.1.3.3 Napthenes and Aromatics

1. Napthenes generally have greater knock tendencies than corresponding aromatics of the same size.
2. Two or three double bonds decrease knock tendency in most cases.
3. Lengthening the side chain on the basic ring structure increases knock tendency.
4. Branching of the side chain on the basic ring structure decreases knock tendency. (Aromatics generally exhibit a significant RON-MON sensitivity.)

2.2 Limitations of the octane rating method

Unfortunately the octane rating method has its shortcomings. Spark knock is not only dependant on the chemistry of the fuel, but also on the geometry of the combustion cylinder, thermodynamic inlet conditions, equivalence ratio and other engine design factors (inasmuch as

these parameters influence the pressure-temperature-time profile that is experienced by the end gas in an engine). Thus for the octane test, the octane rating reflects not only the fuels' chemical properties, but also the thermodynamic test conditions and the geometry of the CFR engine. A single standardized test is insufficient to accurately characterize the knock propensities of a variety of fuels over a range of engine operation, especially those fuels that deviate in chemical structure from the reference fuels.

In many studies related to the octane test and in particular the work of Leppard (1990), the standardized test proved to be lacking in describing the fundamental ignition characteristics of fuels. It was demonstrated in this study that fuels differing chemically from the reference fuels (alkenes, olefins and aromatics) have higher sensitivities. This was attributed to the differences in ignition delay temperature dependence. In this case, the problem is most certainly due to the ignition characteristics of fuel being highly temperature dependant, but not all in a similar fashion.

Another current issue relates to the mechanics of the autoignition process in the CFR engine. The question raised is: are traditional octane rated knock conditions a true representation of that which is measured by a modern knock sensor, as the associated pressure fluctuations in the cylinder? This question challenges octane rating as a direct indicator of incipient autoignition (Yates et al., 2005); the work of Swarts (2006) provides ample evidence that this is not the case. At this point, therefore, it is appropriate to introduce the concept of a fuels ignition delay as a more fundamental knock propensity property.

2.3 Ignition delay

2.3.1 Definition of ignition delay

Autoignition delay or induction time is defined as the time elapsed from an instantaneous increase in temperature to the spontaneous ignition of a hydrocarbon-air mixture through rapid chain-branching chemistry in a suitably pressurized and heated environment. It is characterized and usually measured by a rapid pressure increase in the system. Conventional devices used to produce autoignition and measure ignition delays include rapid compression machines (RCM), shock tubes, constant volume devices and flow reactors. A RCM consists of a piston-cylinder arrangement that adiabatically compresses a homogenous test mixture of fuel and air in a very short increment of time. The time taken for compression to render the required pressure and temperature environment for autoignition is small with respect to the total ignition delay of the

mixture under these conditions. An example of an ignition delay trace obtained in a RCM is shown in Figure 2-1.

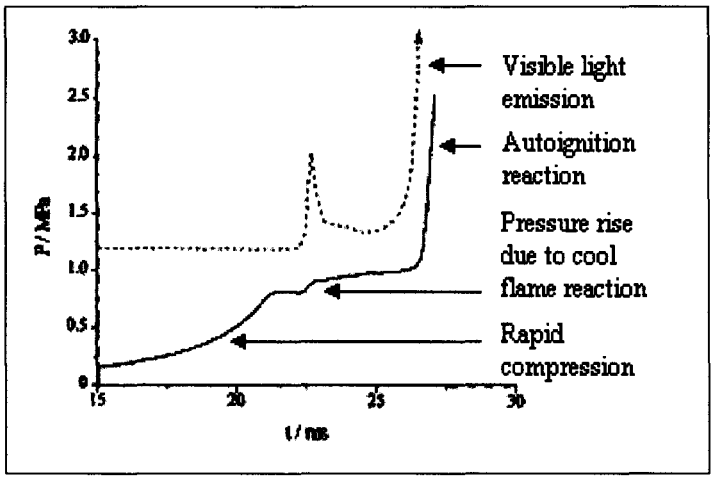

Figure 2-1: Pressure trace showing two-stage ignition in a RCM (supplemented by emitted visible light measurement), courtesy of Griffiths et al. (1997)

For initial temperatures above approximately 850 K (the value being subject to post-compression pressure conditions), single-stage ignition occurs; at initial temperatures below this value, two-stage ignition is found to occur in certain fuels. The first stage culminates in the formation of a cool flame and an associated pressure rise as a result of heat release during the cool flame reaction. The second stage culminates with the characteristic rapid pressure rise indicating combustion. Figure 2-2 shows the autoignition delay characteristics of a range of hydrocarbon fuels over a range of temperatures. Hydrocarbon oxidation is usually categorized into three main regions: low temperature (<700 K), intermediate temperature (700 -1100 K) and high temperature (>1100 K). Typical alkane fuels exhibit a phenomenon known as the negative temperature coefficient (NTC) region (typically 700 – 800 K). In this region, the overall ignition delay is seen to increase with increasing temperature. This is associated with the cool flame reaction; the NTC region reflects the temperature zone where the cool flame ceases to occur as the initial temperature increases. The significance of this is that both the primary reference fuels used for octane definition exhibit such behaviour, and thus this particular chemistry is intrinsically associated with the octane value prescribed to a fuel. This therefore characterises blends of fuel which may or may not exhibit similar chemical kinetic characteristics.

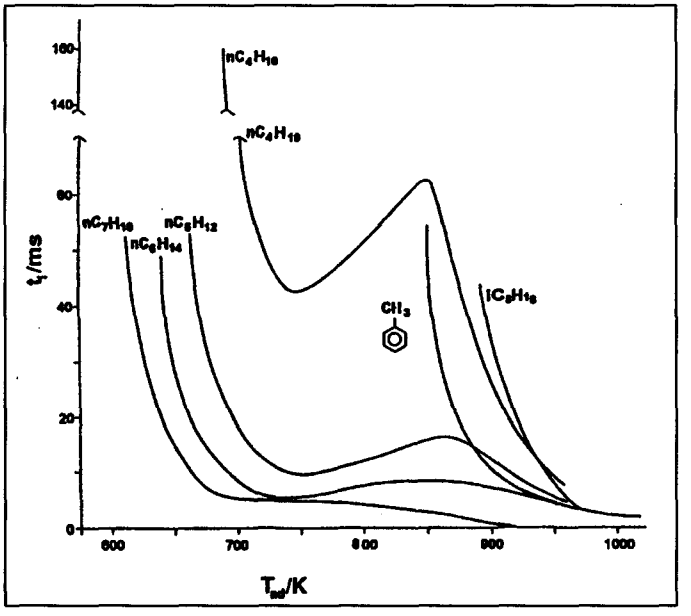

Figure 2-2: Ignition delay characteristics of hydrocarbons tested in a RCM at 0.65 – 0.75 MPa in stoichiometric proportion in air, compliments of Griffiths J. F. and Mohamed C. (1997)

2.3.2 Measuring ignition delay (Griffiths J. F. and Mohamed C., 1997)

2.3.2.1 Constant volume devices (Combustion bombs)

Fuel is admitted into a vessel that is already pressurized and heated to prescribed test conditions. Ignition occurs and is measured. Homogeneity and temperature uniformity of reactants are usually not applicable and uncertainties in equivalence ratio and temperature gradient restrict these results from zero dimensional modelling applications. Precise measurement of experimental conditions is also difficult owing to heat loss from fuel vaporization. Due to conditions in the combustion bomb being locally heterogeneous and non-isothermal, it is difficult to characterize accurately the NTC region of a fuel, as local areas at optimal temperature and equivalence ratio will autoignite first, initiating global autoignition. Many experimental systems involve the use of a two-stage combustion process to simulate quiescent compression ignition (i.e. TDC) conditions. This involves the combustion of lean premixed gases in the first stage to yield products similar in composition to air and result in high pressure and temperature conditions. (Siebers, 1985); (Agarwal et al., 1997)

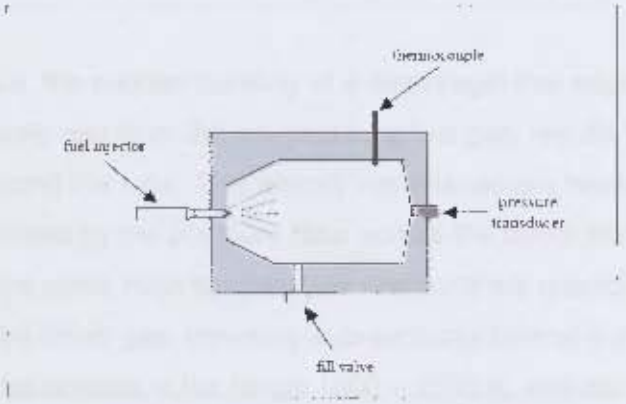

Figure 2-3: Constant volume bomb

2.3.2.2 Flow systems

Laminar or turbulent flow devices can be used for studying hydrocarbon oxidation, usually via the collection of products under fixed state conditions, then through product analysis and thereby reaction chemistry deduction. Reactants are metered, pre-heated and then introduced into the reactor tube under constant pressure and flow rate conditions. The reactor is kept at constant temperature or is varied in a stepped manner as developed by Koert et al (1994). The controlled cool down (CCD) technique involves stabilization of the reactor temperature, followed by systematically controlled temperature reduction. Thus, extracted gas samples may describe an entire reactivity map in one experiment. Conditions achieved in this device include operation at pressures up to 2.0 MPa, temperatures in the range of 500 -1000 K and residence times typically in the order of 200 ms.

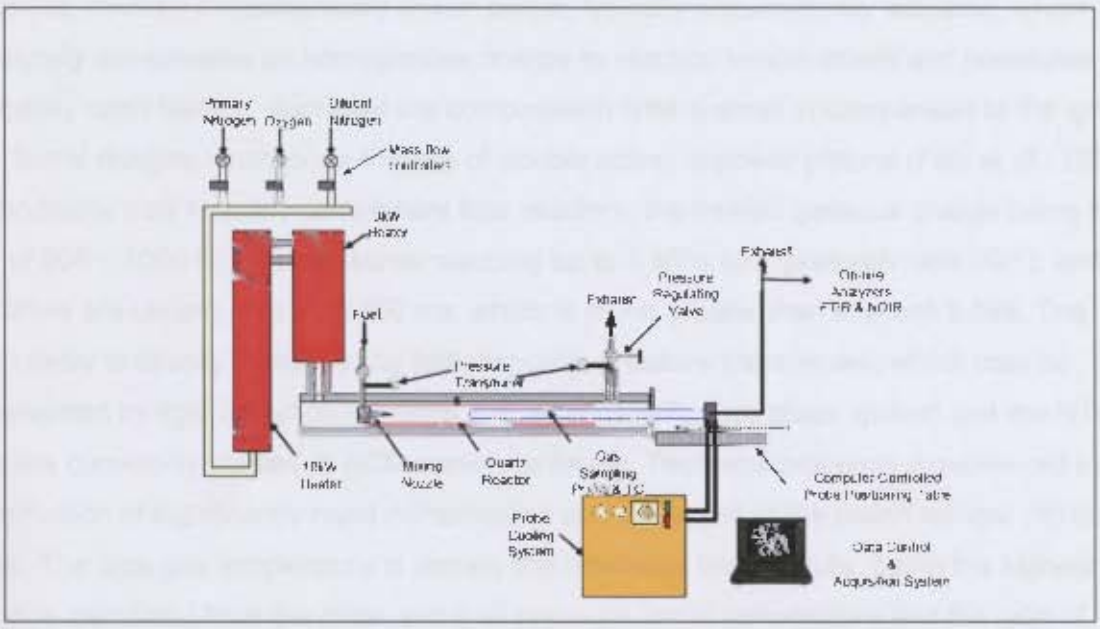

Figure 2-4: Pressurised flow reactor, courtesy of Koert et al. (1994)

2.3.2.3 Shock tubes

In a shock tube apparatus, the sudden bursting of a diaphragm that separates a high pressure section containing the driver gas from the low pressure test gas, results in the propagation of a supersonic shock front along the tube. This almost instantaneously heats and pressurises the test gas to values determined by the pressure ratio across the shock front and the ratio of specific heats of the gases used. High temperature reactions are quenched on the arrival of the cold contact surface of the driver gas, travelling sub-sonically behind the shock front. Typical shocked gas temperatures operate in the range 1500 – 2500 K, well into the high temperature range of typical fuels. The near discontinuous temperature rise resulting from the shock front gives a well defined starting point for the reaction from which the ignition delay may be measured. Ignition delays that are long (in the order of several milliseconds) may result in significant heat losses from the shock tube; this may cause uncertainties in the data

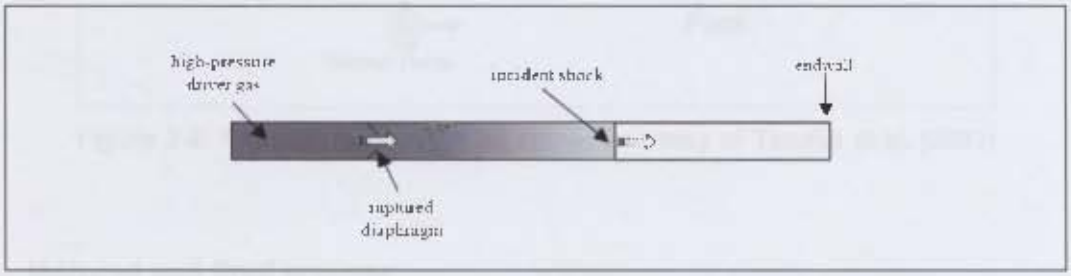

Figure 2-5: Shock tube

2.3.2.4 Rapid compression machines

This device involves a mechanically driven piston, typically pneumatically actuated, which adiabatically compresses an homogenous charge to reaction temperatures and pressures in a significantly rapid fashion, such that the compression time is small in comparison to the ignition delay. Some designs incorporate the use of double acting opposed pistons (Fish et al., 1969). The conditions may typically compliment flow reactors, the heated gaseous charge being in the range of 500 – 1000 K, with pressures reaching up to 5 MPa (compression ratio 10:1). Ignition delay times are usually less than 100 ms, which is much greater than in shock tubes. The ignition delay is usually measured by fast response pressure transducers, which may be supplemented by light detection (Griffiths J. F. et al., 1997). Two stage ignition and the NTC region are commonly studied in RCM experimentation. Technical problems experienced include the production of significantly rapid compression and the arrest of the piston without vibration or bounce. The core gas temperature is usually the reference temperature, being the highest in value; it is calculated from the initial and final pressure, initial temperature and the ratio of specific heats of the reactant mixture.

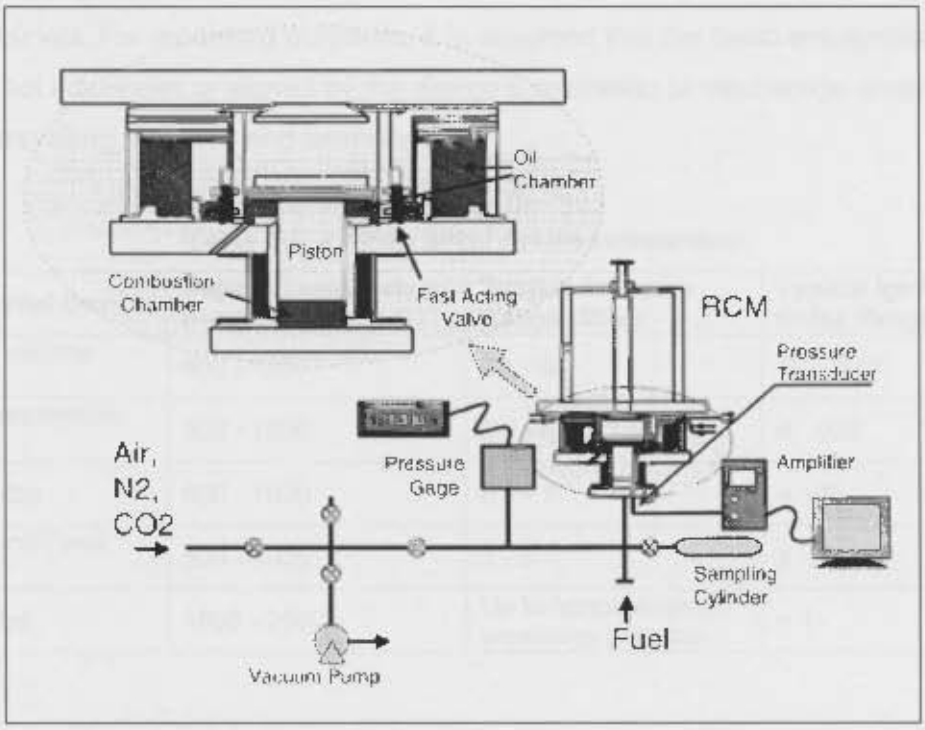

Figure 2-6: Rapid compression machine, courtesy of Tanaka et al. (2003)

2.3.2.5 Motored and fired engines

In this device, an engine is run with an electric motor (the induced charge not being spark ignited in the motored application but purely by compression ignition). Motored engines are typically used to study partial oxidation of hydrocarbons through compression of the charge to autoignition temperatures and pressures. Intermediate species are examined through rapid sampling, probe sampling or exhaust gas analysis. The reaction time is governed by engine speed. Unlike other devices for studying autoignition processes, the charge undergoes constantly changing conditions. The pressure history is usually measured and the temperature history calculated from the pressure values. Overall conditions may be varied by adjustment of the inlet temperature and pressure, engine speed and compression ratio. Extensive work in this arena has been conducted by Leppard (1990). Motored and fired engine data is useful in interpreting results from conventional ignition delay measuring systems as well as giving practical insight into the process of autoignition in spark ignition engines.

Table 2-2 gives a comparative overview of the various devices that have been discussed. From these devices it may be said that constant volume bombs function and may supply information in the low-temperature region; this corresponds to higher ignition delays and therefore less error in the assumption of homogeneity and isothermal conditions. Motored and fired engines, flow devices and rapid compression machines span the low to intermediate temperature region.

while shock tubes give access to the high temperature region of general hydrocarbon autoignition curves. For modelling purposes, it is assumed that the basic autoignition reaction chemistry is not influenced or altered by the device's geometric or mechanical properties, but only by the prevailing pressure and temperature.

Table 2-2: Ignition delay device comparison

Experimental Device	Typical Temperature Range (K)	Typical Pressure Range (MPa)	Typical Ignition Delay Range (ms)
Constant Volume Bomb	600 - 1200	0.1 - 5	10 - 1000
Rapid Compression Machine	500 - 1000	0.5 - 5	4 - 100
Flow Reactor	600 - 1000	0.1 - 1	> 100
Motored and Fired Engine	500 - 1000	1 - 5	1 - 10
Shock Tube	1500 - 2500	Up to typical engine pressures possible	> 1

2.4 Hydrocarbon oxidation chemistry

2.4.1 Autoignition fundamentals

Depending on the pressure and temperature of the mixture, hydrocarbon oxidation can take various forms:

Slow reactions involve low pressure and temperature (<200^{0}C), not usually occurring within engines.

Single or multiple cool flame reactions are low temperature reactions (300 – 400^{0}C), characterised by development of partial combustion accompanied by pale blue emission. Reaction is halted after a fraction of reactants is used up; the accompanied heat release is small.

Two-stage ignition involves a cool flame followed by a hot flame (high temperature autoignition reaction).

Single-stage ignition is a result of the transition from two-stage to single-stage autoignition as high temperature chemistry dominates with increasing initial temperatures.

The autoignition reaction of hydrocarbon fuels consists of hundreds of different possible chemical chain reactions taking place; most of the reactions are sequential. The process can be briefly described in three steps:

Initiation. Highly reactive intermediate species, both molecular and radical, are produced from the more stable fuel and oxygen molecules.
Propagation. Reactant molecules and radicals form further radicals and other sequential products, such that the concentration of reactive species increases rapidly and exponentially. When the reaction rate of radical formation due to chain branching is sufficiently fast, it is termed an autoignition reaction. This is characterized by a rapid increase in temperature and pressure.
Termination. Chain propagation radicals are removed through the formation of more stable species.

It is important to note that autoignition limits may be determined by 1) isothermal limits, in that it is the kinetic features of the reaction that lead to rapid combustion (the reactions themselves being generally exothermic) and 2) thermal limits, in that rapid combustion is brought about via intermediate heat release, requiring intermediate exothermicity and overall activation energy; heat capacity and thermal conductivity of the gases are factors (Walker R. W. and Morley C., 1997).

Some hydrocarbon fuels do not exhibit cool flame or two-stage behaviour. In hydrocarbons that do exhibit this behaviour, the transitions can be explained by the formation of metastable intermediate species, which promote chain branching reactions and whose reactions of formation are temperature dependant. These intermediates may react to form stable molecules or form active radicals; rate and dominance are a function of temperature. Hydroperoxides, intermediates having the form ROOH (R being an organic radical), are responsible for the chain propagation process leading to autoignition in the low temperature ignition process. At temperatures above approximately 950 K, hydrogen peroxide (H_2O_2) is responsible for chain propagation. Below this temperature it is relatively stable, while beyond it the intermediate species decomposes into two highly reactive OH radicals in a reaction known as homolysis. A general oxidation scheme for heavy hydrocarbons is shown in Figure 2-7.

2.4.2 Oxidation mechanisms and the NTC region

In order to explain the reason for NTC characteristics of certain hydrocarbons, an outline of basic hydrocarbon oxidation was proposed in the work of Semenov (Heywood J. B., 1988):

$$RH + O_2 \rightarrow \dot{R} + H\dot{O}_2$$ Equation 2-2

$$\dot{R} + O_2 \leftrightarrow \dot{R}O_2$$ Equation 2-3

$$\dot{R} + O_2 \rightarrow Olefin + H\dot{O}_2$$ Equation 2-4

$$R\dot{O}_2 + RH \rightarrow ROOH + \dot{R}$$ Equation 2-5

$$R\dot{O}_2 \rightarrow R'CHO + R''O$$ Equation 2-6

$$H\dot{O}_2 + RH \rightarrow H_2O_2 + \dot{R}$$ Equation 2-7

$$ROOH \rightarrow R\dot{O} + \dot{O}H$$ Equation 2-8

$$R'CHO + O_2 \rightarrow R'\dot{C}O + H\dot{O}_2$$ Equation 2-9

$$R\dot{O}_2 \rightarrow destruction$$ Equation 2-10

$$H_2O_2 + M \rightarrow 2OH + M$$ Equation 2-11

In the region 500 - 600 K, where the oxidation rate increases with temperature, the equilibrium of Equation 2-3 is strongly rightward dominant. However, for hydrocarbons that exhibit NTC behaviour a drop in reaction rate is observed, as the temperature is increased, usually in the range of 570 – 630 K for most alkanes (measure at 1 bar). In this range, alternative reactions of RO_2 occur besides Equation 2-5, with higher activation energies. At higher temperatures, the equilibrium of Equation 2-3 lies increasingly to the left with the result that the yield of ROOH (the radical responsible for rapid chain branching) decreases. Thus the oxidation rate decreases.

With further temperature increase, the concentration ratio $\frac{[R]}{[RO_2]}$ rises further with increasing leftward dominance of Equation 2-3; this results in oxidation being primarily caused by reactions of R radicals rather than RO_2, the most important being Equation 2-4. H_2O_2 is thermodynamically stable at these temperatures and is removed by Equation 2-7 to H_2O_2. The homolysis of hydrogen peroxide in Equation 2-11 begins above 750 K at a pressure of 1 bar. At higher pressures experienced in internal combustion engines decomposition of H_2O_2 rapidly occurs at temperatures (900-1000 K).

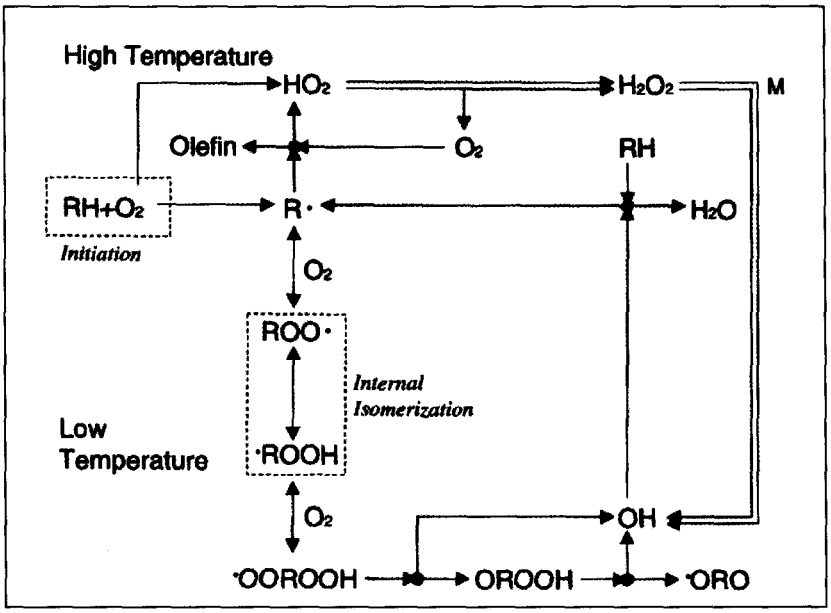

Figure 2-7: General oxidation scheme for heavy hydrocarbons at low and high temperatures, courtesy of Tanaka et al. (2003)

2.4.3 Significance of the cool flame

According to RCM data analysis by Fish et al. (1969), the cool flame occurs as the result of the normal chemical course of the oxidation reaction and is not an insignificant side reaction. It is suggested that primary propagation steps in the cool flame are responsible for isomerisation of alkylperoxy radicals to hydroperoxyalkyl radicals. These are responsible for rapid chain branching and the products necessary for hot ignition are formed by the cool flame.

Another study by Westbrook (1994) holds that the low temperature oxidation (cool flame) has the role of providing heat release early in the reaction, enabling the oxidation process to reach critical temperatures (decomposition temperature of intermediates) at an earlier time than without such heat release. Thus it is proposed that the cool flame reaction is important primarily for the physical conditions it produces, not for its reaction products. Both studies observed that when the cool flame pressure rise is large, hot ignition results quickly, but when cool flame is less intense, ignition is delayed. Thus both studies agree that the effect of the cool flame is responsible for controlling the timing of the hot ignition process.

In the RCM data analysis of Tanaka et al. (2003), the importance of the cool flame effect on the final induction time is recognised. It was noted that the pressure rise resulting from heat release from the cool flame correlated well with the overall ignition delay. Fish et al. (1969), on the other hand, attempted to correlate the pressure rise from the cool flame with the initial pressure in the RCM for a certain fuel.

$$\Delta p = k p_0^{\ m}$$ Equation 2-12

where m is fuel dependant.

2.4.4 Significance of chemical structure

The structure of the hydrocarbon affects the different regimes of chemistry quite significantly, the influence being weaker at higher temperatures. Knock propensity, and therefore octane number, is thus highly dependant on structure, owing to the structure's dependence on low temperature peroxy radical chemistry. Short-chain and branched paraffins have a high resistance to autoignition, resulting in a high octane number. This is due to there being a lower relative number of secondary carbon atoms within the structure available for hydrogen abstraction. Similarly, the ring structure of aromatic fuels results in it being a relatively stable molecule and more autoignition resistant (which means resistance to hydrogen abstraction).

2.5 Empirically derived correlations

Attempts at modelling the ignition process have involved the development of 1) empirically derived ignition delay correlations involving global reaction rate equations or 2) chemical mechanisms which use the full or reduced oxidation mechanisms (as described using Semenov's basic hydrocarbon oxidation process). No detailed models with real blended fuels are currently available for use.

2.5.1 Arrhenius relations

Empirical relations for the ignition delay as a function of test conditions usually involve the Arrhenius equation form:

$$\tau = A p^n e^{\frac{\beta}{T}}$$ Equation 2-13

Where: τ is in milliseconds (ms)
p is absolute pressure in bars
T is in Kelvin (K)
A, n, β are fuel dependant parameters

Douaud and Eyzat (1978) have done an extensive study on this form of correlation, including induction time as a function of fuel octane value, the following equation is valid for PRF fuels in the range 100>ON>80:

$$\tau = 17.68\left(\frac{ON}{100}\right)^{3.402} p^{-1.7} e^{\left(\frac{3800}{T}\right)}$$

Equation 2-14

The equation is a derivation of the reaction rate governed Arrhenius equation and expresses the ignition delay as a global reaction rate.

A study was undertaken by Yates et al. (2005) whereby representative fuel compounds of a gasoline blend were modelled using reduced chemical kinetics in order to investigate their respective ignition delay characteristics. The resulting ignition delay response in the pressure-temperature domain was reduced to a simple system of three coupled Arrhenius equations, effectively matching data in the low-intermediate and high temperature regions.

$$\tau_{total} = \left\{\left(\tau_1 + \tau_2\right)^{-1} + \left(\tau_3\right)^{-1}\right\}^{-1}$$

Equation 2-15

A_i, n_i and β_i parameters for each of the three stages were calculated using a regression technique, effectively fitting the data from chemical kinetics results.

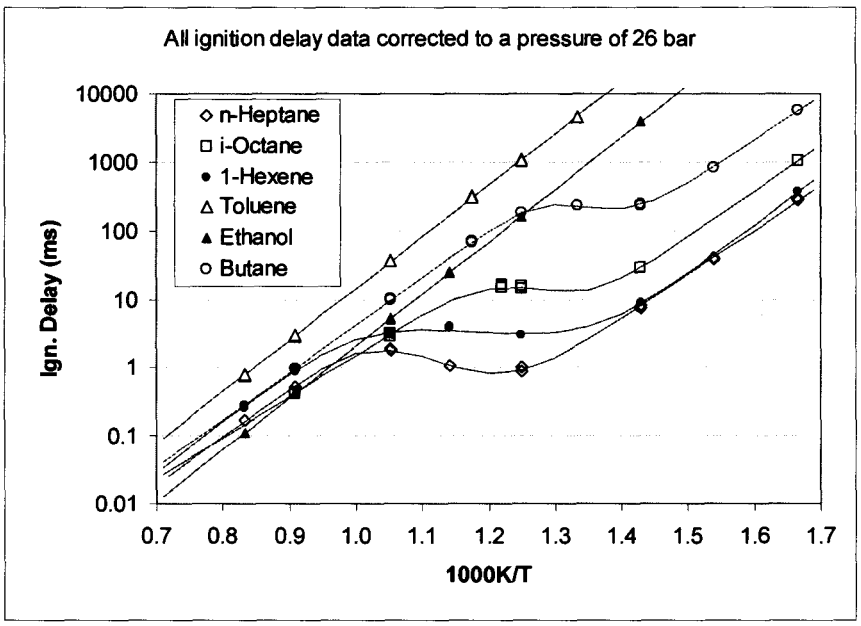

Figure 2-8: Three Arrhenius equation correlation results for various hydrocarbon fuels, courtesy of Yates et al. (2005)

2.5.2 Application for motored engine data

In a motored or a fired engine, such as the CFR octane rating engine, reactions of a homogenous charge are occurring in a constantly changing physical environment. As a point of note, the reaction time to autoignition in this case cannot be said to be an ignition delay, as this definition is strictly for the special case whereby the physical state of the fuel-air mixture is regarded as constant. Therefore it is necessary to devise a correlation scheme which will match a global reaction to the state-time history in the engine. Livengood and Wu (1955) proposed such a correlation in their motored engine research using a single-staged Arrhenius expression whereby autoignition of the charge occurs when

$$\int_{t=0}^{t_{crit}} \frac{dt}{\tau} = 1 \qquad \text{Equation 2-16}$$

(t_{crit} being the total time taken for autoignition of the mixture, $\tau_{autoignition}$.) The equation is derived based on two main assumptions:

1. The rate of production of critical species for autoignition (for a certain mixture) is dependant only on the gas state.
2. The concentration of critical species required for autoignition is constant (critical concentration).

The three Arrhenius formulation given in Equation 2-15 was proposed purely as a numerical correlation and was not meant to describe the underlying chemistry. To supplement this deficiency, a new approach was attempted to incorporate the physical changes that occur in the autoignition reaction history. The global reaction of autoignition was represented as two integral steps describing the relatively stable intervals separated by the abrupt gas transition of the cool flame, characteristic of two-stage ignition:

$$\int_{t_0}^{t_1} \frac{dt}{\tau_{(i)}} + \int_{t_1}^{t_2} \frac{dt}{\tau_{(CF)}} = 1 \qquad \text{Equation 2-17}$$

where t_1 describes the time of the occurrence of the cool flame, and t_2 the hot flame ignition (total ignition delay). The ignition delays τ_i and τ_{cf} describe the principle autoignition chemistry, characterized by the decomposition of peroxides evaluated at the initial conditions and post-cool flame conditions respectively.

If, in the preceding equation, the gas state is approximated as constant and solved for the total ignition delay (t_2) the integral reduces to:

$$t_2 = \tau_{(CF)} + t_1\left(1 - \frac{\tau_{(CF)}}{\tau_{(i)}}\right)$$ Equation 2-18

It was also discovered through detailed chemical kinetic modelling that the cool flame temperature transition (ΔT) is strongly dependant on initial temperature and pressure. The observance of pressure rise from heat release being a function of initial pressure (Equation 2-12) was similarly discovered by Fish et al. (1969) through empirical analysis. The proposed formulation by Yates et al. (2007) was:

$$\Delta T = C_1 T_i + C_2 {p_i}^m$$ Equation 2-19

for $$T_i \leq -\frac{C_2}{C_1} {p_i}^m$$ Equation 2-20

The abrupt transition at ΔT = 0 was remedied by using an equation resulting in a rounded, more realistic profile.

$$\Delta T' = 0.5\left(\Delta T + \sqrt{(\Delta T)^2 + C_0}\right)$$ Equation 2-21

2.6 *Motored and fired engines*

2.6.1 Fuel studies involving motored engines

As previously mentioned in Section 2.2, Leppard undertook extensive research with motored engines testing fuels including n-butane (Leppard, 1987), isobutane (Leppard, 1988) and a variety of alkanes, alkenes and primary reference blends (Leppard, 1990). His method included the variation of compression ratio in a CFR engine for a given engine speed, intake temperature and pressure; this was for the measurement of intermediate species over a continuous range starting from negligible fuel reaction up to the point of autoignition. These were attempts to study the reaction chemistry up to autoignition in order to provide experimental data for the development and validation of a knock model.

Work conducted by Livengood and Wu (1955) provided important insight into correlating transient motored and fired engine data with static RCM data. Experiments were done with n-heptane and a PRF 55 blend and were performed in a CFR engine, varying compression ratio to the threshold of knock. Good correlation resulted when using a single Arrhenius function, although as the experimental range was insufficiently spread to characterize the entire fuel autoignition model, the extent of success of the method and results is uncertain. Revisitation of this study and useful insight is given by Yates et al. (2005). See Figure 2-9.

A similar study was performed by Rifkin and Walcutt (1957) using iso-octane in a motored engine to reconcile data extracted from experiments with a RCM and from motored engine ignition points. The study was unsuccessful in that correlation between the simple autoignition model and their engine results was poor. The reason behind this, offered by Yates et al. (2005), was due to the use of a single Arrhenius function derived from RCM data in the low temperature region to describe both high and low temperature regions that were effectively covered in the engine tests.

It was the intention of this study to reproduce autoignition in a motored engine under similar experimental conditions and correlate this data to the new autoignition model for verification of the numerically derived parameters. The primary objective was to obtain experimental points straddling the NTC region and low and high temperature range of the fuel so that the scope of the proposed fuel autoignition model is sufficiently met.

2.6.2 Representing motored engine data

A useful technique to represent the gas conditions and autoignition properties of the fuel together for comparison was explored by Rifkin and Walcutt (1957) as well as by Livengood and Wu (1955), whereby isodelay contours of the autoignition properties of the fuel were overlaid on the pressure-temperature history of the in-cylinder gas under knock or autoignition limited conditions. The value of the ignition delay was then practically explored in relation to peak conditions of pressure and temperature of the gas mixture undergoing autoignition. Due to the problem in the mismatch of time scales, Douad and Eyzat (1978) proposed the calculation of a "mean effective" pressure and temperature, constrained to lie on the chosen isodelay curve. The proximity of the data points to the theoretical contour line where threshold knock occurrs is indicative of the accuracy of the autoignition model. For the current project application, this procedure was used in conjunction with the integral technique in order to validate the fuel autoignition model that was used.

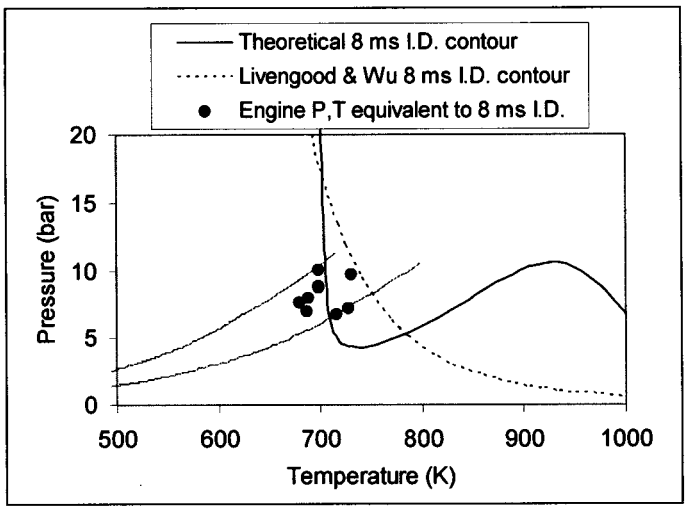

Figure 2-9: The representation of the Livengood and Wu engine data for n-heptane onto the predicted ignition delay map, courtesy of Yates et al. (2005)

2.6.3 Explaining fuel sensitivity

A study by Leppard (1990) explains the fundamental physical causes of sensitivity. It is explained that the first step in understanding fuel sensitivity lies in appreciating the comparison of MON engine conditions with those of the RON method, namely: higher temperatures, slightly lower pressures (due to pressure drop in the inlet system, owing to higher engine speed) and lower reaction times (due to higher engine speed). Secondly, the octane scale is defined according to the autoignition behaviour of the reference fuels, which exhibit NTC behaviour. It is the combination of these factors which lend to result in what is known as fuel sensitivity (defined as (RON – MON).

Paraffinic NTC behaviour becomes less pronounced as conditions change from RON to MON. This equates to higher compression ratios being required to induce autoignition in the MON test than would be required in a fuel displaying no NTC behaviour. Thus, fuels displaying NTC behaviour are super-rated by the motor octane number. Since the reference fuels are paraffinic, this behaviour is incorporated into the octane scale itself. Sensitive fuels not exhibiting NTC behaviour will thus appear to be under-rated by their motor octane number.

3 Experimental Method

3.1 Test point determination

In order to predict the required thermodynamic conditions for autoignition in the experimental engine, a zero-dimensional autoignition model was developed. The engine conditions were prepared so that the final range of autoignition points would provide sufficient information to confirm the accuracy of the ignition delay model. Equations for ideal gases under polytropic conditions were incorporated in the model using geometric and dynamic values specific to the engine used. For the purpose of simplification, an averaged value for the ratio of specific heats (α) for a stoichiometric mixture of n-heptane and air was used in the prediction model. An ignition delay model for the fuel undergoing autoignition was incorporated, based on the three Arrhenius equation with parameters specific to n-heptane; this was developed by Yates, et al (2005) and was discussed in chapter 2.

$$\tau_{total} = \left\{\left(\tau_1 + \tau_2\right)^{-1} + \left(\tau_3\right)^{-1}\right\}^{-1}$$

Equation 2-15

$$\int_{t=0}^{t_{crit}} \frac{dt}{\tau} = 1$$

Equation 2-16

Using the conservation of ignition delay correlation developed by Livengood and Wu (1955) (as mentioned in chapter 2), autoignition was designated as occurring when the integral, calculated from the summation of the reaction rate for each time step, had reached a value of unity. The results of the model were used to establish the points and likelihood of autoignition in the engine cycle for varied thermodynamic inlet conditions and engine speeds. The conditions which would best describe the region of interest on the ignition delay surface map, the NTC region, were also determined. This then led to the determination of the design and modification criteria for inlet conditions of the engine.

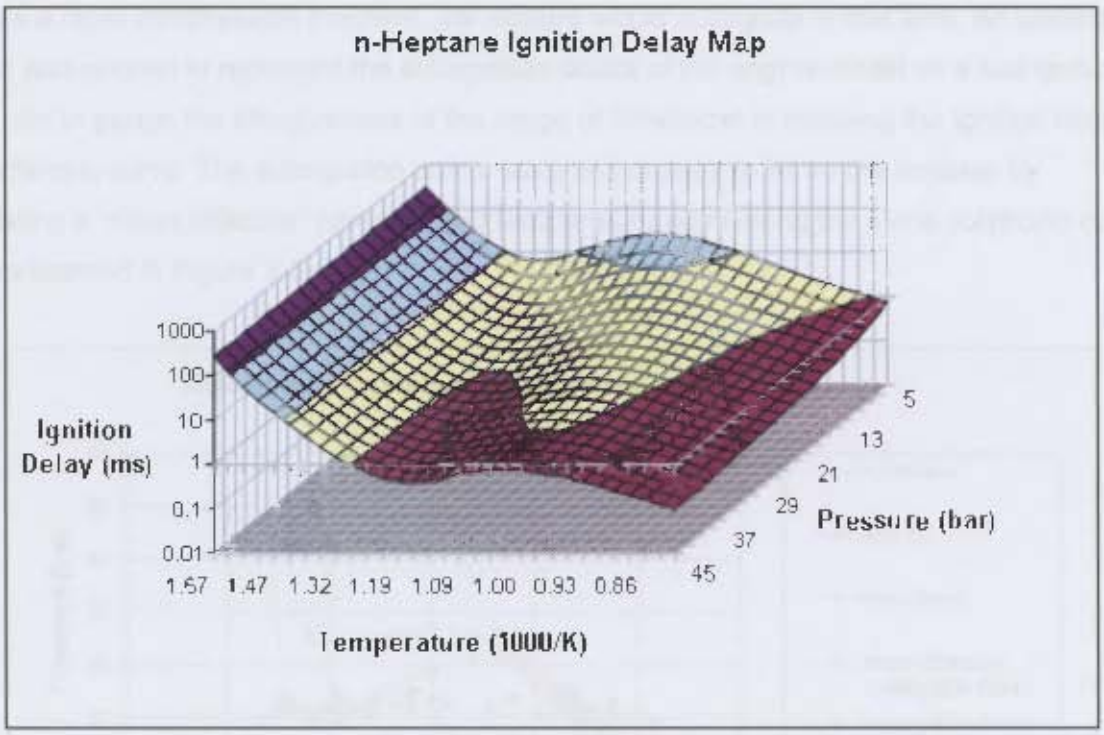

Figure 3-1: The ignition delay characteristic map for n-heptane

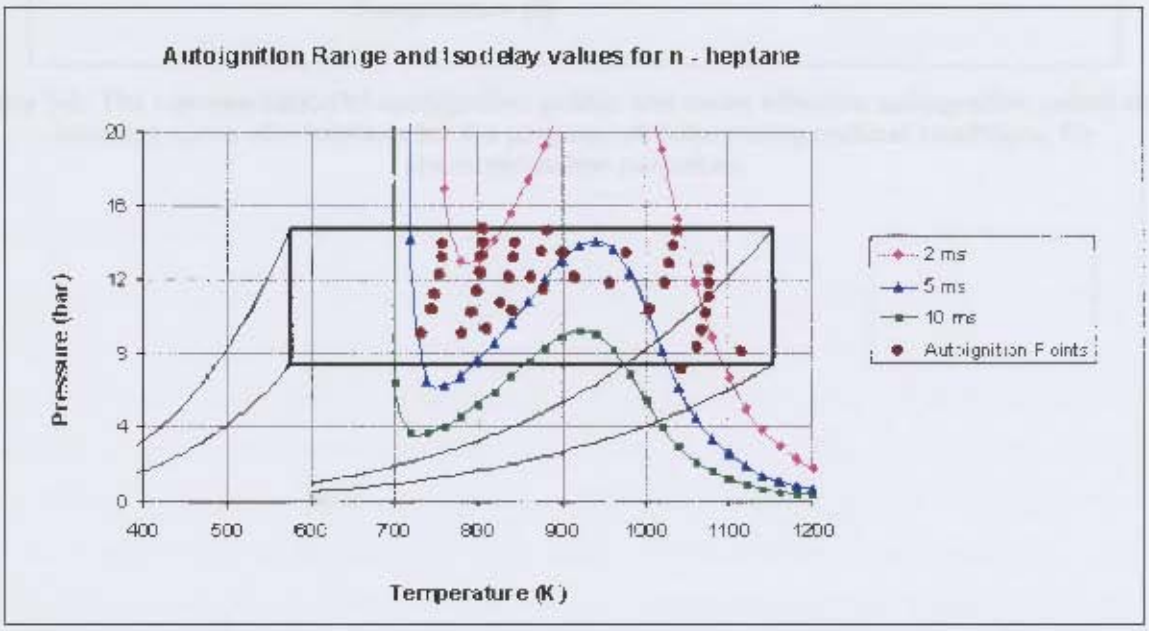

Figure 3-2: The representation of predicted autoignition points for design engine conditions on isodelay curves of n-heptane

Possible autoignition points occurring from between 0 – 15° ATDC (brought about by peak conditions of temperature and pressure in the engine model according to adjusted inlet conditions) were found to lie mostly in the region between isodelays of 2 and 5 ms (as represented in Figure 3-2). Practically, this means that at points of autoignition, conditions in the

such as a rapid compression machine, the mixture would autoignite in that time. An isodelay of 2.5 ms was chosen to represent the autoignition points of the engine model on a fuel ignition delay plot to gauge the effectiveness of the range of conditions in mapping the ignition delay characteristic curve. The autoignition points were constrained to lie on the isodelay by calculating a "mean effective" pressure and temperature point along the same polytropic curve (as represented in Figure 3-3).

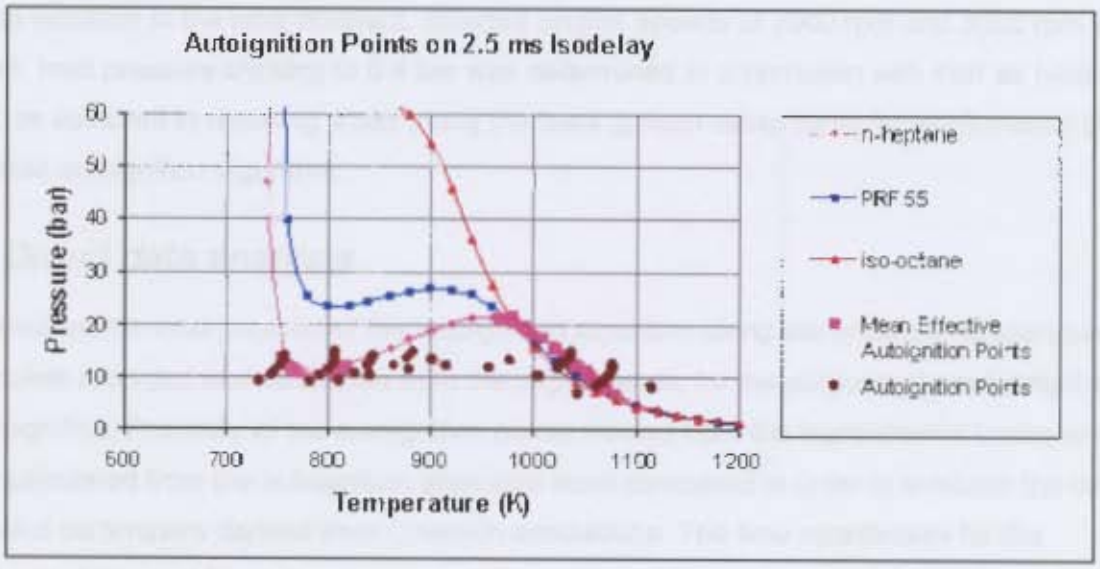

Figure 3-3: The representation of autoignition points and mean effective autoignition points on an isodelay curve of n-heptane for the purpose of determining optimal conditions for characterisation purposes.

3.2 Modelling results

By adjusting parameters such as compression ratio and inlet thermodynamic conditions, the conditions for autoignition were determined for the fuel in study, n-heptane, as well as other fuels. The current compression ratio in conjunction with obtainable variation in inlet conditions was sufficient in describing the ignition characteristics of n-heptane in the required range. To provide variation in the time constant, different engine speeds of 2000 rpm and 3000 rpm were chosen. Inlet pressure choking to 0.4 bar was determined in conjunction with inlet air heating to 600 K as sufficient in reaching areas along the fuels ignition delay curve for confirmation of the proposed autoignition algorithm.

3.3 Direct data analysis

This involved the incorporation of the autoignition algorithm using the pressure-temperature data points recorded and calculated from the experiments, for the purpose of predicting the time of autoignition. Proximity of the autoignition points viewed from the experimental traces and those calculated from the autoignition algorithm were compared in order to evaluate the original Arrhenius parameters derived from Chemkin simulations. The time coordinates for the beginning of the cool flame reaction were also compared between the actual and theoretically determined values.

3.4 Autoignition engine model

An engine model was set up in an attempt to match the pressure and temperature histories measured from the engine experiments. The purpose of the model was twofold: firstly, the model was used, in conjunction with the measured data, to investigate the effect of modification of autoignition parameters describing the ignition delay characteristics of the fuel; secondly, thermodynamic trends deduced from the model were used to expose experimental errors associated with the study, as well as to investigate the effectiveness of the device in characterising ignition delay. Initial pressure measurements were adjusted using the model, owing to uncertainty existing between the value of the pressure measured upstream from the inlet valve (proposed as the initial pressure) and the actual value at inlet valve closure; this was as a result of the inlet manifold air dynamics for the experimental engine being unknown. The method of data correction is described in chapter 5.

For convenience, the equations constituting the autoignition algorithm are repeated below:

$$\tau = Ap^n e^{\frac{\beta}{T}}$$ Equation 2-13

$$t_2 = \tau_{(CF)} + t_1\left(1 - \frac{\tau_{(CF)}}{\tau_{(i)}}\right)$$ Equation 2-18

$$\Delta T = C_1 T_i + C_2 p_i^{\ m}$$ Equation 2-19

Thus it is seen that two sets of A, n, β are necessary to define the autoignition history profile. The first set constitutes the reaction chemistry leading to overall autoignition and the second set constitutes the reaction chemistry leading to the cool flame reaction. The Arrhenius parameters A, n and β approximate the global reaction chemistry in both cases and were determined from empirical data. The values of parameters n and β, however, have a smaller error margin as they are more strongly associated with fundamental reaction chemistry. The parameter A (although also associated with fundamental reaction chemistry) represents the intercept of the ignition delay curve and is determined from empirical data. This parameter in both cases was therefore subject to modification to coerce correlation between the model and test data reaction times. In calculating the temperature rise from the cool flame event, the parameter C_1 was modified for correlation purposes. Originally this parameter was calculated using a function of initial temperature versus temperature increase from Chemkin results; and since it is only a proposed theoretical value, it may therefore be subjected to modification. Chemkin derived Arrhenius coefficient values used in this thesis is given in Table 3-1.

Table 3-1: Table of Arrhenius coefficient values used

Model	$\ln(A_1)$	n_1	B_1	$\ln(A_2)$	n_2	B_2	C_0	C_1	C_2	m
n-Heptane	18.89	0.066	14825	11.18	0.950	15041	3000	1.975	1642	0.046

4 Experimental Setup

In this chapter, the commissioning of the experimental apparatus, test procedures and data acquisition are discussed.

4.1 Experimental apparatus

The requirements of the project are reviewed here for the purpose of discussing the design and modification of the experimental apparatus accordingly.

1. Modify an existing single cylinder engine with the capabilities for heated inlet manifold air temperature to 600 K and choked inlet air pressure to 0.4 bar.
2. Modify the inlet system so that it can be operated with a fuel injection system, with the potential of adjustability for different fuels, equivalence ratios and air densities through heating and choking of the inlet air.
3. Insert the relevant transducers and equipment for engine test data acquisition and analysis.
4. Build a dynamometer system, consisting of a frame, driving element and load control system. The engine should have motoring speed variability from 600 – 3000 rpm.

An existing Briggs and Stratton engine-generator unit was provided by Sasol for the research project. The rapid heat release characteristic of uncontrolled autoignition in engines results in a corresponding rapid pressure rise of the in-cylinder gases. This usually results in severe engine damage if allowed to continue over a prolonged period, so for the purposes of this project a small, easily replaceable engine was chosen. A smaller engine with a reduced induction volume also has the advantage of having a higher relative safety factor with regard to continual in-cylinder pressure stresses when compared to an engine with larger capacity and thus was more suited to the type of experimentation undertaken.

Table 4-1: Engine specifications

Specification	Units	Values
Bore	mm	72
Stroke	mm	26
Swept Volume	cc	215
Compression ratio	-	8.5:1
Power rating	hp	7.5

4.2 Modifications and design of the inlet manifold

A new inlet manifold was designed for the purposes of experimentation including:

1. Air-mass meter (feedback to the fuel measuring control unit)
2. Inlet air throttle device (control of inlet air pressure)
3. Air plenum (dampening pulsations from single cylinder induction for pressure measurement in the air inlet)
4. Inline air heater (control of inlet air temperature)
5. Electronic fuel injection (control of the rate of fuel metering with accuracy)
6. Fuel injector cooling

Details of design and specification are in Appendix B.

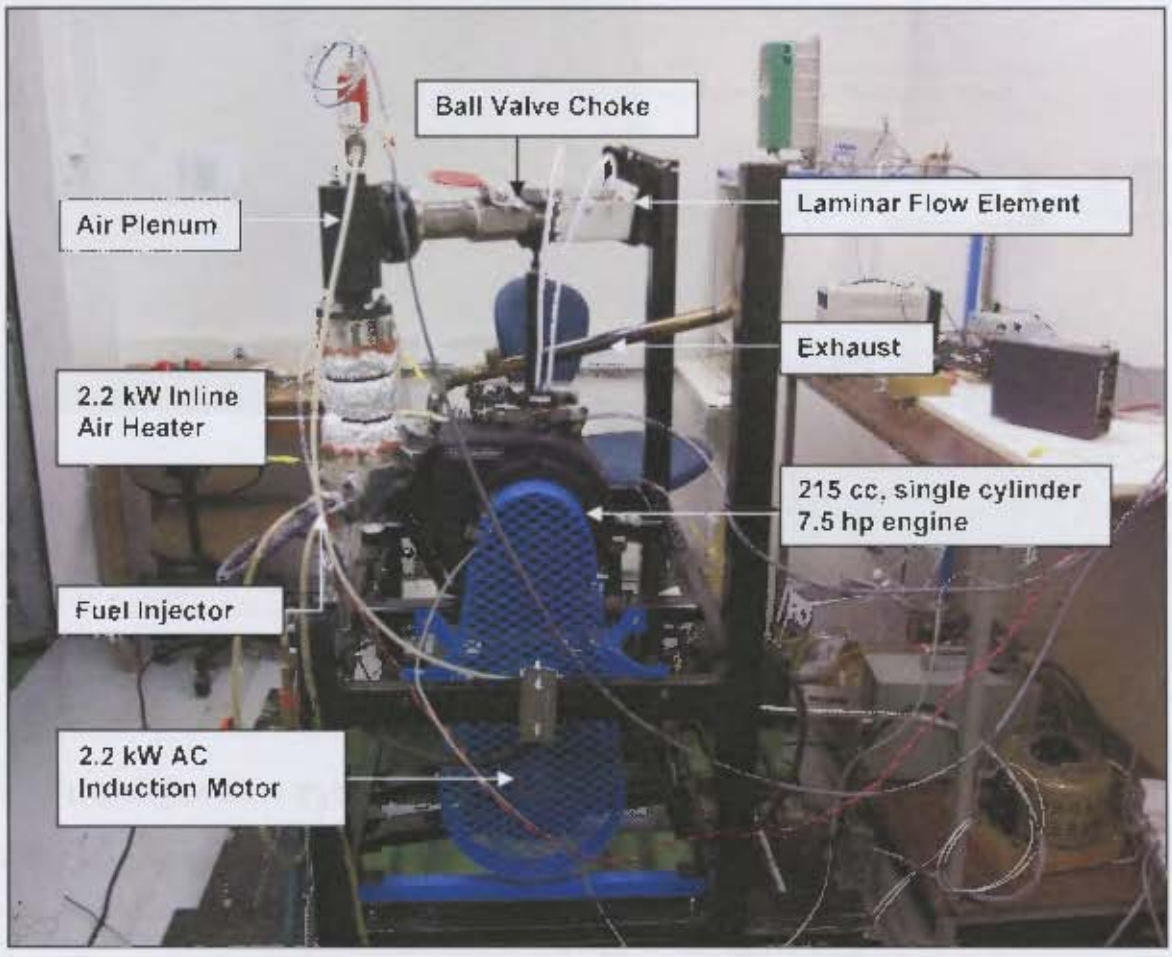

Figure 4-1: Engine dynamometer setup and inlet manifold modifications

4.3 Experimental engine dynamometer system

An AC induction motor with a variable speed drive controller was specified for motoring the engine at the desired speeds. Under firing or autoignition conditions a load control system was required for speed control via the generator. A resistor bank of 8 kW, mounted in the extractor system for safety purposes and a 10 kW maximum load dimmer were used to control the power shedding of the generator and thus the speed of the engine. A dynamometer frame was constructed to mount the machines. The details of design and specification for the dynamometer system are in Appendix A.

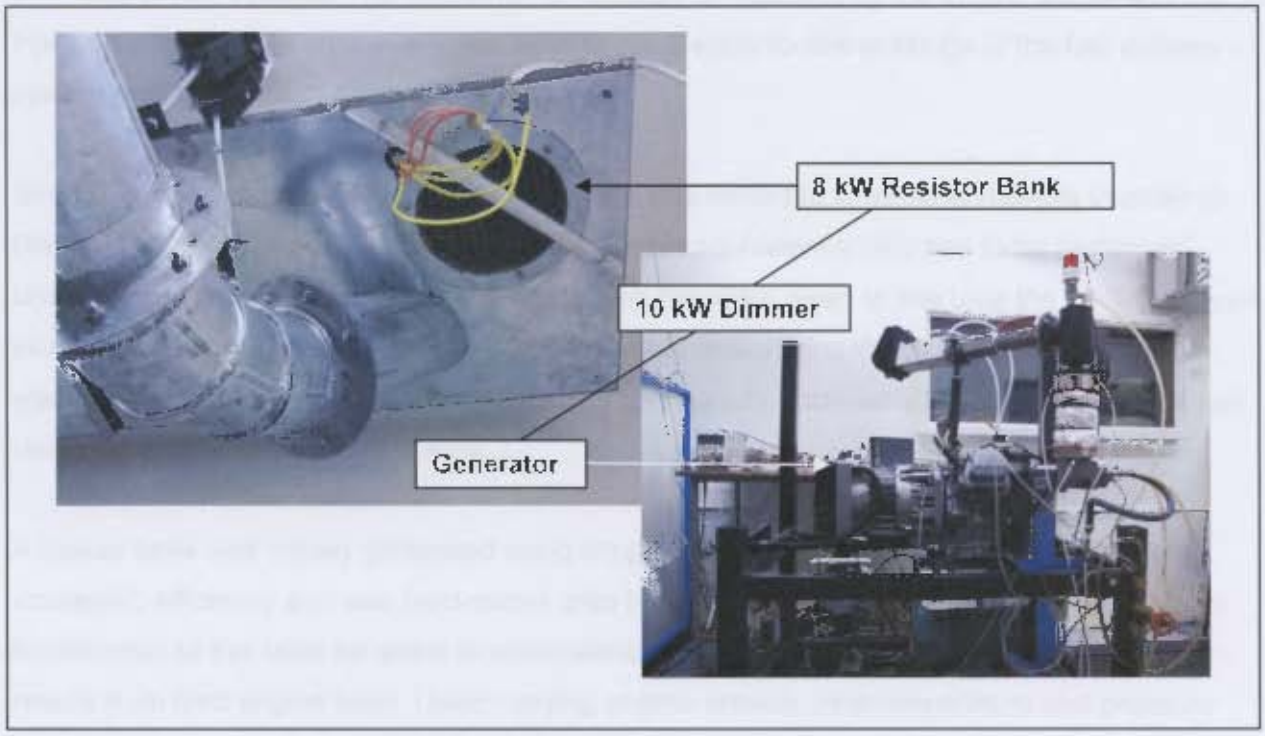

Figure 4-2: Load control system

4.4 Fuel injection system

The first step for fuel metering under conditions using different fuels, equivalence ratios and dynamic air density variation involved the replacement of the carburettor with a fuel injection system. An electronic control unit consisting of a Motorola JK1 8-bit flash memory microcontroller with onboard ADC regulated the fuel injector pulse width and frequency according to input signal values. The input signals, consisting of the revolution counter and laminar flow element air mass flow, were compared with values arranged in a lookup table stored on the chip before an output signal was fed to the injector (See Figure 4-3).

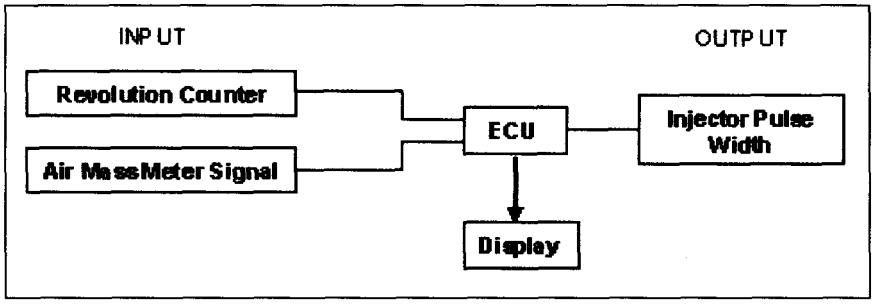

Figure 4-3: Control loop for fuel delivery system

The lookup table contains values that may be altered and uploaded to the ECU memory via a serial port to a computer. Linear interpolation between the values results in an output pulse width signal controlling the length of time that the injector solenoid remains open and therefore the mass of fuel injected. The frequency of injection is regulated by the engine speed and the injection event occurs once every two revolutions. Details for the workings of the fuel delivery system may be found in Appendix C.

Since fuelling of the engine in autoignition mode was limited to small time intervals in order to prevent engine damage, the calibration for a certain equivalence ratio had to be performed under normal fired conditions; sufficient time was therefore given to fine tune the fuelling without incurring damage to the engine. For purposes of commissioning the device, the lookup table was calibrated under stoichiometric conditions for a locally obtained 95 octane commercial fuel using the technique described below.

A lookup table was initially generated using simple airflow calculations involving a constant volumetric efficiency and was hard-coded onto the chip as the default storage setting. Further modification to this table for exact stoichiometric conditions was performed using empirical results from fired engine tests. Under varying engine speeds, inlet temperature and pressure conditions, the air fuel ratio was adjusted manually by overriding the air mass signal with a variable DC voltage source. The tests were performed under firing conditions with the use of a spark plug to initiate burning. The speed of the engine was controlled using the load shedding system during engine firing. Stoichiometric conditions were then adjusted using negative feedback from a lamda sensor mounted in the exhaust stream.

The data collected from the tests was used to develop an empirical volumetric efficiency function to calculate input values in the lookup table under stoichiometric conditions. The injection duration function that best correlated the experimental with calculated values was discovered to be of the form:

$$ID = A_0 + \rho(A_1 N + A_2 N^2 + A_3 N^3)(1 + A_4 T_i)(1 - \frac{A_5}{P_{atm} - P_i})$$ Equation 4-1

where: ID is the injection duration value (corresponding to mass of fuel per cycle)

ρ is the air density (based on inlet temperatures and pressures)

N is the engine speed

T_i is the inlet temperature

P_i is the inlet pressure

The volumetric efficiency function consisted of the product of a polynomial function of engine speed, an initial temperature term and an initial pressure term. The last term in the equation describes the change in pressure between inlet and exhaust, indicative of its effect on volumetric efficiency. Details on the technique are described in Appendix C.

4.5 Transducers and data acquisition

For the purposes of the project, four measured inputs were required for simultaneous sampling and capturing:

1. TDC marker
2. Inlet absolute pressure
3. Inlet temperature
4. In-cylinder pressure

Other measurements (taken for control purposes) are labelled in Figure 4-4, and including the thermocouples for control of the heater temperature.

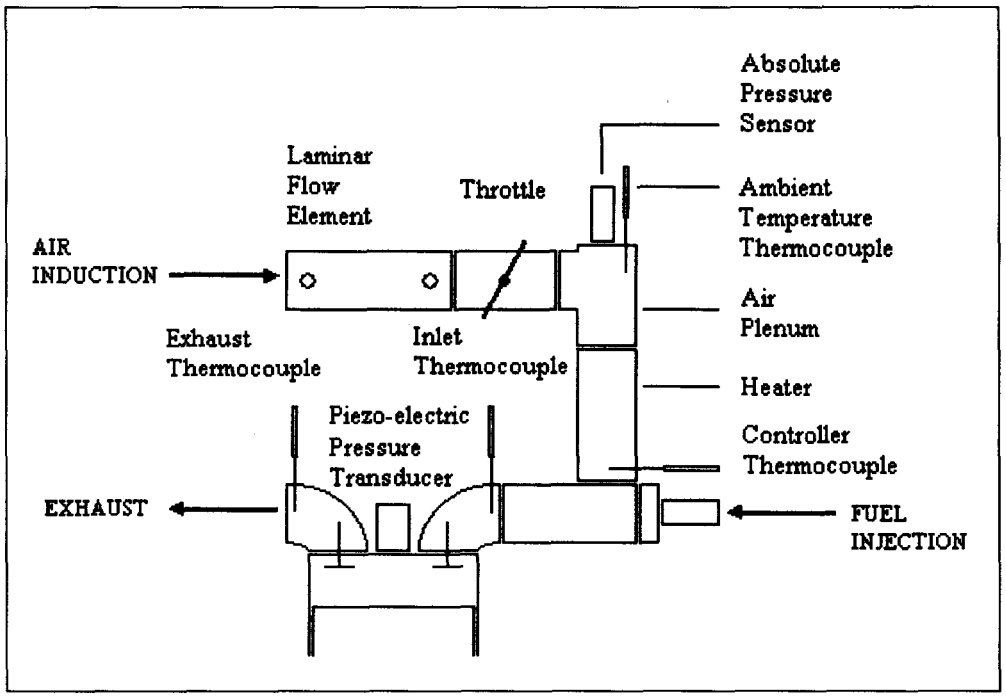

Figure 4-4: Schematic of inlet manifold modifications and attached transducers

4.5.1 TDC marker

The previously mentioned revolution counter consisted of an optical sensor that was triggered every revolution by a disk attached to the engine flywheel. The signal was fed to the ECU which regulated fuelling, as well as being a requirement for data acquisition for positioning of the in-cylinder trace as a function of crank angle. A technique was used to calculate the offset of the signal marker to true TDC, which is described in Appendix D.

4.5.2 Inlet pressure

The inlet pressure was measured using a Huba Control (691.90000005) absolute pressure transducer mounted in the air plenum.

4.5.3 Inlet temperature

The inlet temperature was measured using a thermocouple mounted directly above the inlet valve.

4.5.4 In-cylinder pressure

A Kistler piezoelectric pressure transducer was mounted in the spark plug thread in the cylinder head.

4.6 Data acquisition

Data was recorded on a four-channel simultaneous sampling oscilloscope with capabilities of storage onto USB drive. The data files were imported and analysed using Microsoft Excel.

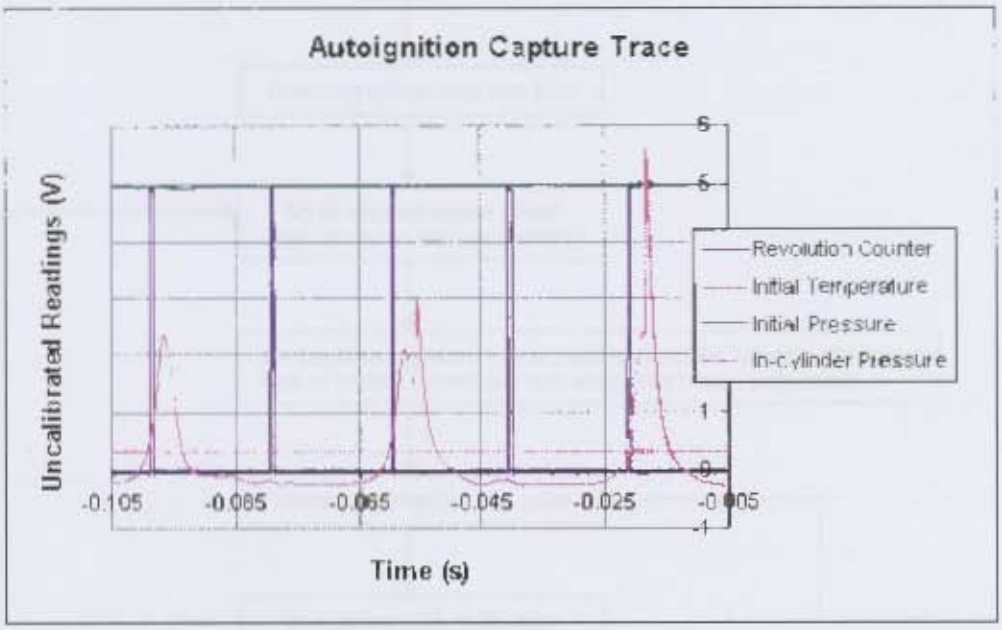

Figure 4-5: Progression of motoring to autoignition development in three successive cycles with simultaneously logged inlet condition signals.

4.7 Experimental procedure

The autoignition experiments using n-heptane were performed within the parameters described in Table 4-2 (obtainable with the device), the intention being that the variation of conditions would provide sufficient information to describe the characteristic ignition delay map, including the NTC region.

Table 4-2: Experimental operating parameters

Parameter	Range
Inlet pressure range	0.4 – 1 bar
Inlet temperature range	300 – 550 K
Engine speed range	1500 – 3000 rpm

Six autoignition test points were acquired as a means to confirm the proposed Arrhenius parameters of the new autoignition algorithm. Fuel was injected after thermal conditions had reached equilibrium. Due to heat loss from the inlet as a result of cooling of the injector, it was not possible to reach the maximum design temperature at low flow rates (low engine speed) without running the risk of damage to the heater.

Figure 4-6 shows a flowchart of the experimental procedure.

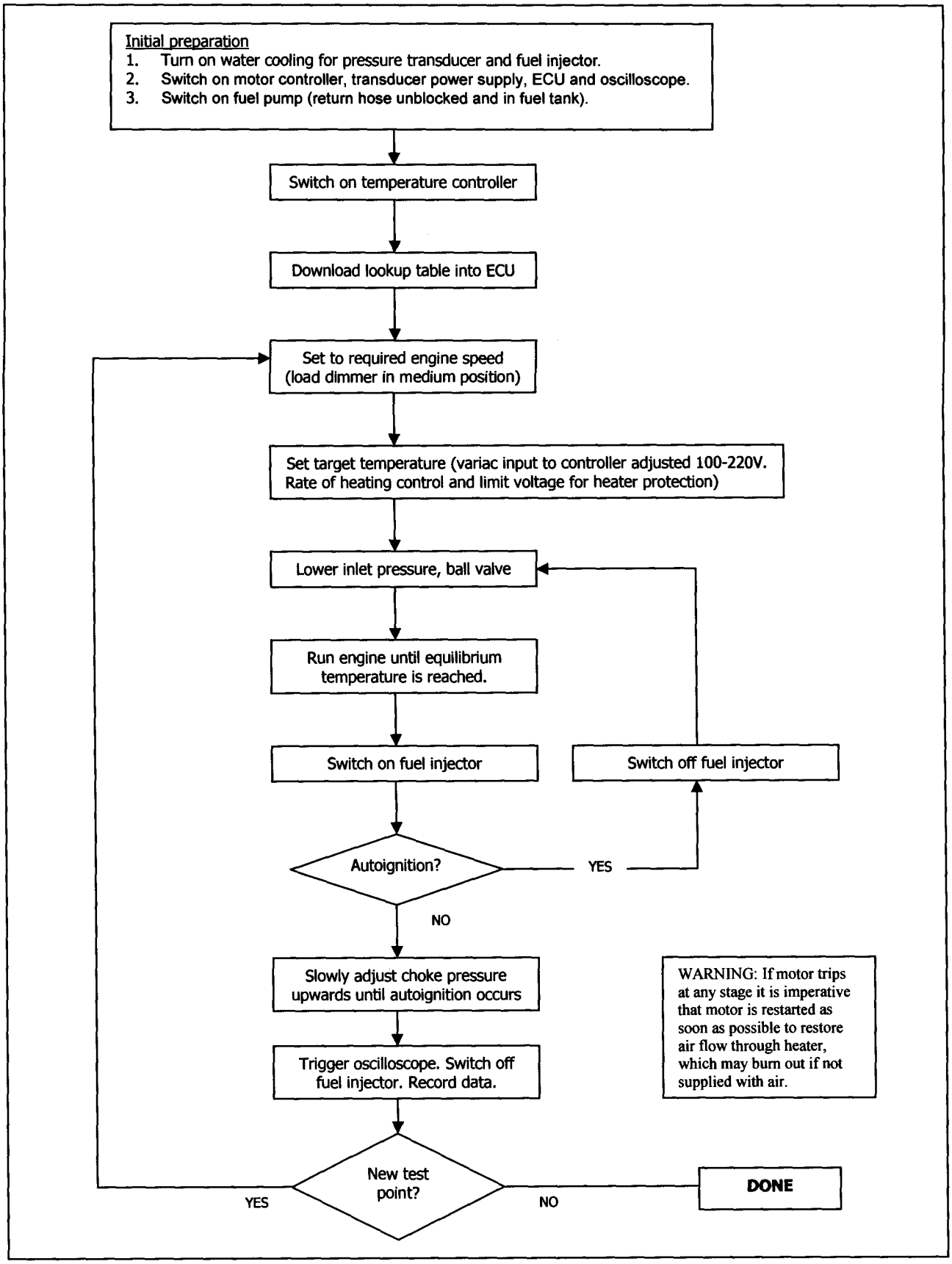

Figure 4-6: Experimental procedure flow chart

5 Preliminary Data Correction

5.1 *Initial pressure correction*

The pressure at inlet valve closure was initially assigned the value measured upstream in the air plenum. This assumption was rejected after discovering that a series of motored engine tests under different inlet air choking conditions and speeds indicated otherwise. The pressure at the inlet valve was different from that which was measured upstream due to air dynamics arising from the conditions and geometry of the inlet system.

A motored engine model was prepared using ideal gas relations and a polytropic compression coefficient of 1.4 for air. Initial pressures were adjusted in the model until the maximum pressure correlated with the maximum compression pressure for each test. A correlation equation was then developed to incorporate the pressure difference in the initial pressure value measured in the autoignition experiments. The equation included initial pressure measured in the air plenum and engine speed as variables. Initial temperature was found to have a negligible effect on this normalised pressure value after investigating its effect in further motored air experiments. The proposed equation was of the form:

$$Pi_{normalised} = a_0 + a_1.P_{i\ measured} + a_2/rpm \qquad \text{Equation 5-1}$$

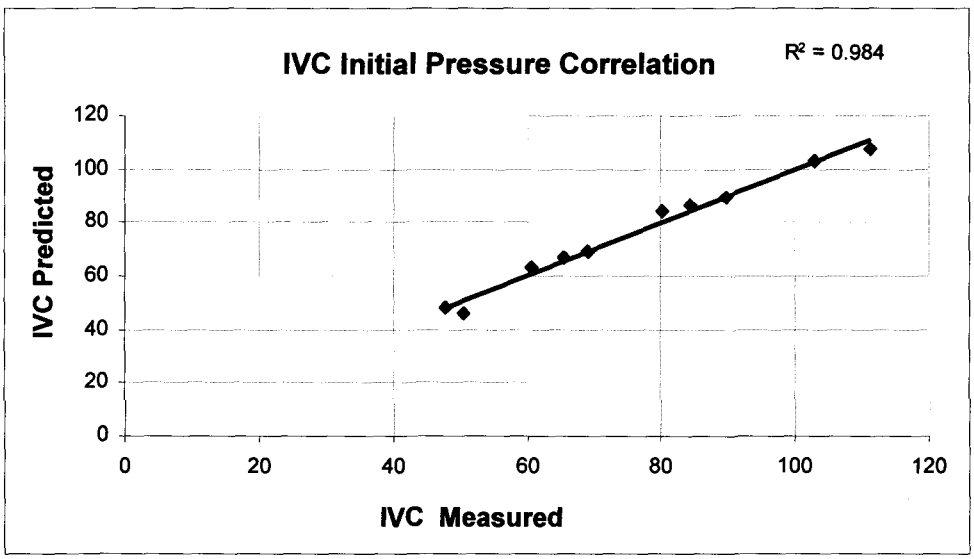

Figure 5-1: Graph showing inlet pressure correction correlation

Table 5-1: Test points from motored tests with proposed inlet pressure corrections

Speed (rpm)	Pi measured (kPa)	Pi normalised (kPa)
997	99.2	82.8
1003	81.0	64.2
1010	60.6	49.6
2013	98.6	100.9
2007	80.9	78.7
2013	60.3	59.5
3000	97.9	109.0
3008	80.3	88.0
3000	60.9	67.7
3000	40.0	47.0

5.2 Autoignition trace modelling

An engine model was developed for the purpose of establishing correlation with the autoignition test data traces. The model included the incorporation of the autoignition algorithm, the effects of which could be investigated and modified in a motored engine system. The effect on the autoignition model as a result of modifying engine variables could also be studied. The model could also be a useful tool in explaining possible sources of experimental error.

Compression of an ideal gas may be described using polytropic gas equations, where the polytropic coefficient equals the ratio of specific heats under isentropic compression conditions. Unfortunately, the exact values of these polytropic coefficients were not known from the autoignition experiments. The coefficient is a function of the heat transfer and the constituents of the gas mixture being compressed, which comprises of air, fuel and residual exhaust gas. Since the exact proportion of each constituent as well as the heat transfer was not known, the coefficient value could not be determined. The presence of residual exhaust gas was reduced during experimentation by recording the first autoignition trace after slowly increasing inlet pressure in the inlet under choked conditions. This, however, did not eliminate pre-reactions from occurring in the preceding compression traces to autoignition. A single polytropic coefficient was used in the model for each test to best approximate the compression portion of the trace. These values, however, did not serve to strictly represent a particular path of heat transfer in each case, but rather to validate a method that would best correlate the simplified model with the test compression traces. It was necessary to investigate a specific value in each case and two methods were devised.

5.2.1 Method I

In each autoignition test trace a cool flame reaction was seen to occur before the autoignition reaction. Polytropic coefficients were adjusted in the model in each case until the maximum compression temperature value reached an extrapolated line from the compression portion of the autoignition temperature trace just before the cool flame reaction. The heat transfer effect was not explicitly included in the model using this method and it was discovered from comparison between the model and test traces that significant heat gain appears to have occurred in the compression stroke. The values derived from this method, however, are under estimates of the isentropic values, indicating net heat loss. A heat transfer model could therefore assist correlation with the actual test data traces in the use of this method.

5.2.2 Method II

The second method involved the use of compression pressure traces preceding the autoignition trace. Polytropic coefficients were adjusted in the model in each case until the maximum pressure of the test data compression trace was reached. These coefficients were then used to derive an experimentally determined correlative equation, in order to assign a polytropic coefficient for the model in each case. Upon investigating the test data temperature traces derived from pressure, it was seen that in each case preceding reactions to global autoignition (cool flame reactions) occurred; this was seen as a temperature rise in the trace. This did not offset the dependency of this method, as the cool flame reaction in the test data helped to offset the heat transfer effect which was not included in the model. For this reason, the second method was preferred in the modelling application for obtaining and discussing results. The equation describing the value of the polytropic coefficient of the model for each test showed the best correlation using the variable of initial temperature measured at IVC. Having achieved good correlation in the determining equation gave credibility to this method as an empirically justifiable means for the modelling of the autoignition data.

$$k = a_0 + a_1.T_i \qquad \text{Equation 5-2}$$

between the model and test traces that significant heat gain occurred in the compression stroke. A heat loss model would therefore assist correlation with the actual test data traces in the use of this method. For the present purposes, however, the adiabatic approximation sufficed.

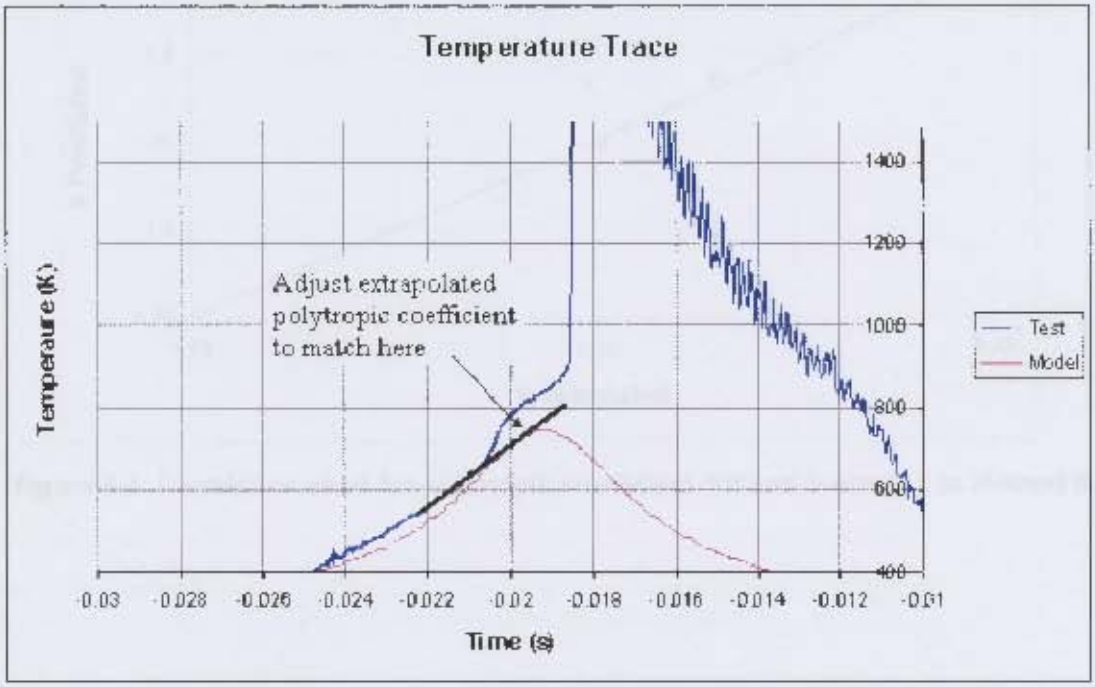

Figure 5-2: Graph showing definition of value of polytropic coefficient defined according to Method I

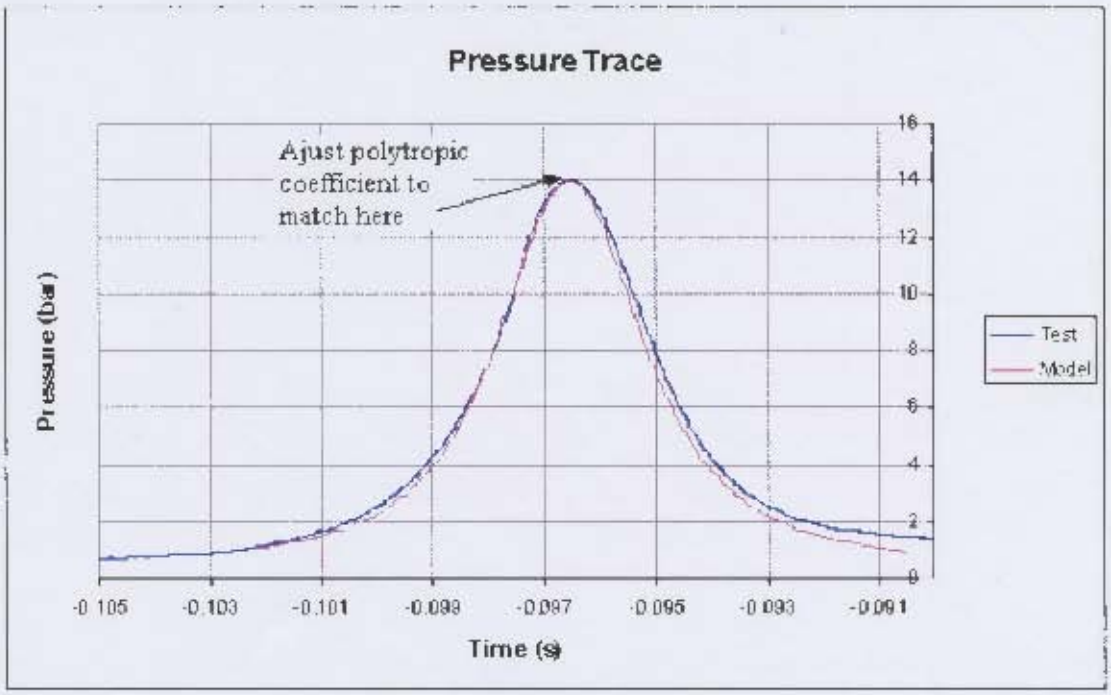

Figure 5-3: Graph showing definition of value of polytropic coefficient defined according to Method II

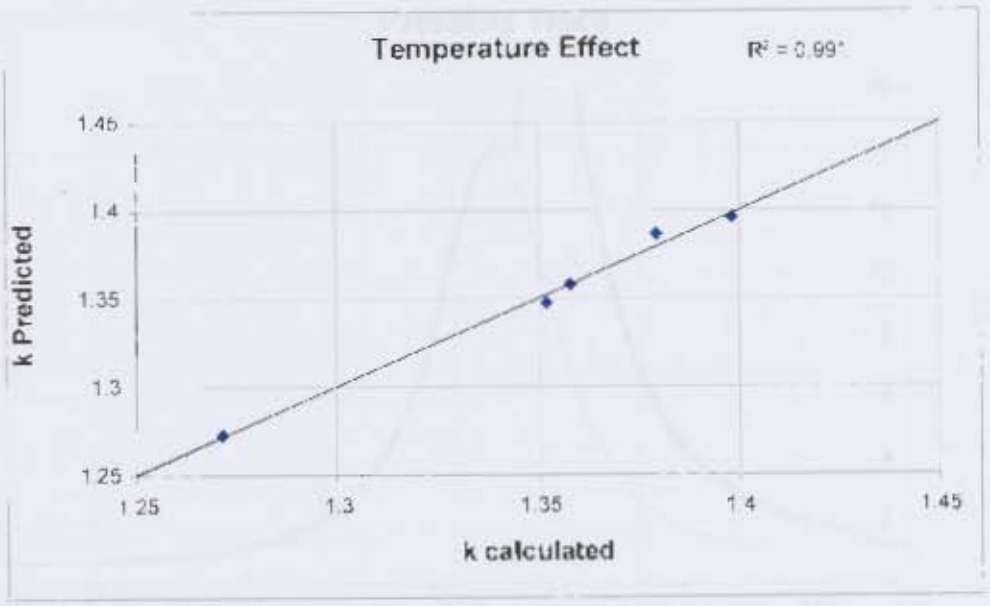

Figure 5-4: Correlation chart for polytropic coefficient defined according to Method II

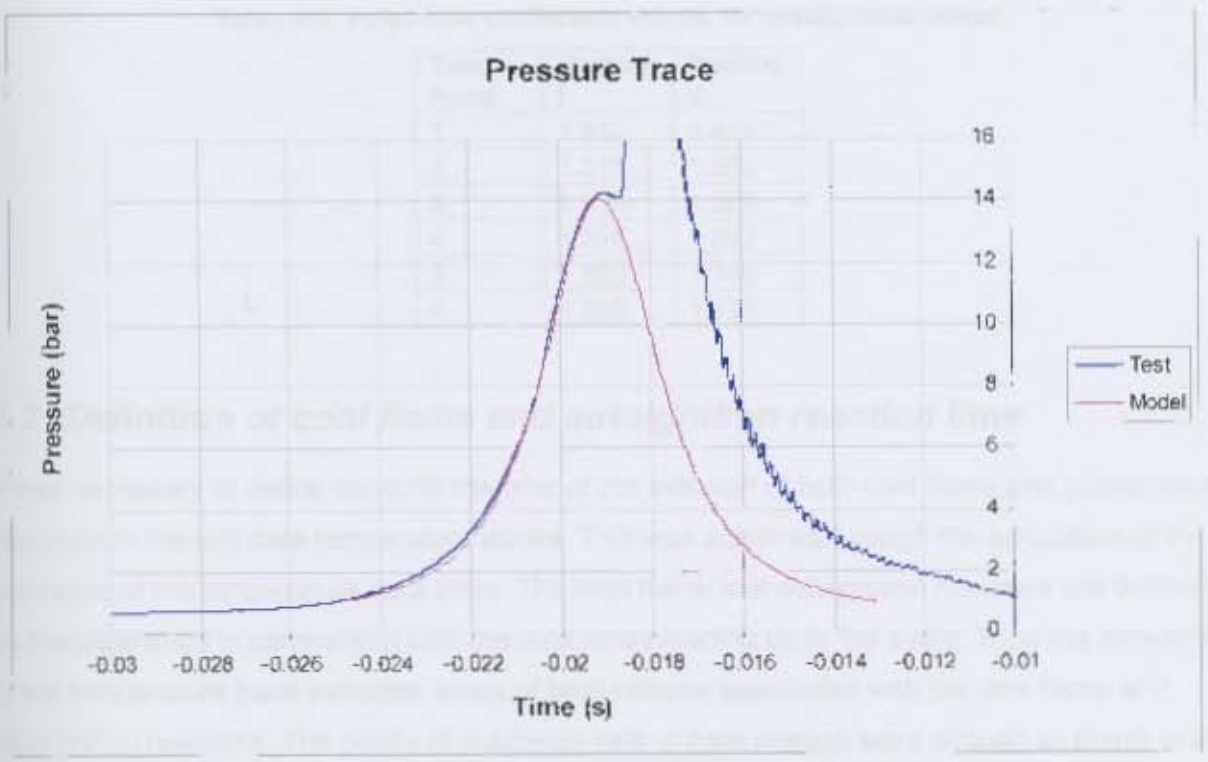

Figure 5-5: Test data pressure trace with model compression trace using polytropic coefficient defined according to Method II

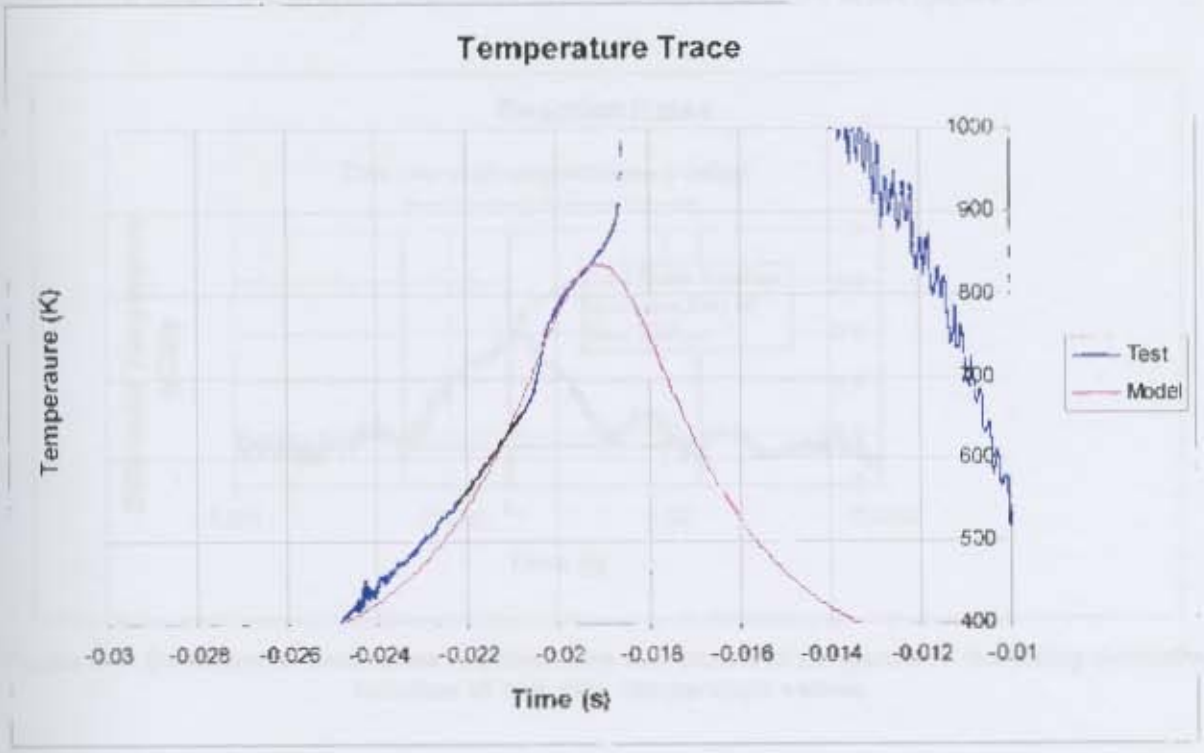

Figure 5-6 Test data temperature trace with model compression trace using polytropic coefficient defined according to Method II

Table 5-2: Polytropic coefficient values for autoignition model

Test Point	Method I	Method II
1	1.332	1.474
2	1.316	1.389
3	1.315	1.359
4	1.336	1.392
5	1.320	1.346
6	1.289	1.280

5.3 *Definition of cool flame and autoignition reaction time*

It was necessary to define correctly the time of the initiation of both cool flame and autoignition reactions in the test data temperature traces. This was achieved through the calculation of the derivative of the temperature data trace. The cool flame and autoignition reactions are defined as instantaneous in comparison with the time delay leading up to the event. Thus the derivative of the temperature trace indicates areas of heat release associated with the cool flame and autoignition reactions. The points of maximum rate of heat release were defined as points in the time scale of the initiation of reaction. The temperature rise in the cool flame was defined as the temperature difference between the two points on either side of the protrusion in the temperature differential graphs, examples of which are Figure 5-7 and Figure 5-9.

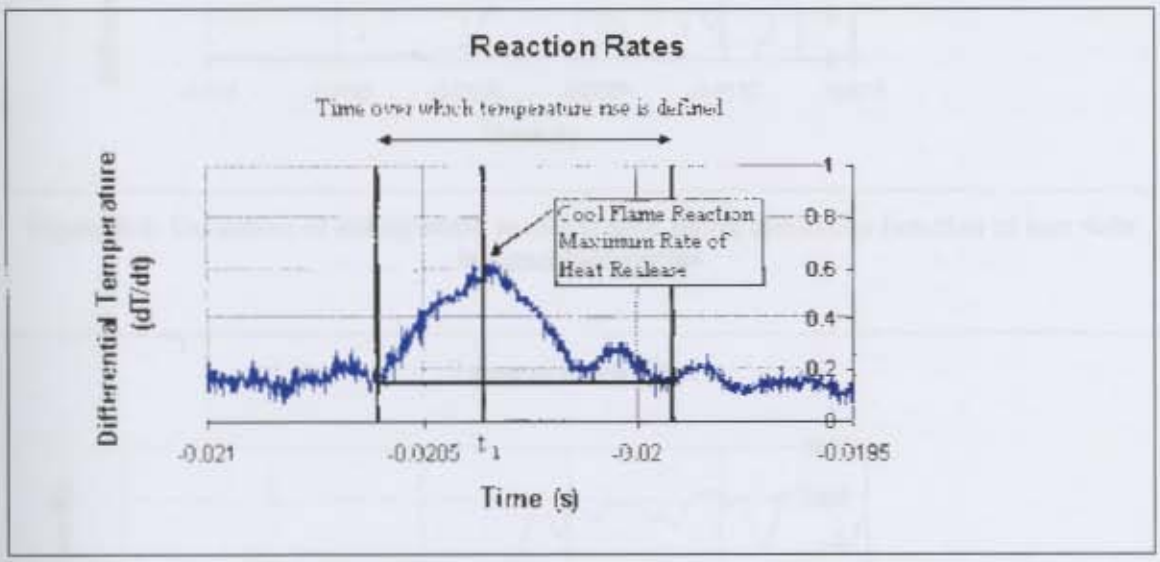

Figure 5-7: Definition of cool flame reaction time and extent of temperature rise using derivative function of test data temperature values

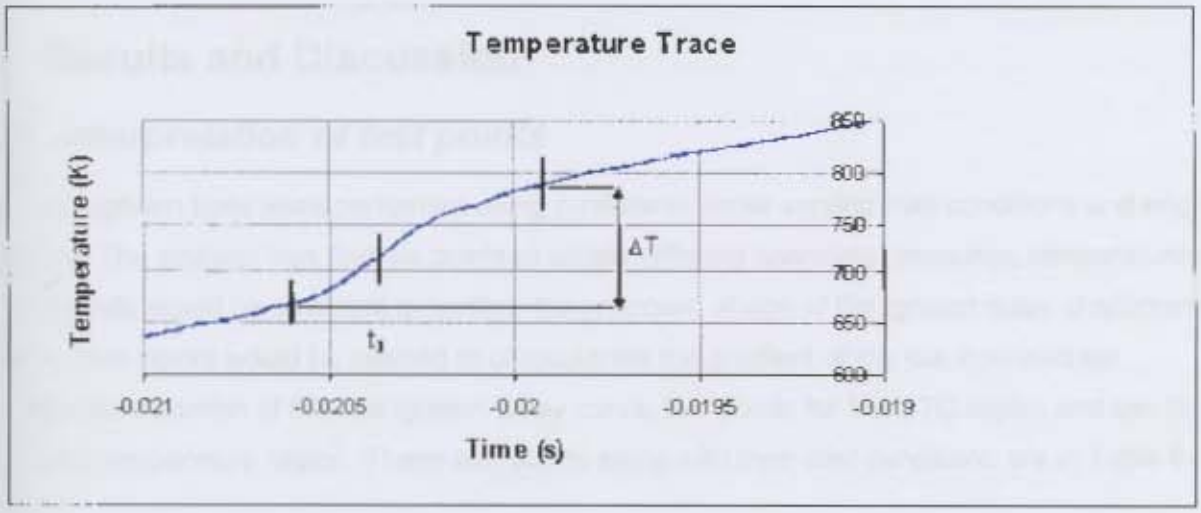

Figure 5-8: Position of cool flame reaction time and extent of temperature rise as shown on temperature trace

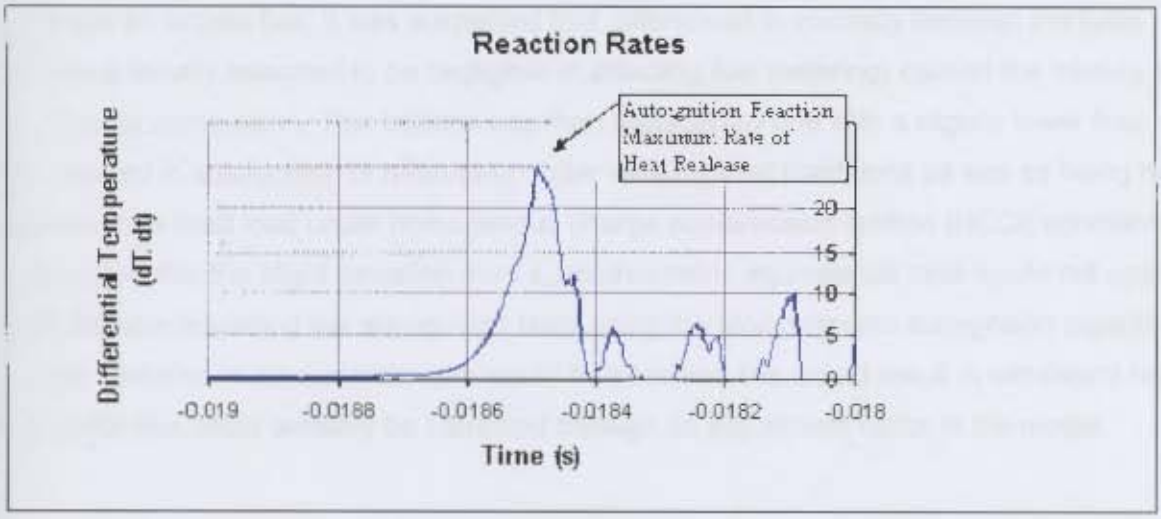

Figure 5-9: Definition of autoignition reaction time using derivative function of test data temperature values

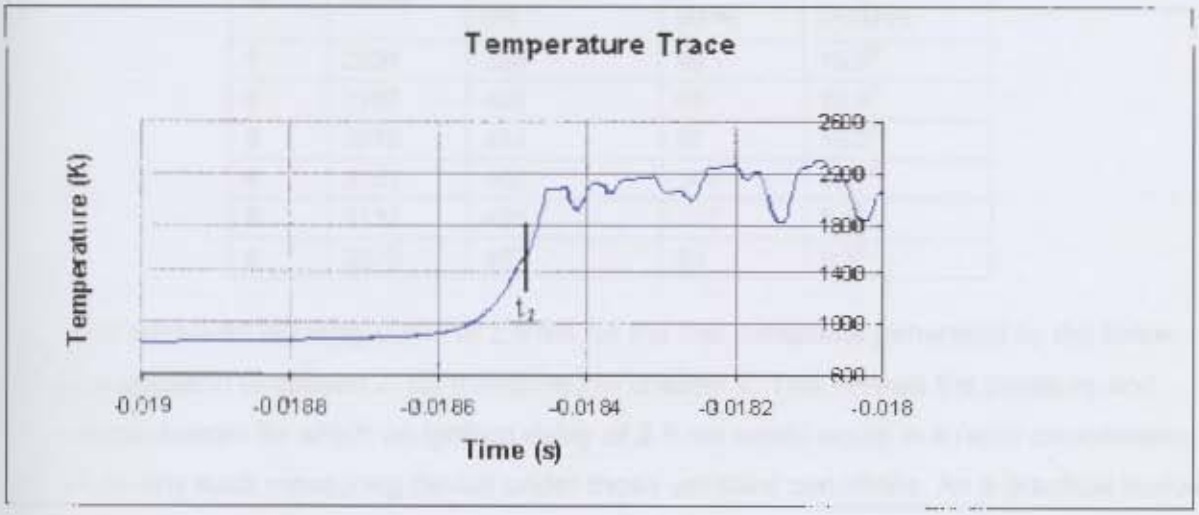

Figure 5-10: Position of autoignition reaction time shown on temperature trace

6 Results and Discussion

6.1 *Interpretation of test points*

Six autoignition tests were performed using n-heptane under varying inlet conditions and engine speeds. The strategy was that six points at widely differing operating pressures, temperatures and speeds would be sufficient to confirm the proposed shape of the ignition delay characteristic curve. Two points would be needed to characterise the gradient of the low-intermediate temperature domain of the fuel ignition delay curve, two points for the NTC region and two for the high temperature region. These test points along with their inlet conditions are in Table 6-1.

Unfortunately, the n-heptane mixture failed to ignite in the engine below an inlet air temperature of 100^{0}C or using the original injector which was used for calibration of the lookup table with the commercial 95 octane fuel. It was suspected that differences in viscosity between the fuels (which were initially assumed to be negligible in effecting fuel metering) caused the mixture to be too rich for combustion. This injector was then replaced by one with a slightly lower flow rate, which resulted in autoignition of n-heptane under variable inlet conditions as well as being run constantly for a fixed load under homogenous charge compression ignition (HCCI) conditions. It was assumed that the slight deviation from a stoichiometric equivalence ratio would not upset the results from modelling the autoignition tests using the stoichiometric autoignition algorithm. Since the deviation in equivalence ratio would be constant, this would result in consistent results and an error that could possibly be corrected through an adjustment factor in the model.

Table 6-1: Autoignition test conditions

Test no.	Speed (rpm)	Initial Temperature (K)	Initial Pressure (kPa)	Autoignition Angle (ATDC)
1	2056	356	95	19.9^0
2	2107	408	95	10.9^0
3	2070	424	87	15.8^0
4	3151	402	107	13.1^0
5	3132	435	107	5.4^0
6	3076	482	84	0.7^0

Figure 6-1 shows an isodelay curve of 2.5 ms for the fuel n-heptane generated by the three-Arrhenius equation (Equation 2-15) mentioned in chapter 2. This reveals the pressure and temperature domain for which an ignition delay of 2.5 ms would occur in a rapid compression machine or any such measuring device under those constant conditions. As a practical feature, the test points are represented on this curve, so that the conditions that the fuel experiences in

the engine may be compared with the properties of the fuel itself. To obtain these points, the actual pressure and temperature values at which autoignition occured were transformed into "mean effective" pressure and temperature values. These values represent the points in the engine's compression cycle that would render a measured ignition delay of 2.5 ms in an ignition delay measuring device under these conditions, yet in a statically controlled environment. The ignition delay values were calculated by applying the three-Arrhenius autoignition delay algorithm derived from Chemkin results directly to the measured temperature and pressure history of the engine. The Arrhenius parameters were not adjusted to correlate exactly with the measure ignition delay time from the test data, since firstly; the predicted autoignition reaction time was observed to be close enough to the time measured and secondly; this was not required for the purpose of showing the general position of the test points in relation the characteristic ignition delay curve of the fuel.

It is seen from Figure 6-1 that four of the points lie in the high temperature region and two points from the lower engine speed lie in the high temperature region of the isodelay curve. No points indicate having been mapped in the NTC region.

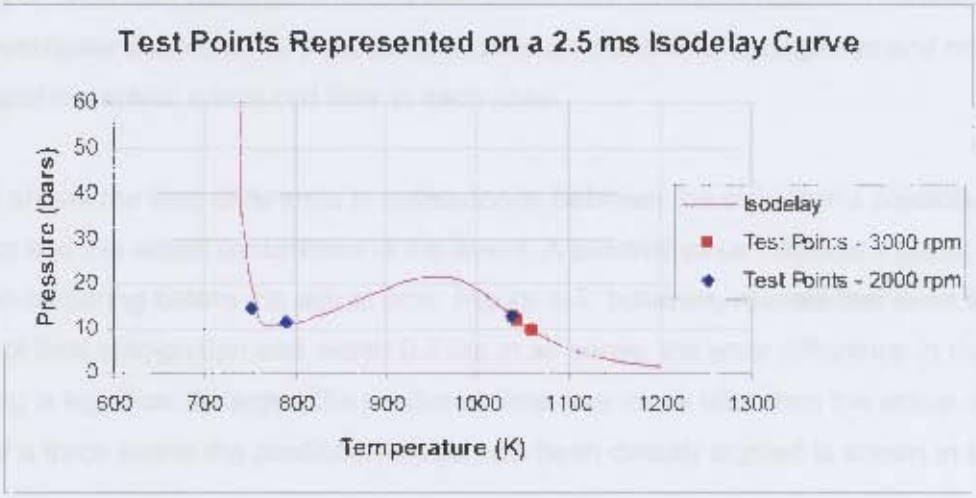

Figure 6-1: Test points transformed and represented on a 2.5 ms isodelay for n-heptane

Figure 6-2 shows the interception of a compression trace with an isodelay curve of n-heptane. It is seen that the NTC region is difficult to characterise as its gradient and the gradient of the compression trace are very similar. A small shift in any direction results in the NTC region being missed, which explains why no points were mapped in the NTC regions despite having raised the temperature in small increments. Therefore, despite the possibilities of points in the NTC region shown in Figure 3-3 no points were mapped in the experiments.

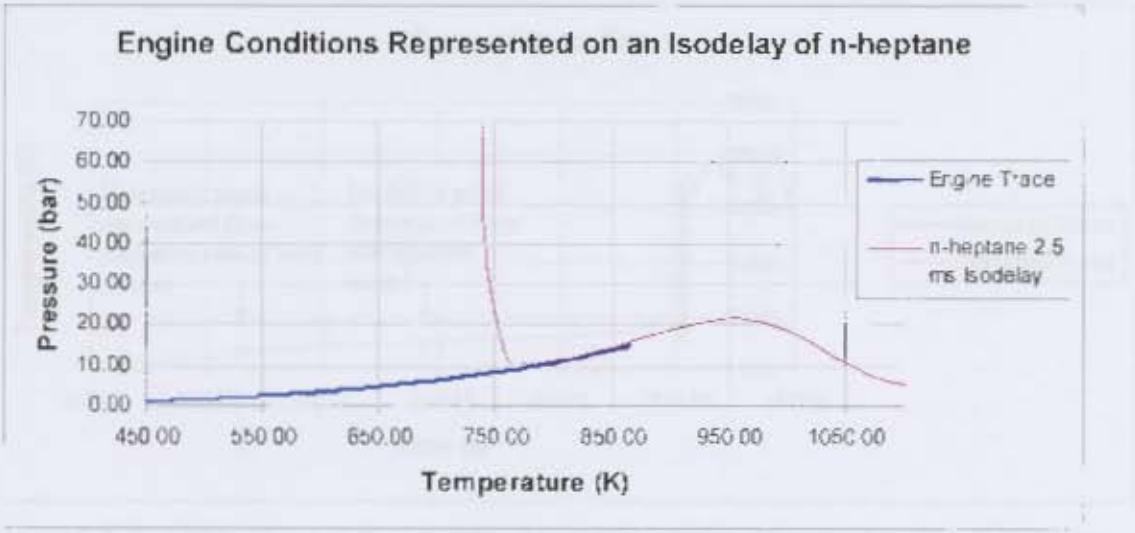

Figure 6-2: Typical compression trace of test engine represented on an isodelay curve of n-heptane

6.2 *Direct data analysis*

As an initial test, the new autoignition model was applied directly to the pressure-temperature data points of each test, using parameters calculated from Chemkin results. This was done in order to investigate the proximity between the calculated points of autoignition and cool flame reactions and the actual measured time in each case.

Figure 6-4 shows the time difference in milliseconds between the algorithm's prediction of autoignition and the actual occurrence of the event. A positive value displays a predicted time of autoignition occurring before the actual time. Figure 6-5, however, reveals that even though prediction of final autoignition was within 0.1 ms in all cases, the error difference in the cool flame timing is significantly larger; the predicted time was much later than the actual event. An example of a trace where the prediction model has been directly applied is shown in Figure 6-3.

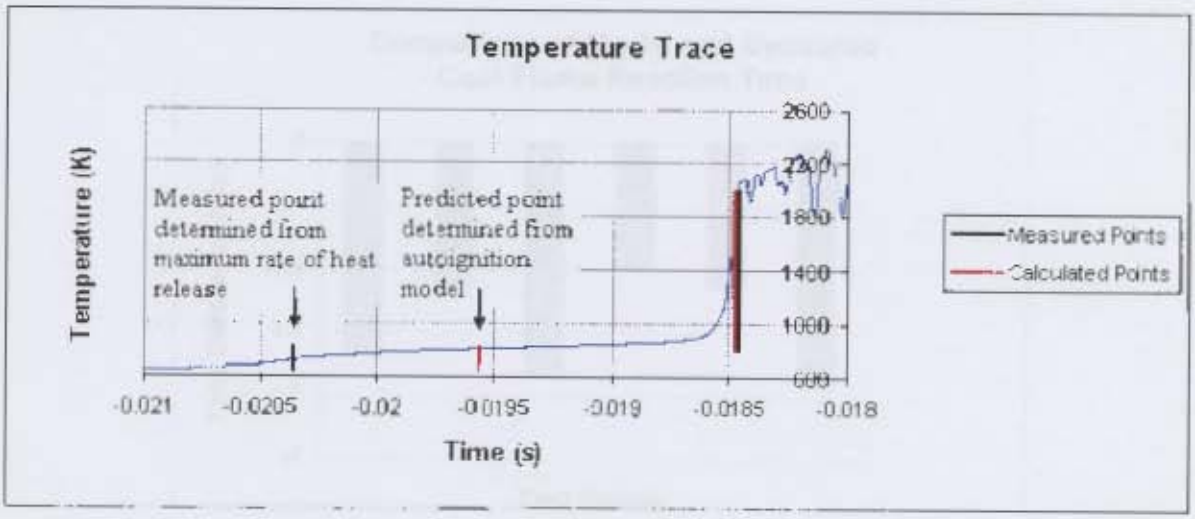

Figure 6-3: Example of prediction points of reaction versus measured points of reaction

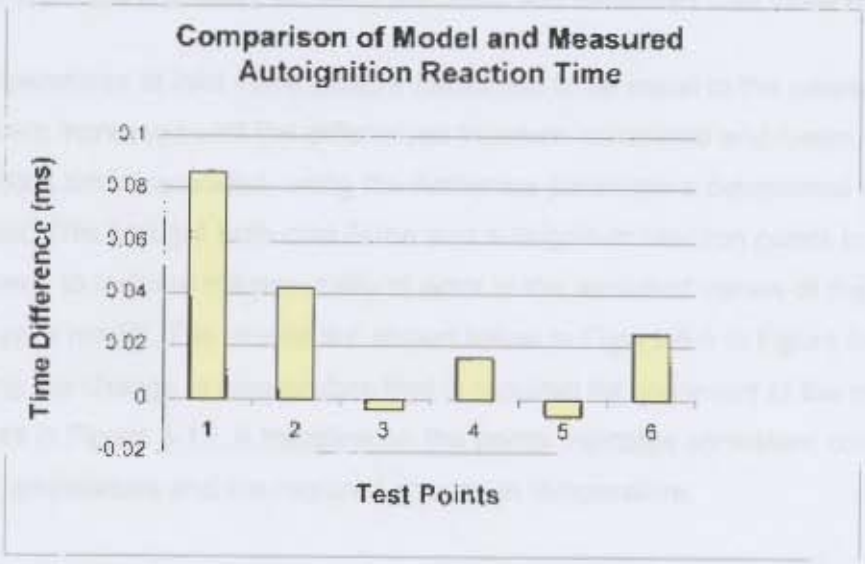

Figure 6-4: Time difference between predicted and measured autoignition reaction

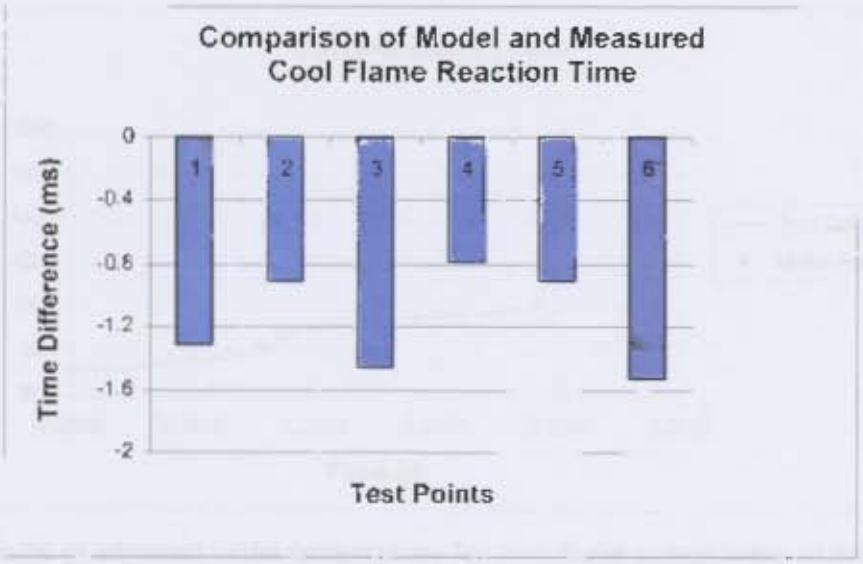

Figure 6-5: Time difference between predicted and measured cool flame reaction

The model temperatures at inlet valve closure (assumed to be equal to the measured manifold temperature) were increased until the differences between calculated and measured values of cool flame reaction times coincided, using the Arrhenius parameters determined from detailed Chemkin models. This brought both cool flame and autoignition reaction points in line in each set, which seemed to indicate the possibility of error in the assumed values of the temperature used for the engine model. The results are shown below in Figure 6-6 to Figure 6-11, as well as a graph showing the change in temperature that is required for alignment of the measured and calculated points in Figure 6-12. A trendline on the points indicates consistent correlation between initial temperature and the required change in temperature.

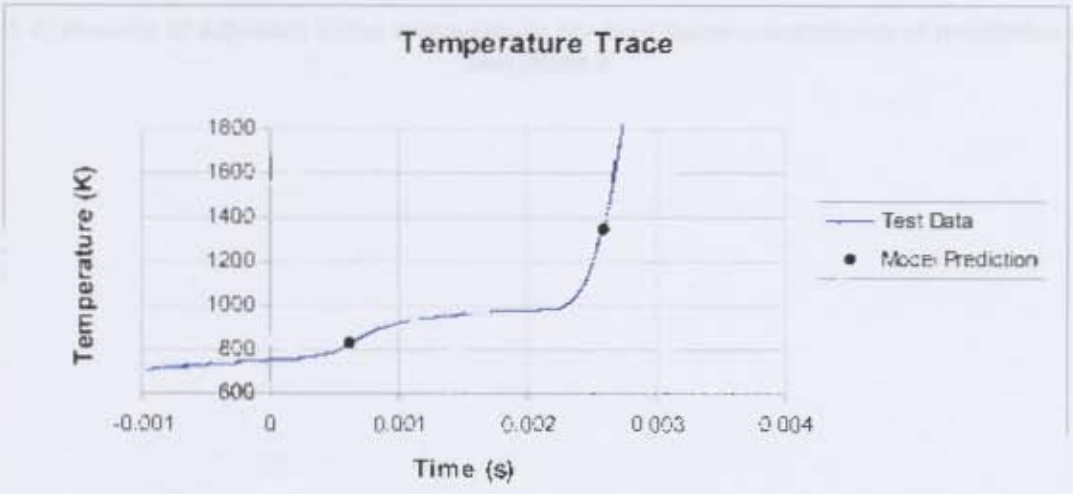

Figure 6-6: Results of adjusted initial temperature for cool flame coincidence of prediction model, test point 1

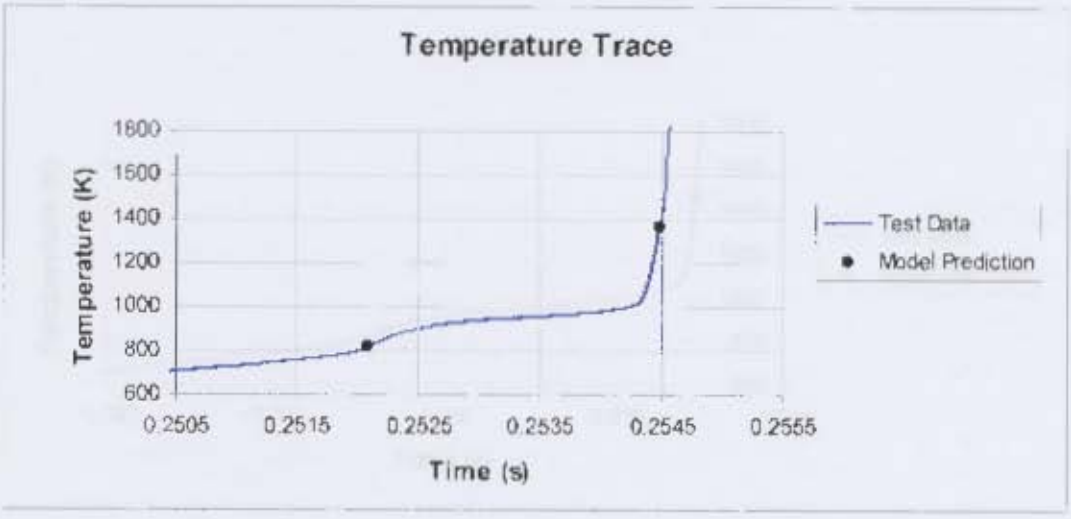

Figure 6-7: Results of adjusted initial temperature for cool flame coincidence of prediction model, test point 2

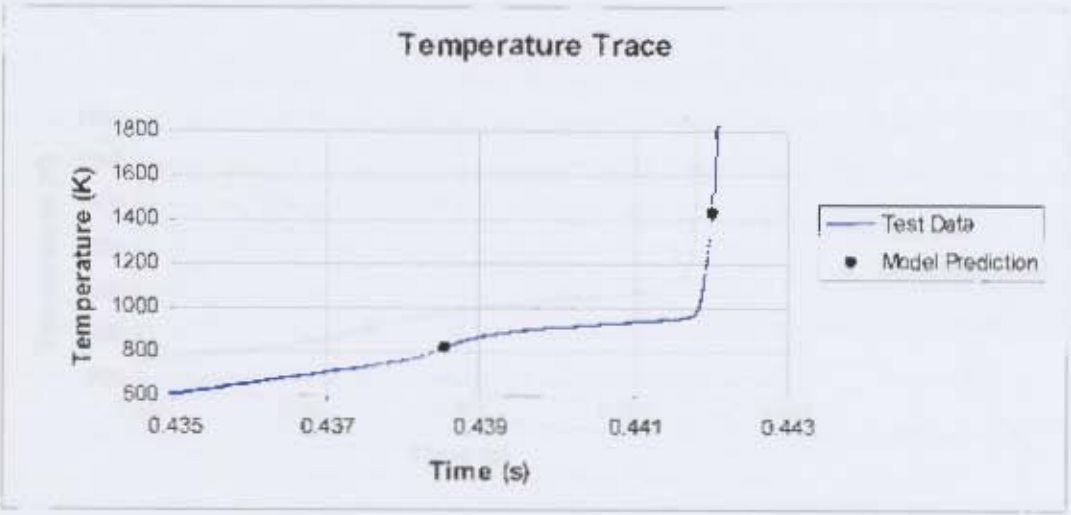

Figure 6-8: Results of adjusted initial temperature for cool flame coincidence of prediction model, test point 3

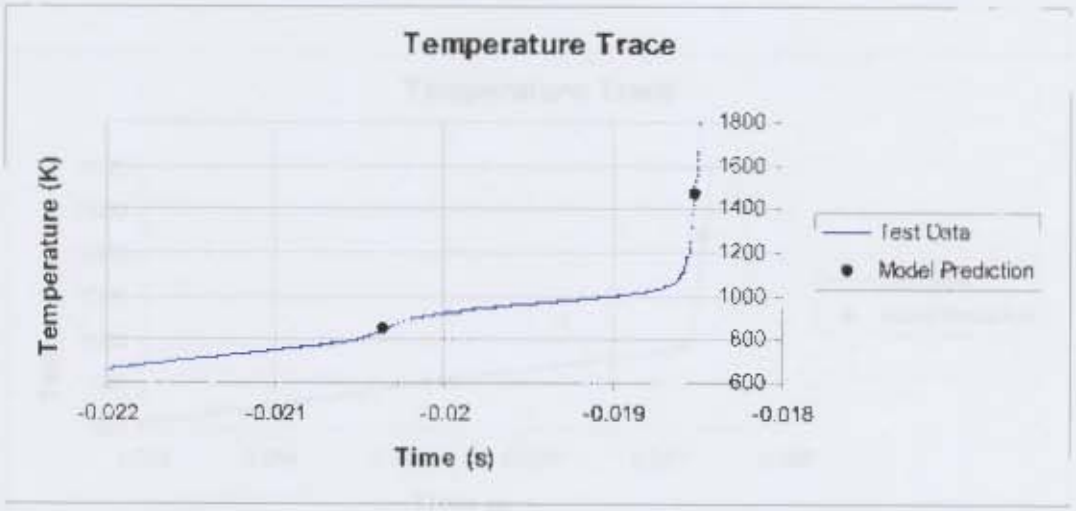

Figure 6-9: Results of adjusted initial temperature for cool flame coincidence of prediction model, test point 4

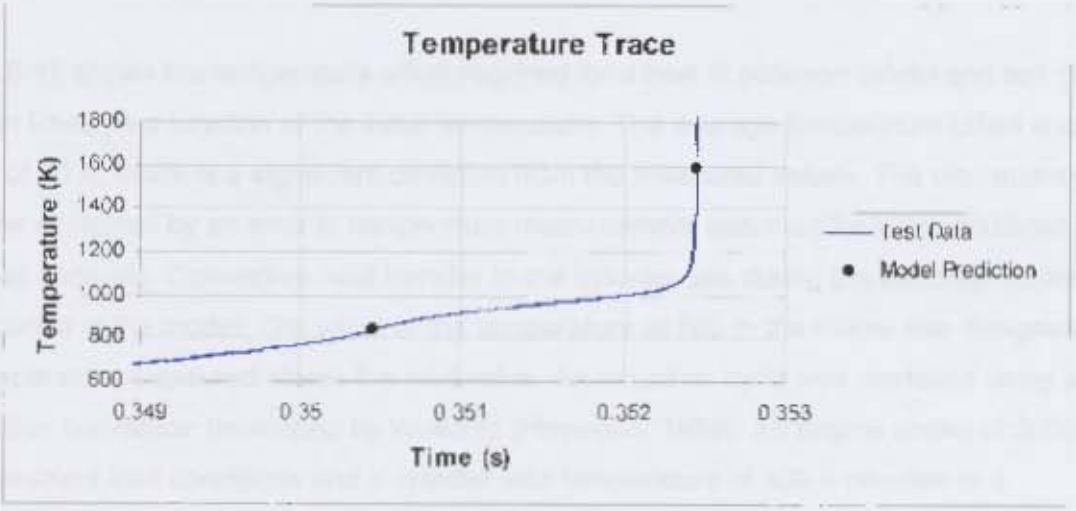

Figure 6-10: Results of adjusted initial temperature for cool flame coincidence of prediction model, test point 5

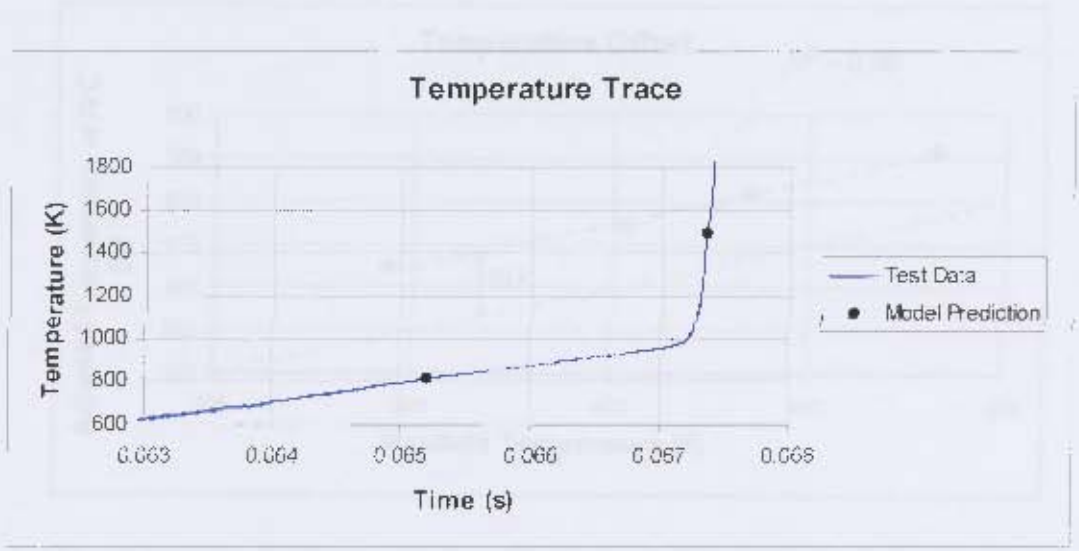

Figure 6-11: Results of adjusted initial temperature for cool flame coincidence of prediction model, test point 6

Figure 6-12 shows the temperature offset required for a best fit between model and test data reaction times as a function of the initial temperature. The average temperature offset was in the region of 70 K, which is a significant deviation from the measured values. The discrepancy could be explained by an error in temperature measurement assumed for inlet conditions at IVC or in fuel metering. Convective heat transfer to the cylinder gas during the induction stroke was not included in the model. The value of the temperature at IVC in the model was designated as the temperature measured above the inlet valve. An induction cycle was modelled using a convection correlation developed by Woschni (Heywood, 1988). An engine speed of 3000 rpm under ambient inlet conditions and a cylinder wall temperature of 400 K resulted in a temperature increase of approximately 30 K at the end of the induction stroke. This indicates that the deviation in the autoignition points could in part be attributed to the error in the assumed initial temperature at IVC as a result of this convective heating effect, as heat loss correction was not applied to the data. The discrepancy could also be attributed to fuel droplets landing on the thermocouple. This would result in readings being lower than actual manifold temperatures, which would be consistent with the findings of Figure 6-12.

Another possibility of error exists if the fuelling conditions were leaner than stoichiometric. A richer mixture would autoignite quicker, which explains the need for the inferred temperature to be increased in order for the model to coincide with the experimental data. A linear correlation further supports this observation. The fuel metering system was calibrated for a stoichiometric air-fuel ratio using a standard 95 octane fuel, which means that any systematic discrepancy in the air-fuel ratio as a result of an error in fuel metering would explain a constant error offset

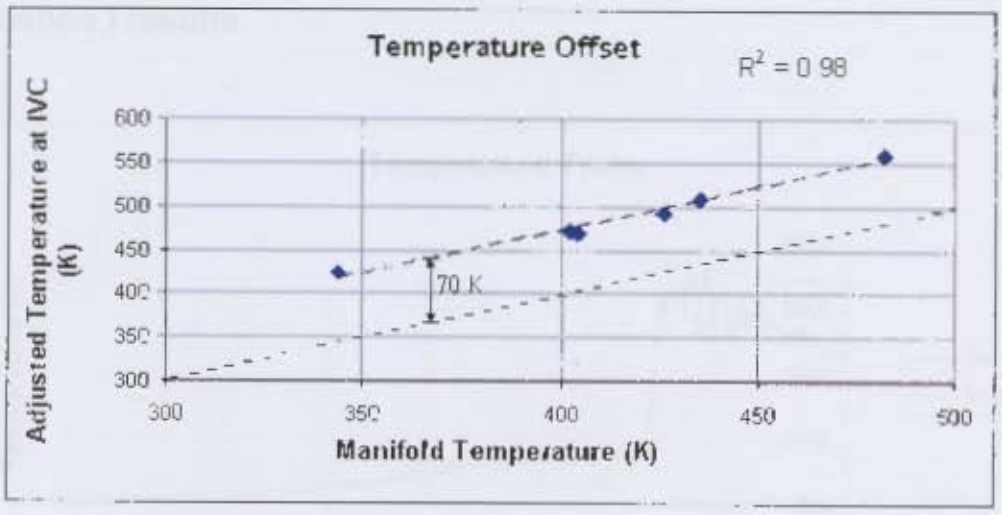

Figure 6-12: Initial temperature versus adjusted initial temperature for cool flame coincidence of prediction model

6.3 *Autoignition engine model*

Further investigation of the test data was conducted through the construction of a model trace with autoignition prediction capabilities for the purpose of correlation along with the test data traces. Two approaches were devised to obtain realistic polytropic coefficient approximations for use in the model. The first method involved the adjustment of the coefficient until the model compression trace reached the linear extrapolation of the test data temperature curve before cool flame reaction. In a similar manner, the second method involved the use of compression traces in each test occurring before the autoignition trace. A correlative equation dependant on initial temperature was then used to define the polytropic coefficient. These methods are explained in more detail in chapter 5.

6.3.1 Method I results

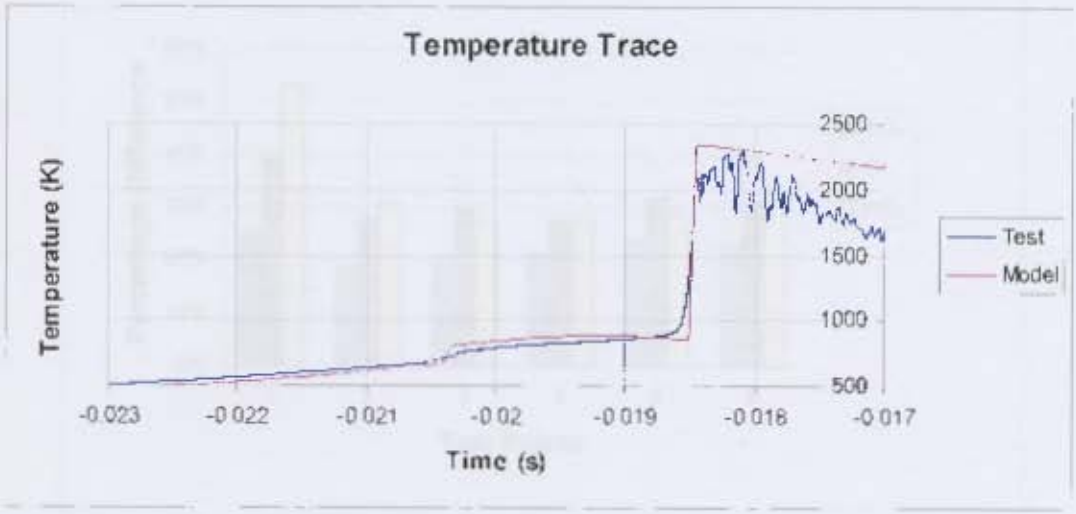

Figure 6-13: Model and test data correlation with modified Arrhenius parameters (A_1, C_1, A_2), test point 4

Figure 6-14 shows the percentage difference that each Arrhenius parameter set (A_1, C_1, A_2) would have to be modified in order for the positions of cool flame and autoignition reaction times of the model to coincide with values measured from the test data (an example of which is represented in Figure 6-13). These results were captured using a model with polytropic coefficients defined according to the first method discussed. Figure 6-14 reveals that, except for the obvious outlier being the first data set, the rest of the tests exhibit an Arrhenius set change of very similar proportions. This may again indicate deviance in temperature readings recorded from the thermocouple and the actual inlet temperature condition at IVC. In this case, the fairly consistent modification to Arrhenius values that was required indicates either a consistent error value in the temperature readings or a fuelling error, whereby the fuelling in the test cases were consistently either too rich or too lean.

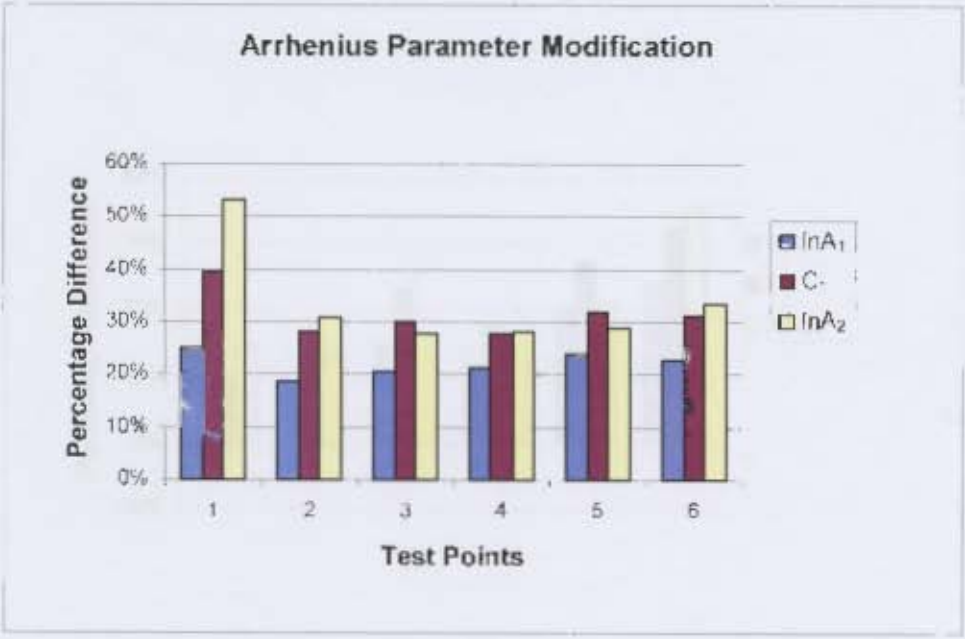

Figure 6-14: Arrhenius parameter modification required for coincidence of cool flame and autoignition reaction time; and cool flame temperature rise using polytropic coefficients derived from Method I

6.3.2 Method II results

When the second method was employed to define a model polytropic coefficient, the following results were collected as shown in Figure 6-15. The graph shows the results to be strongly temperature dependent (as the test data are arranged in two speed sets of increasing initial temperature). This is expected, as the polytropic coefficients were defined by initial temperature in the correlative equation. This may also indicate, however, the effect of radiation heat loss on the temperature readings, as the required Arrhenius parameter modification is greater when the initial temperature is higher. A higher initial temperature means higher radiation heat losses from the thermocouple, which was not shielded in the experiments.

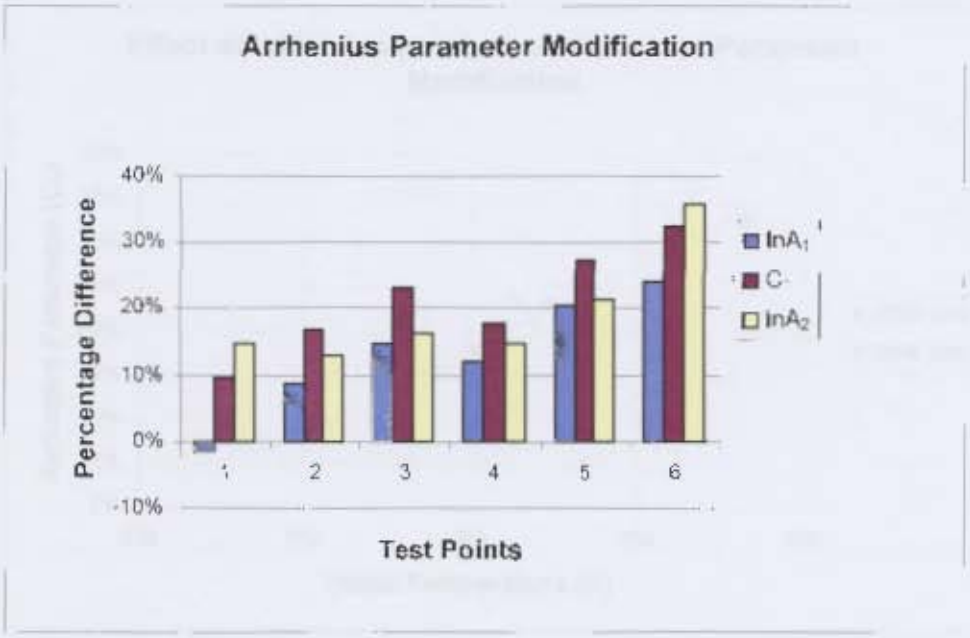

Figure 6-15: Arrhenius parameter modification required for coincidence of cool flame and autoignition reaction time, and cool flame temperature rise using polytropic coefficients derived from Method II

The following graphs, Figure 6-16 to Figure 6-18, represent plots of the modifications made to the Arrhenius parameters as a function of initial temperature, the obvious trend being that the required parameter modification increases with increased initial temperature.

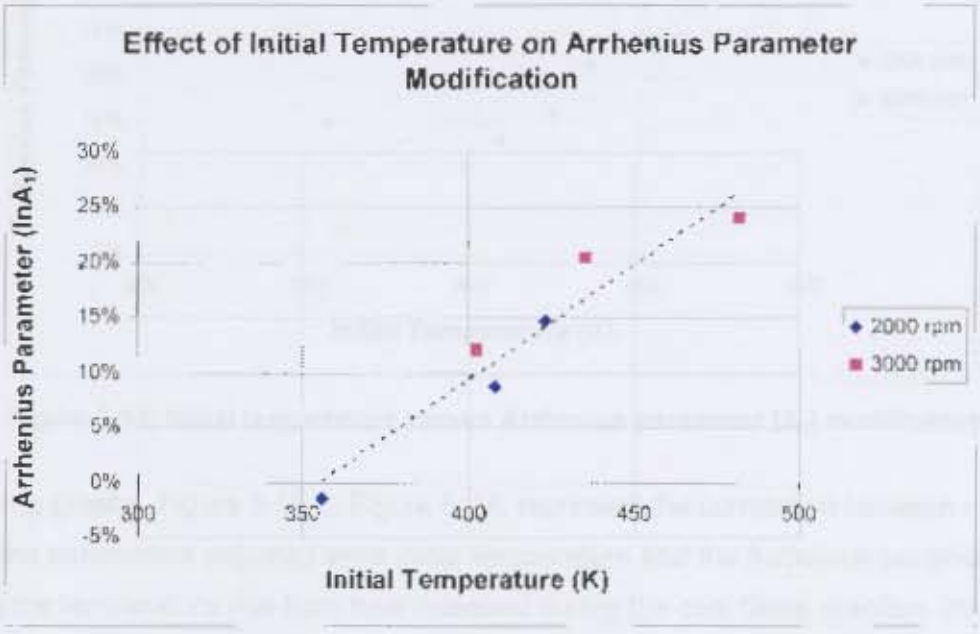

Figure 6-16: Initial temperature versus Arrhenius parameter (A_1) modification

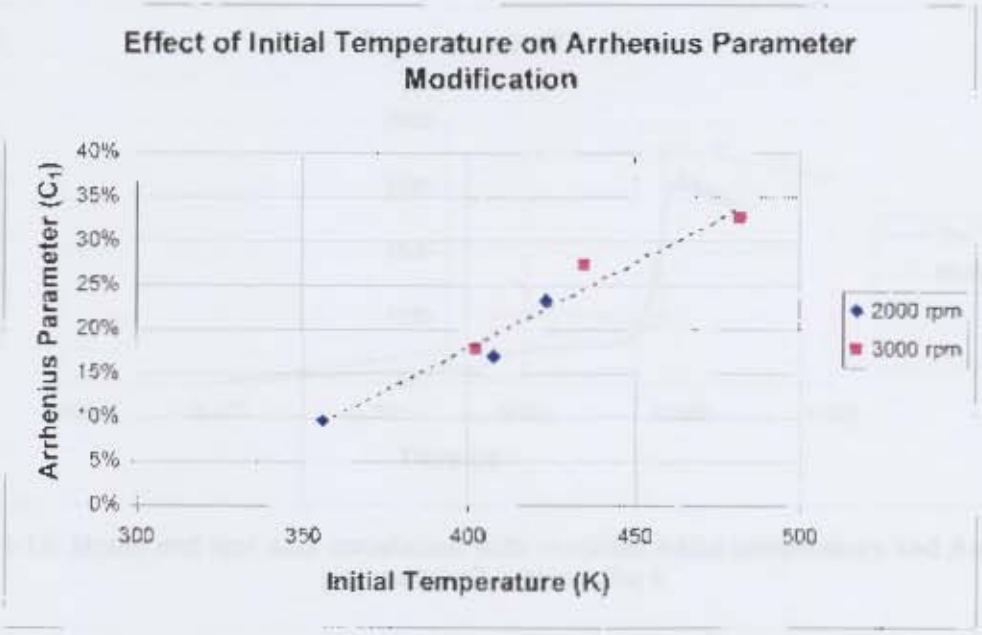

Figure 6-17: Initial temperature versus Arrhenius parameter (C_1) modification

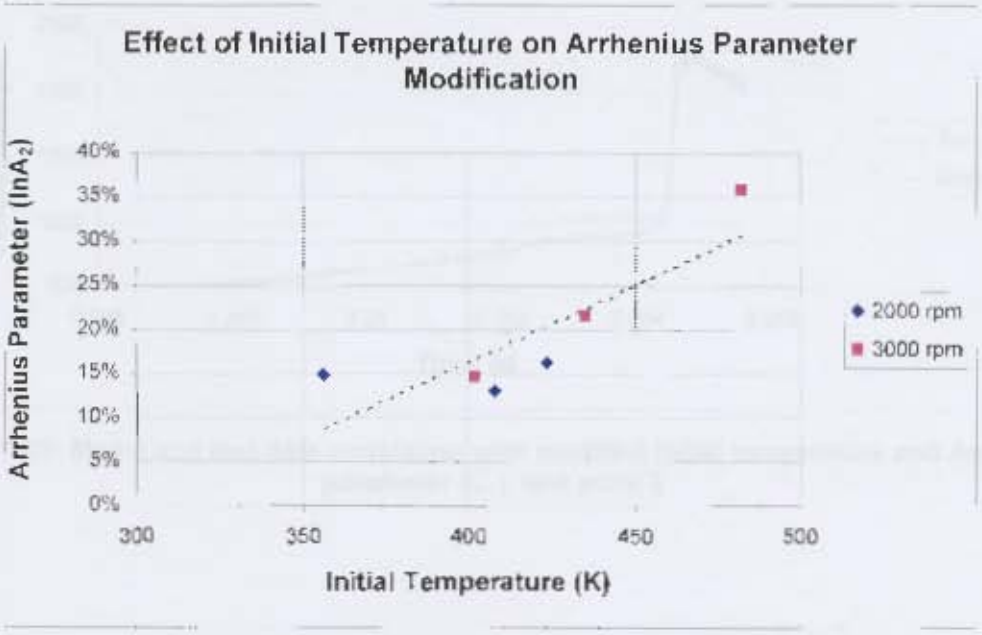

Figure 6-18: Initial temperature versus Arrhenius parameter (A_2) modification

The following graphs, Figure 6-19 to Figure 6-24, represent the correlation between model and test data; the parameters adjusted were initial temperature and the Arrhenius parameter describing the temperature rise from heat released during the cool flame reaction. Initial temperature was increased until the cool flame reaction times coincided and parameter value C_1 was adjusted until total autoignition reaction times coincided.

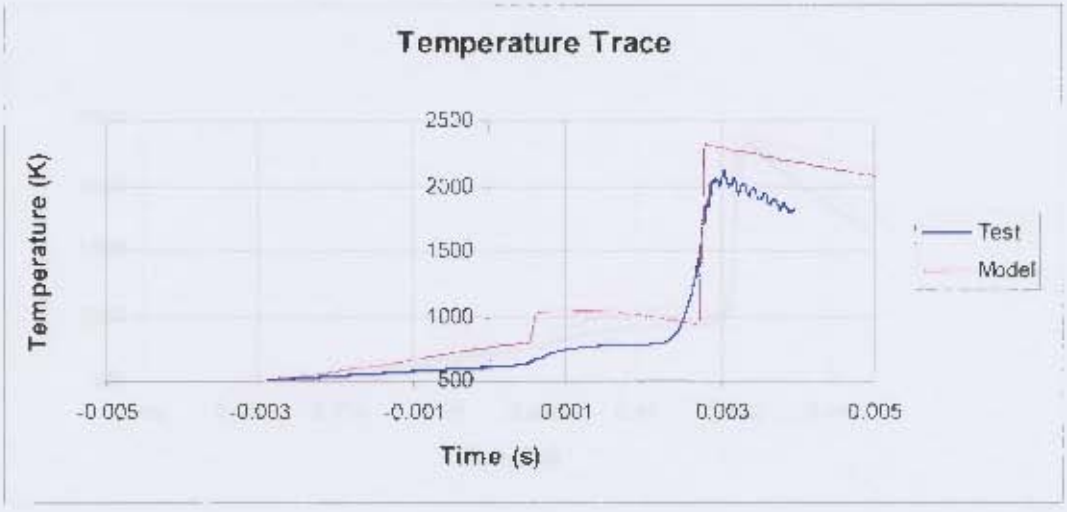

Figure 6-19: Model and test data correlation with modified initial temperature and Arrhenius parameter (C_1), test point 1

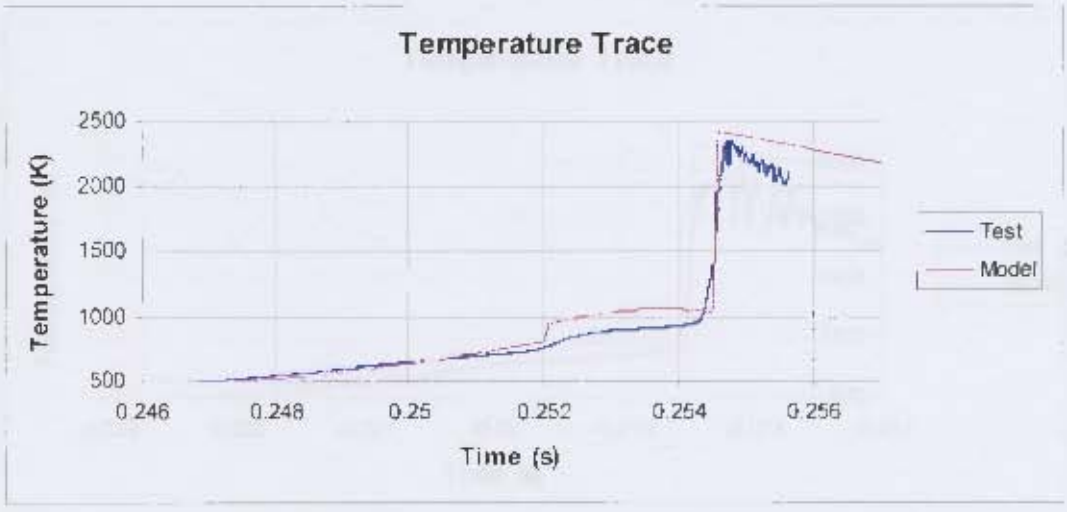

Figure 6-20: Model and test data correlation with modified initial temperature and Arrhenius parameter (C_1), test point 2

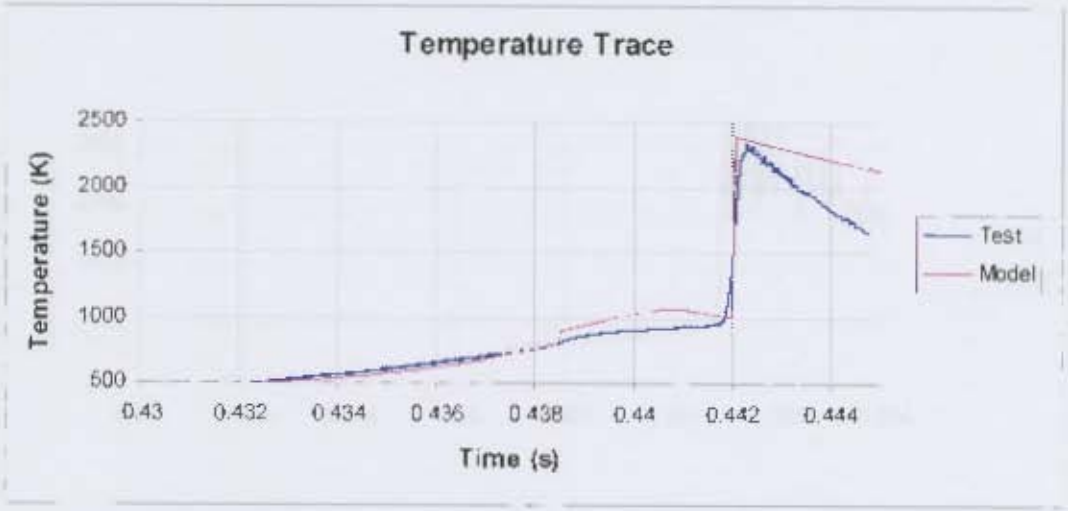

Figure 6-21: Model and test data correlation with modified initial temperature and Arrhenius parameter (C_1), test point 3

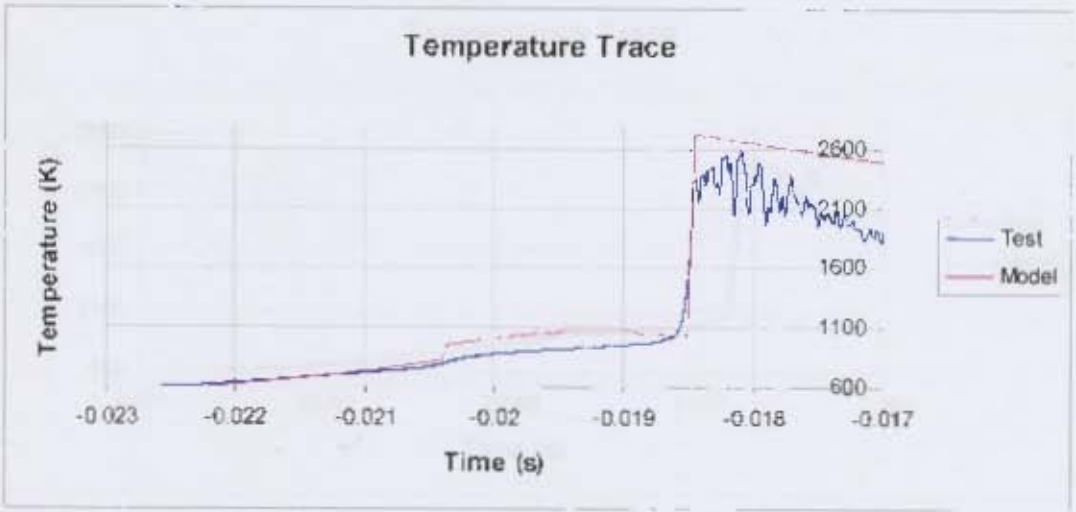

Figure 6-22: Model and test data correlation with modified initial temperature and Arrhenius parameter (C_1), test point 4

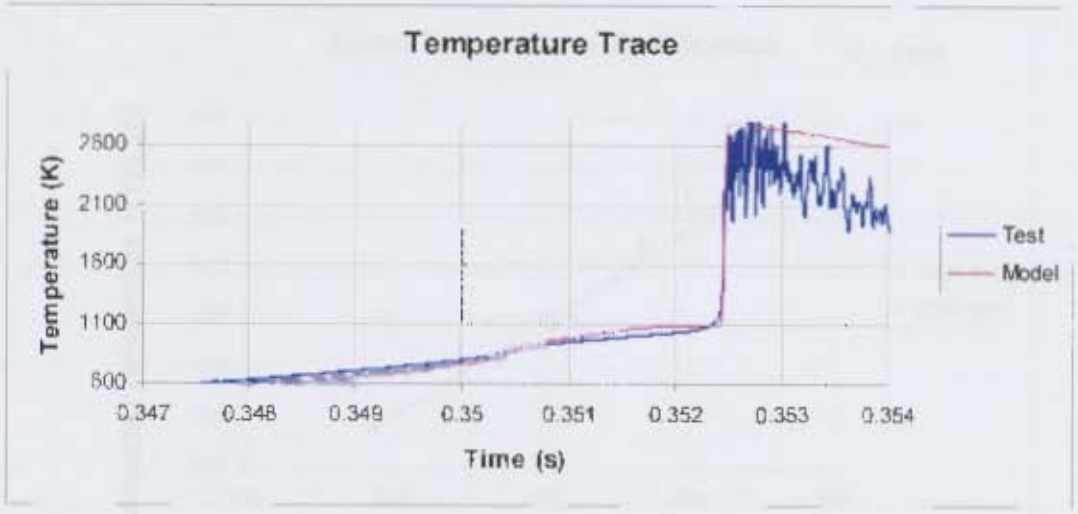

Figure 6-23: Model and test data correlation with modified initial temperature and Arrhenius parameter (C_1), test point 5

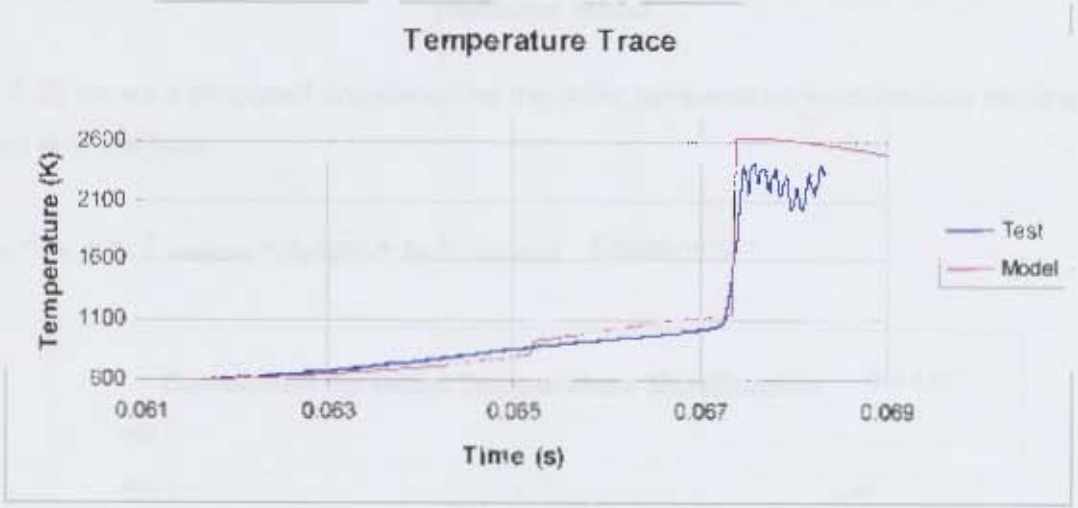

Figure 6-24: Model and test data correlation with modified initial temperature and Arrhenius parameter (C_1), test point 6

Figure 6-25 shows the modification of the initial temperature from the original value to secure correlation of the model and test traces. This graph is consistent with Figure 6-16 to Figure 6-18, which show that an increase in initial temperature results in an increase in required Arrhenius parameter modification.

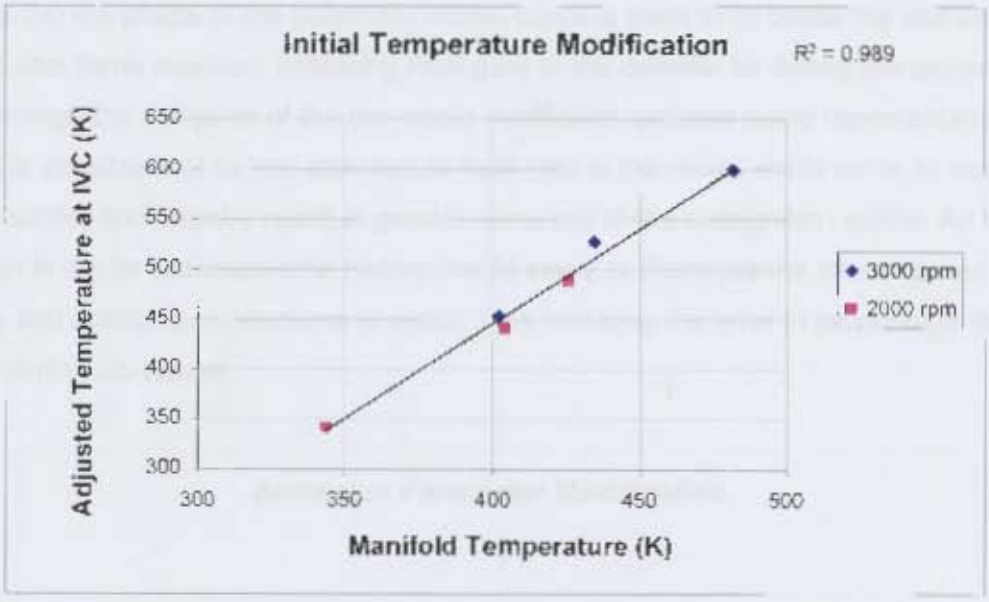

Figure 6-25: Initial temperature versus adjusted initial temperature for cool flame coincidence of prediction model

Figure 6-26 shows a proposed correlation for the initial temperature modifications required. The equation is of the form:

$$T_{i\,modified} = a_0 + a_1.T_{i\,measured} + a_2/rpm + a_3.P_{\,normalised} \quad \text{Equation 6-1}$$

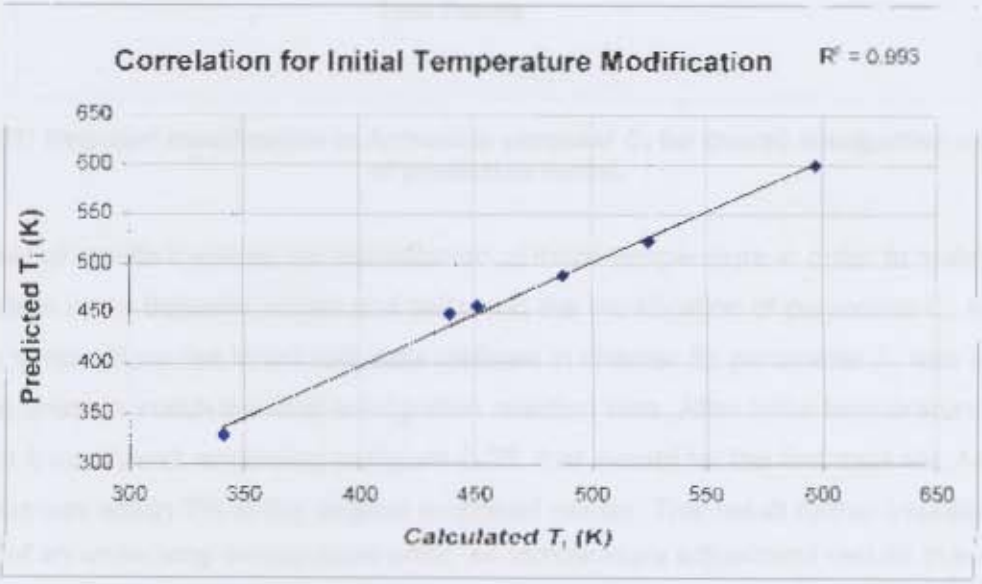

Figure 6-26: Graph showing correlation for equation developed to describe temperature adjustment for cool flame coincidence of prediction model

Figure 6-27 shows the modification of the Arrhenius parameter (C_1) from the original value to secure correlation of the model and test traces. The adjusted values caused an exaggerated cool flame reaction temperature rise in all cases. Generally, in the previous figures (Figure 6-19

to Figure 6-24) the shape of the polytropic model curve is seen to lie below the test data curve before the cool flame reaction, indicating heat gain of the cylinder air during the compression stroke. Although the definition of the polytropic coefficient included some representation of heat transfer, it is possible that further attention to heat loss in the model could serve to represent this heat transfer and thereby result in greater accuracy of the autoignition model. An increase in heat gain in the temperature-time history would serve to decrease the time required for both cool flame and autoignition reactions to occur, thus reducing the error in percentage difference to original Arrhenius values.

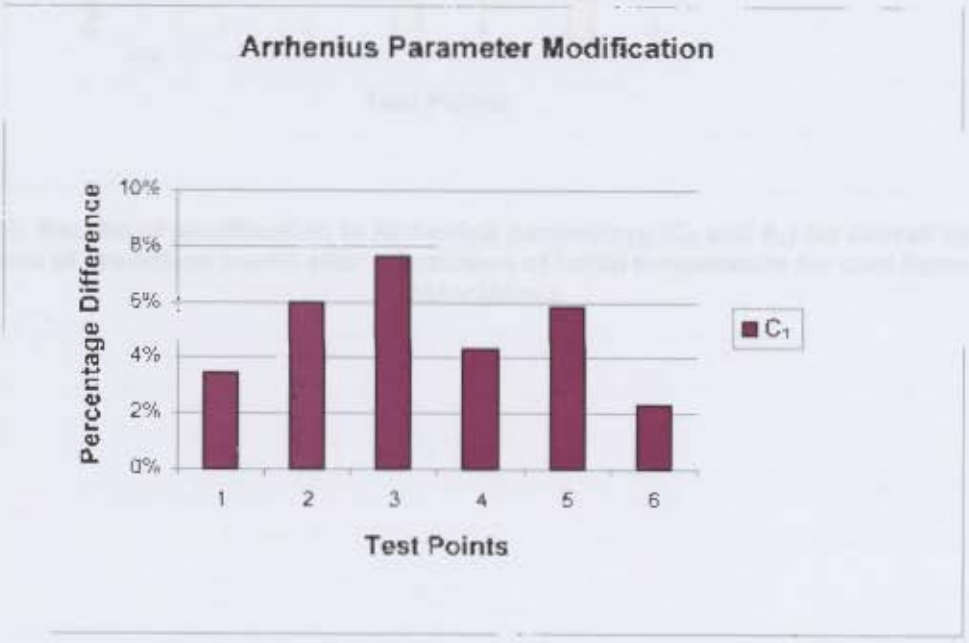

Figure 6-27: Required modification to Arrhenius parmeter C_1 for overall autoignition coincidence of prediction model.

The next set of results involved the modification of initial temperature in order to match cool flame reaction times between model and tests and the modification of parameter C_1 in order to match the temperature rise in the test data (defined in chapter 5); parameter A_2 was also modified in order to match the final autoignition reaction time. After initial temperature adjustment it was found, according to Figure 6-28, that except for the first data set, Arrhenius modification was within 7% of the original proposed values. This result further indicates the possibility of an underlying temperature error, as temperature adjustment results in a smaller error range of Arrhenius parameter differences.

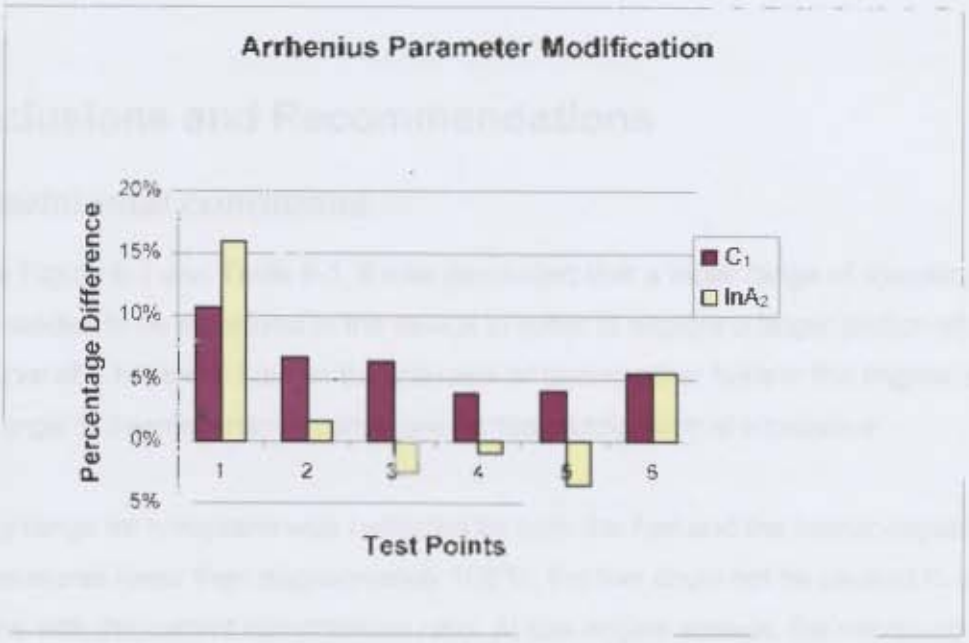

Figure 6-28: Results of modification to Arrhenius parameters (C_1 and A_2) for overall autoignition coincidence of prediction model after adjustment of initial temperature for cool flame reaction coincidence

7 Conclusions and Recommendations

7.1 Experimental conditions

Referring to Figure 6-1 and Table 6-1, it was concluded that a wider range of operating conditions needed to be employed in the device in order to explore a larger portion of the isodelay curve of n-heptane. Also, in the interests of testing other fuels in the engine, a larger operating range of thermodynamic conditions for fuel autoignition is imperative.

The heating range for n-heptane was restricted by both the fuel and the heater capabilities. At initial temperatures lower than approximately 100^{0}C, the fuel could not be caused to autoignite in the engine with the current compression ratio. At low engine speeds, the maximum usage of the heater was also limited. At speeds beyond 3000 rpm the heater's maximum temperature was not restricted, but for lower engine speeds, where air flow over the heater was less, care had to be taken that the surface temperature of the heater did not exceed 600 ^{0}C or damage to the ceramic sheath would occur. Since the heater control device was not fast-acting enough for limiting the temperature, the maximum power usage of the heater was limited manually, perhaps too safely below the maximum operating temperature of the heater. A recommendation therefore would be the inclusion of a fast-acting control device that would enable the operator to increase the initial temperature in the lower engine speed experiments.

Another experimental restriction was on the lower speed operation of the engine, which was 2000 rpm. The engine could not be accurately calibrated due to the generator not being able to operate effectively for load control below this speed. A lower engine speed would allow more time for the autoignition of the fuel over the compression cycle. This would therefore allow for operation of the engine at lower initial temperatures, and thus would also allow an extension of the operable range in the lower temperature regions of the isodelay curve.

Greater variability in engine operation could also be achieved through the variation of the compression ratio without having to extend the capabilities of the heater. It was initially intended that a wide variety of fuels would be tested for the commissioning of the device by using different compression ratios. Changing of the compression ratio would be achieved by using spacers on the cylinder block after the machining of the cylinder head to its minimum allowable thickness. This method would only allow one compression ratio to be experimented with at a time, where a more desirable feature would be the variability of the compression ratio during

engine operation. Greater variability in engine operation could also be achieved through supercharging the inlet.

7.2 Ignition delay characterisation

From a previous discussion of Figure 6-2 the NTC region proves difficult to characterise as a small shift in any direction results in the region being missed, despite attempts to raise the temperature in small increments. Possibly the best method to reach the NTC region would be to use a variable compression ratio test engine; this would allow for controlled incremental variation of thermodynamic properties without having to be concerned with controlling thermodynamic equilibrium of the inlet air through modification of inlet pressure as in the experiments undertaken.

7.3 Experimental results from direct modelling

Results from modelling the test data with an Arrhenius based autoignition prediction model indicated good correlation of overall autoignition when applied directly to the engine thermodynamic test data. Correlation with cool flame reaction times was improved significantly by artificially increasing initial temperature values. The increase of initial temperature did not adversely affect overall autoignition times, which seemed to indicate that the points were close to the confines of the NTC region (where overall ignition delay becomes independent of initial temperature). It was interesting to observe that the increment of the temperature increase for correlation was similar in all cases, indicating a constant offset of error. From these results, it was concluded that either an error in the equivalence ratio of the test mixture or an error in temperature measurement existed from the experiments (or both). A discrepancy could be explained by an error in the temperature measurement assumed for inlet conditions at IVC, which was consequently incorporated in the model. It was discussed that the deviation in the autoignition results could in part be attributed in part to the convective heating effect of the cylinder gases during the induction stroke. An induction model could be used to adjust the measured temperature at the inlet valve. Another explanation given was that fuel spray droplets landing on the thermocouple would explain the discrepancy in the measured to expected manifold temperatures.

Temperature measurement was calibrated from a signal largely isolated from the electronic noise source, although it is possible that aerial transmission of electronic noise affected the temperature readout of the calibration device. It is therefore in the best interests of further usage of the test device to calibrate the initial temperature signal under varying inlet conditions where

no noise is present or where the calibration device is ensured against picking up a transmitted noise signal.

The errors involved in the reaction time correlation could also be explained as a result of metering an equivalence ratio that was different from a stoichiometric fuel mixture. Calibration for stoichiometry was performed for a 95 octane commercial fuel, but autoignition tests were performed on n-heptane and with a different fuel injector, as the original injector flow rate was concluded to result in too rich a mixture for autoignition. Any deviation in metering would therefore be a constant offset of equivalence ratio, which would seem to explain the similar amount of modification required for correlation with the stoichiometric autoignition model. It would therefore be advisable to retest the fuel metering system. Preferably, the fuel to be tested should be calibrated to stoichiometry. This would require testing to occur either under firing or autoignition HCCI conditions. Occurrence of damage to the piezoelectric pressure transducer is possible if the autoignition conditions are not controlled. This is why this method was not attempted in this project. Another possible method includes calibrating the test fuel metering under firing conditions, which implies the use of a test engine with variable compression ratio. Feedback for calibration would be achieved by the use of an oxygen sensor in the exhaust stream.

7.4 Experimental results from indirect modelling

Results from the modelling of the autoignition traces were presented according to two methods, which described the definition of a model polytropic coefficient. Results using the first method led to conclusions very similar to those proposed from direct analysis of the data. Direct data analysis using the new Arrhenius model and initial temperature modification led to a conclusion of experimental errors existing in either temperature measurement or fuel metering or both. Modification of Arrhenius parameters in the second set required for correlation of the model was very similar in most cases, which led to the conclusion that a constant error offset must be present in either fuelling or temperature measurement. Results from the model using a polytropic coefficient defined by the second method gave a slightly different indication. Modification to Arrhenius parameters required for correlation was strongly temperature dependent, with increased error difference with a required increase in initial temperature. This led to the conclusion that if a temperature measuring error exists, it may be due to radiation heat loss from the thermocouple, as the thermocouple used was not shielded against radiation. A recommendation therefore would be to use a shielded thermocouple and to improve insulation at the inlet valve in order to prevent heat loss.

7.5 Further work

A summary of recommendations for further work include:

1. A greater range of operating conditions is required for testing other fuels. This invariably implies the use of different compression ratios of the engine to reach thermodynamic conditions capable of causing the higher octane fuels to autoignite. With the current setup, changing the compression ratio on the engine is a large undertaking if many iterations are required. The best approach would be either to modify the current engine for compression ratio variability during engine operation, or the use of an already existing variable compression ratio test engine.
2. To increase the range of experimental conditions, it is recommended that a system be investigated that will allow tests to be run at lower speeds than those limited by the generator operation. A DC motor regenerative drive system would be more effective in controlling speed, as well as load, in a dynamometer setup, rather than one where separate elements are required to control these aspects. A system that would completely eliminate any generation of noise would doubtlessly avoid many unnecessary signal cleaning and precautions that may have compromised an easier attainment of data in this project.
3. A heater controller with greater capabilities than the one in current use would be necessary if the engine were to run at lower engine speeds. Another option would be the use of a cartridge heater with capabilities of use at lower flow rates. It is recommended that if the current setup is used, the thermocouples installed should be shielded. This will allow for correct readings at the heater outlet and inlet valve, where the effect of radiation is most prominent. In addition, calibration of the thermocouples should be performed with a meter that will not be affected by noise transmission as a result of motor controller operation.
4. The problem of calibration of the fuelling system proved to be more complicated an undertaking than originally foreseen. Each fuel needs to be calibrated separately for reliable results to be acquired. This may only be possible with a variable compression ratio engine, where the fuel may be calibrated under autoignition and not under firing conditions. The best method would be through obtaining results where the equivalence ratio could be certified through negative feedback from an oxygen sensor in the exhaust stream. Care obviously would have to be taken that transducers under these conditions would not be damaged.

8 Bibliography

Agarwal A., Assanis N. (1997) *Modelling the Effect of Natural Gas Composition on Ignition Delay Under Compression Ignition Conditions*, SAE Technical Paper, No. 971711

ASTM Method D2699-01a (2003) *Standard Test Method for Research Octane Number of Spark-Ignition Engine Fuel*

ASTM Method D2700 (2003) *Standard Test Method for Motor Octane Number of Spark-Ignition Engine Fuel*

Bradley D., Morley C. (1997) *Autoignition in Spark-Ignition Engines*, Comprehensive Chemical Kinetics, Vol. 35, Ch. 7, Elsevier

Cengal Y. A. and Boles, A. B (1994) *Thermodynamics – An Engineering Approach*, International Ed. McGraw Hill, London

Chapman, A. J (1967) *Heat Transfer*, Macmillan, New York

Douaud A. M., Eyzat P. (1978) *Four Octane Number Method for Predicting the Anti-Knock Behaviour of Fuels and Engines*, SAE Technical Paper, No. 780080.

Fish A. et al. (1969) *The Controlling Role of Cool Flames in Two-Stage Ignition*, Combustion & Flame, 13.

Griffiths J. F. et al. (1997) *Spontaneous Ignition Delays as a Diagnostic of the Propensity of Alkanes to Cause Engine Knock*, Combustion & Flame, 111: 327-337.

Griffiths J. F., Mohamed C. (1997) *Experimental and Numerical Studies of Oxidation Chemistry and Spontaneous Ignition Phenomena*, Comprehensive Chemical Kinetics, Vol. 35, Ch. 6, Elsevier

Heywood J. B. (1988) *Internal Combustion Engine Fundamentals*, International Ed. McGraw Hill, London, p371-478

Hughes E and Boles, A. B (1994) *Hughes – Electrical Technology*, Longman, Singapore

Koert D. N. et al. (1994) *Experimental Studies of Propane Oxidation through the Negative Temperature Coefficient Region at 10 and 15 Atmospheres*, Combustion & Flame, 96: 34-49.

Lenhert, D. B. (2003) *The Oxidation of an ISF Surrogate and Its Components in the Negative Temperature Coefficient Region*, 3rd Joint Meeting of the U.S. Sections of the Combustion Institute, Session Name: RIC Engines III, Paper Number: B16

Leppard W. R. (1987) *The Autoignition Chemistry of n-Butane: An Experimental Study*, SAE Technical Paper, No. 872150

Leppard W. R. (1988) *The Autoignition Chemistry of Isobutane: A Motored Engine Study*, SAE Technical Paper, No. 881606

Leppard W. R. (1990) *The Origin of Fuel Octane Sensitivity*, SAE Technical Paper, No. 902137

Livengood J. C., Wu P. C. (1955) Correlation *of Autoignition Phenomena in Internal Combustion Engines and Rapid Compression Machines*, 5th Symp (Intl) on Combustion, p347-356.

Rifkin E. B., Walcutt C. (1957) *A Basis for Understanding Anti-Knock Action*, Trans SAE, Vol 65, p552-566

Siebers D. L. (1985) *Ignition Delay Characteristics of Alternative Diesel Fuels: Implications on Cetane Number*, SAE Technical Paper, No. 9852102

Swarts A (2006) *Insights Relating to Octane Rating and the Underlying Rate of Autoignition*, PhD Thesis, University of Cape Town

Tanaka S. et al. (2003) *Two-Stage Ignition in HCCI Combustion and HCCI Control by Fuels and Additives*, Combustion & Flame, 132: 219-239.

Viljoen C.L. et al. (2005) *An Investigation of the Ignition Delay Character of Different Fuel Components and an assessment of Various Autoignition Modelling Approaches*, SAE Technical Paper, No. 2005-01-2084.

Walker R. W., Morley C. (1997) *Basic Chemistry of Combustion*, Comprehensive Chemical Kinetics, Vol. 35, Ch. 1, Elsevier

Warnatz J. (2000) *Hydrocarbon Oxidation High-Temperature Chemistry*, Pure Appl. Chem., Vol. 72, No. 11, pp.2101-2110, 2000.

Westbrook C. K. (2000) *Chemical Kinetics of Hydrocarbon Ignition in Practical Combustion Systems*, Proc. Comb. Inst., Vol 28, 1563-78.

Yates A. et al. (2007) *An Accurate Determination of the Cetane Number of Sasol GTL Diesel*, SAE Technical Paper, No. 2007-01-0026

Yates A., Swarts A. (2004) *In-Cylinder Fuel Evaporation and Heat Transfer Information Inferred from the Polytropic Character of the Compression Stroke in a Spark-Ignition Engine*, SAE Technical Paper, No. 2004-01-1856

Yates A., Swarts A., Viljoen C. L. (2005) *Correlating Auto-Ignition and Knock-Limited Spark-Advance Data for Different Types of Fuel*, SAE Technical Paper, No. 2005-01-2083

Appendix A Dynamometer Setup

A.1 Engine specification

A Briggs and Stratton engine-generator unit was provided by the Sasol Advanced Fuels Laboratory for the research project. The engine had previously been used for valve deposit tests for a range of fuels and fuel additives.

Table A-1: Engine specifications

Hardware	215cc, 7 hp overhead valve 4-stroke engine
Model	138432 (OHV)
Company	Briggs and Stratton Corp.

Table A-2: Engine mechanical specifications

Displaced volume	215 cc
Power rating	7.5 hp
Crank throw	26 mm
Conrod length	90 mm
Cylinder bore	72 mm
Compression ratio	8.5
Valve diameter	24 mm
Maximum valve lift	5.5 mm
Inlet valve opening angle	17^0 BTDC
Inlet valve closing angle	225^0 ATDC
Exhaust valve opening angle	135^0 ATDC
Exhaust valve closing angle	17^0 BTDC

Figure A-1: Engine maximum power curve

Figure A-2: Engine maximum torque curve

A.2 Generator specification

The coupled generator was used to load the engine during testing. The unloaded potential difference produced for different motored speeds of the generator is recorded in Figure A-3. From experimentation it was deduced that the minimum usable engine speed for loading purposes was 1800 rpm (including the effect of hysteresis which is not shown on the graph). Constant loading of the engine (and thus

speed control) was required for fuelling calibration under engine firing conditions whereas for the actual autoignition tests loading was only required to prevent "runaway" of the engine once the fuel had begun to autoignite.

Table A-3: Generator specifications

Hardware	Single-phase synchronous brushless alternator
Model	ES100 D
Company	NSM
Voltage	230V at 50 Hz (3000 rpm)
Current	13 A

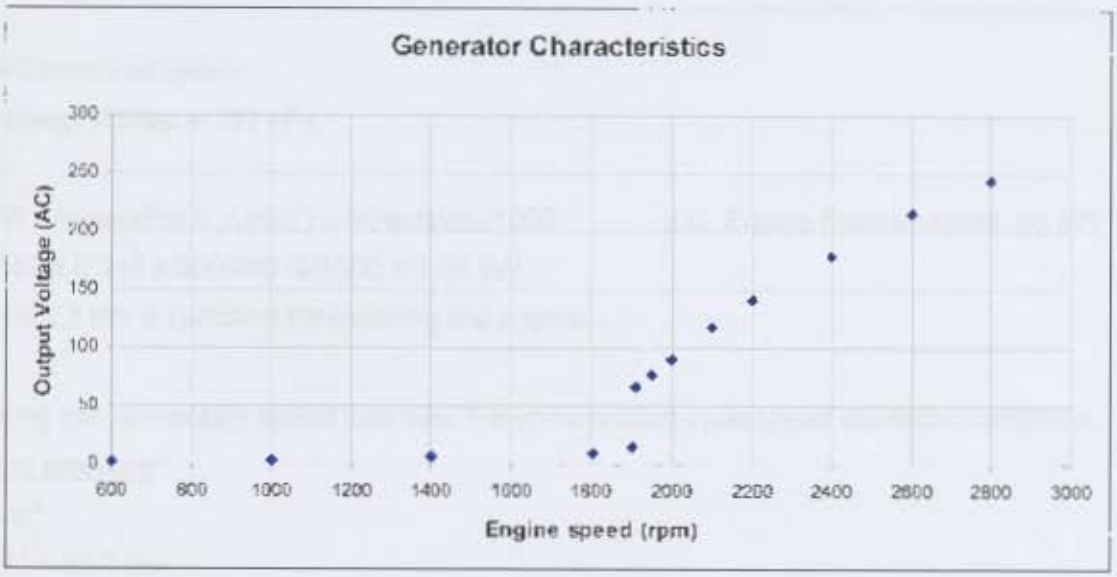

Figure A-3: Generator voltage output at varied engine speed

A.3 Motor specification

A separate driving element was required for motoring the engine at set speeds. A 2.2 kW AC asynchronous induction motor with a variable speed inverter controller was used.
The desired engine operating parameters under motored conditions included:

1. The option of increasing compression ratio up to 20:1
2. Maximum engine speed of 3000 rpm

Theoretically, the net work done in a motoring cycle for compression and expansion of the gases (excluding pumping losses and friction) is zero units. Equations were used from Cengal A. Y. and Boles, A. B; Thermodynamics – An Engineering Approach (1994) and Heywood J. B; Internal Combustion Engine Fundamentals (1988).

bmep (brake) = imep (indicated) – tfmep (total friction) (I.C. Engine Fundamentals, pg 715)

tfmep (bar) = $0.97 + 0.15(N/1000) + 0.05(N/1000)^2$ (I.C. Engine Fundamentals, pg 722)

tfmep = 1.87 bar (using fired engine approximation at maximum 3000 rpm)

bmep = 0 (motored cycle)

imep = bmep + tfmep = 187 kPa

$P_{total}(kW) = imep(kPa) \times V_d(dm^3) \times N(rev/s)/n_R/1000$ (I.C. Engine Fundamentals, pg 50)

$P_{total} = 187 \times 0.215 \times 3000/60 /2/1000 = 1.01$ kW

Therefore 2.2 kW is sufficient for motoring the engine.

Calculating the momentary speed loss over the compression cycle under adiabatic conditions...

Maximum pressure

$P_2/P_1 = cr^{\alpha}$

$P_2 = 20^{1.4} = 66.3$ bar

Maximum temperature

$T_2 = (P_2/P_1)^{\alpha-1/\alpha} .T_1$

$T_2 = 994$ K

Required power at 3000 rpm

3000 rpm... $6.3(10)^{-3}$ kg/s (air)

$W_c (kW) = mC_{v(av)}\Delta T$

C_v at 650 K (average temp) = 0.776

$W_c = 6.3(10)^{-3} \times 0.776 \times (994 - 300) = 3.4$ kW

Difference = 3.4 – 2.2 = 1.2 kW

Energy from flywheel

For the 200mm diameter, 3 kg flywheel:

$E_k = \frac{1}{2} I (\omega_{22} - \omega_{12})$, $I = \frac{1}{2} m r^2$

The power required over the compression cycle for a compression ratio of 20:1 results in a deceleration in engine speed by 7 rpm converted from the energy "stored" in the flywheel. The motor is sufficient to maintain the engine speed over the other cycles.

Table A-4: Motor specifications

Hardware	3-phase induction motor
Model	LS100L T
Company	Leroy Somer
Power rating	2.2 kW
Synchronous speed	1425 rpm

A.1.1 Motor controller

The motor controller used was a 2.2 kW Digidrive Inverter which generated the 3-phase frequency for governing the speed of the motor. The motor operated at 50 Hz brought the engine over 3000 rpm.

Table A-5: Motor controller specifications

Hardware	Variable speed inverter drive
Model	SE2D200220
Company	Leroy Somer
Power rating	2.2kW

A.1.2 Pulley specification

The synchronous speed of the motor is 1425 rpm while the design maximum motoring speed is 3000 rpm. Thus the speeding up ratio required for the belt drive is 1425/3000 = 0.48:1. A 95 mm diameter aluminium pulley was used, mounted on a transmission hub which was located centrally on the engine flywheel. A 200 mm diameter taper lock pulley was specified for the motor shaft.

A.1.3 Belt specification

Calculations taken from specification catalogue for "Wraxall belts and pulleys catalogue"

Load factor

Light duty (compressor), no idler, speeding up, 10 hrs and under operation...

(1+0.1) x 1.25 x 1 x 2.2 kW = 2.75 kW (Table F6)

Belt type

3000 rpm and 2.75 kW... 90 x 1 SPA (Table F7)

Speed ratio

3000/1440 = 2.08... F52, sr = 2.1

driven d = 95 mm, driver D = 200 mm... 4.6 kW (1 belt)

Max bore (driver/driven)... 28/50

Centre distance, belt length

C = 2 x sqrt [(D+d) x d] = 335 mm

L = 2C + (D-d)2 /4C + 1.57 (D+d) = 1141 mm

Power rating

3000 rpm and d = 95 mm... 3.55 kW / belt (Table F12)

Additional power rating

For sr = 2.1 and 3000 rpm increase... 1.17 kW/ belt (Table F13)

Power correction factor

SPA and L = 1120 (1141)... 0.88 (Table F8)

Arc of contact

(D-d)/C = 0.31...163° wrap angle and 0.96 correction (Table F8)

Power calculation

(3.55+1.17) x 0.88 x 0.96 = 3.99...4

No of belts

4/2.75 = 1.4... 1 belt required (90 x1 SPA), standard belt length = 1180 mm

A.4 Dynamometer frame

The frame was welded together from 1.5 mm mild steel rectangular and square tubing. The motor was located underneath the engine and mounted on pivoting arms, its weight being used to tension the belt. The single-cylinder engine produced significant vibration when run at speeds of 1000 and 2000 rpm.

The vibration was reduced at these speeds by clamping the frame to the test cell rail (and not on rubber mounts as previously supported). This helped to stiffen the overall spring constant and thereby dampen the vibration significantly.

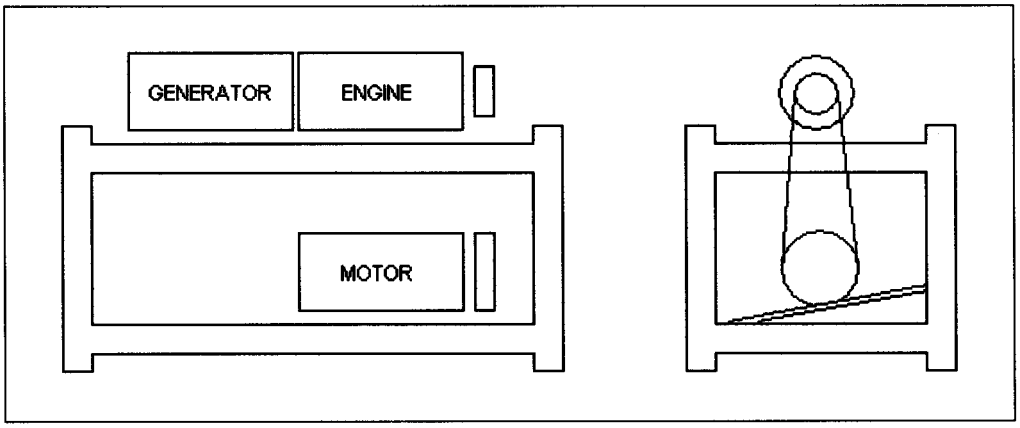

Figure A-4: Dynamometer setup schematic

A.5 Load control system

A resistor bank was constructed for converting the power generated by the engine under firing conditions into waste heat. The maximum power produced by the engine is 6 kW. The 8 kW resistor bank consisted of 4 2kW elements (25 Ω each) which were mounted in the extractor system air stream for heat removal and as a safety precaution. A 10 kW (maximum power output) dimmer was purchased to control the power shedding and thus speed of the engine under fired and autoignition conditions. The system enabled speed control under fired conditions for fuel calibration purposes and speed limiting control under autoignition conditions of the engine.

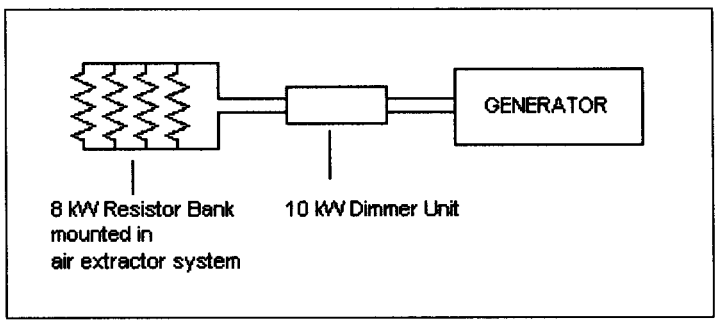

Figure A-5: Load shedding system schematic

Appendix B Inlet Manifold Design Modifications

In order to meet the requirements for varying and measuring inlet conditions, the air inlet system of the engine needed to be modified and the following components incorporated:

1. Air-mass meter (feedback to the fuel metering control unit)
2. Inlet air throttle device (experimental control of inlet air pressure)
3. Air plenum (dampening pulsations from single cylinder induction for pressure measurement in the air inlet)
4. Inline air heater (experimental control of inlet air temperature)
5. Fuel injector (experimental control of fuelling) with water cooling facility.

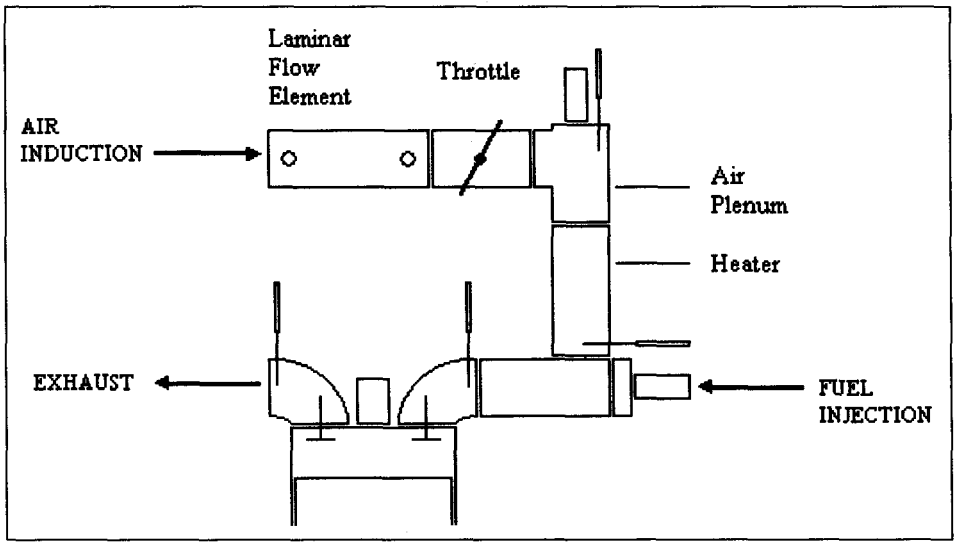

Figure B-1: Inlet manifold modification schematic

B.1 Air plenum

The induction stroke in a 4–stroke engine occurs once every two revolutions of the engine, resulting in one induction pulse in a single cylinder engine. The purpose of the air plenum was to reduce pulsation so that the pressure sensor readings would not fluctuate. The combined effect of an increased volume and surface area from the inlet tube to the plenum through tapering of the pipe was designed to buffer this pulsation effect.

Volume = $(\pi D^2/4).L = \pi \times (80)^2 \times 120/4 = 603$ cc (approx. 3 times the swept volume)

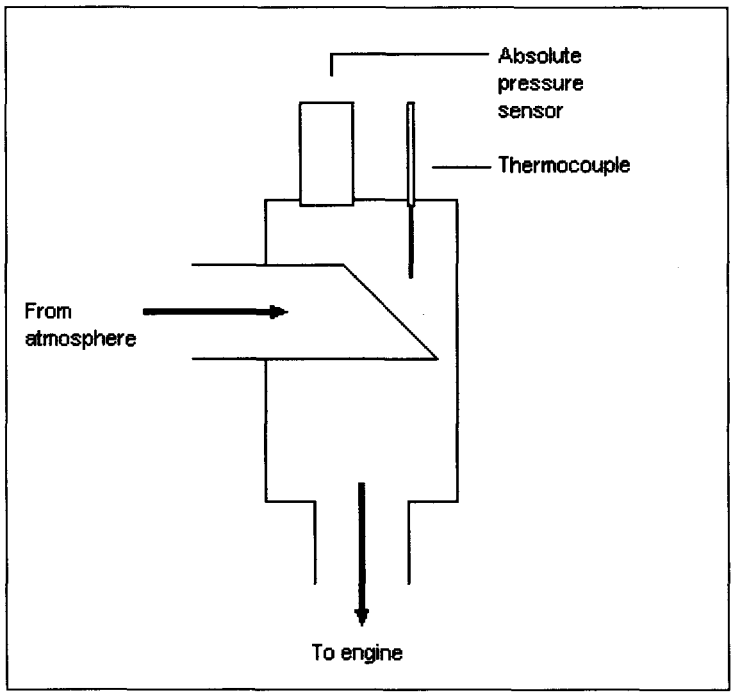

Figure B-2: Air plenum

B.2 Air mass-meter design

An air mass meter was required for signal feedback to the electronic control unit in order to inject the correct required amount of fuel into the inlet. Initially, a Bosch hot film mass-meter (0 280 217 110) (a BMW component) was considered for use. When this device was mounted in the inlet, however, the effects of pulsation were clearly seen and resulted in non repeatable readings. Linear correlation of averaged readings (after attaching a 200 l drum in series as a buffer tank situated before the mass-meter) was fairly good after about 1400 rpm, although the impracticality of the set up and the original desire for operating below 1400 rpm led to the consideration of an alternative measuring device, a laminar flow element.

Figure B-3 below shows the calculated versus actual results of the engine speed tests, when using the BMW massmeter and the 200 l drum. The straight lines are devised from the correlative data of calibration tests performed on the massmeter using a Horiba flow system.

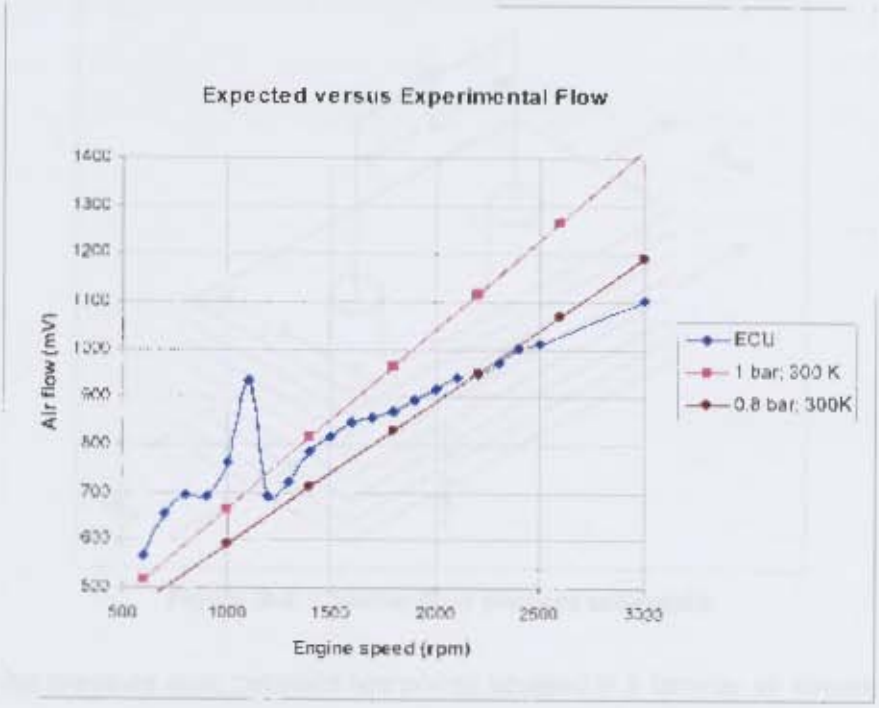

Figure B-3: Results of tests using BMW massmeter

A laminar flow element was designed and constructed to measure the air mass flow rate through the inlet manifold. It consists of several layers of closely arranged parallel plates through which the flow of the induced air is laminar. Since the flow characteristics are steady and uniform, the pressure drop across two points in the laminar air stream is a linear function of the flow rate.

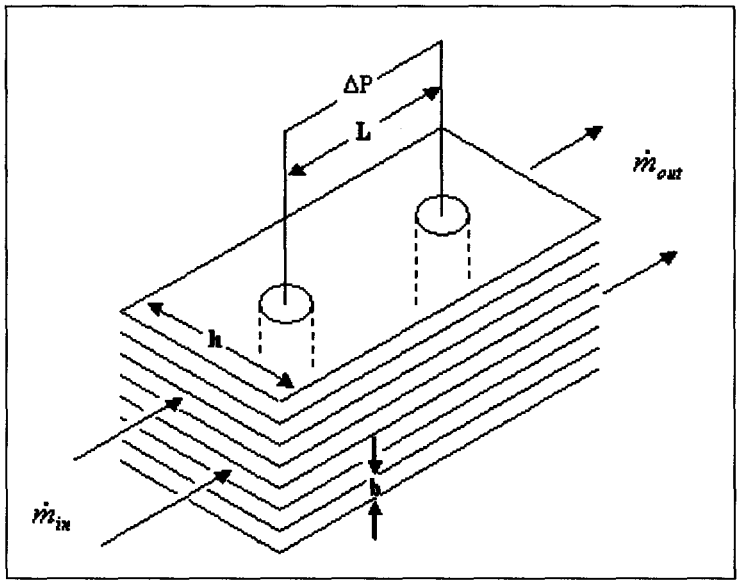

Figure B-4: Laminar flow element schematic

The equation for the pressure drop between two points situated in a laminar air stream between parallel plates is given as:

$$p_1 - p_2 = \frac{12\mu V}{b^2} L$$

(Pao, H. F., Fluid Mechanics, pg 176)

A differential pressure transducer was purchased with an operating pressure range of 0 – 1 psi (0 – 6.9 kPa) and the laminar flow element dimensions were designed for the pressure drop to be within that range.

Table B-1: Design parameters of laminar flow element

Number of plates (N)	19
Distance between plates (b)	0.5 mm
Width (h)	43 mm

When the flow element was connected in the inlet and tests were performed, the pressure transducer attached across the flow element showed unsteady pulsating flow readings. Electronic noise was also present in the signal as a result of the operation of the motor controller inverter. It was discovered that the average value of the pressure trace was a linear function of engine speed (and thus flow rate) over the design range for unchoked inlet conditions. This meant that the device could be used as a flow

meter despite the presence of a pulsating signal over the test range. To average the signal a rectifier circuit was built and connected on the signal output. The signal was also adjusted for the input range of the ADC input for the ECU (0 – 1.5 V) and filtered so that the error in reading would not exceed 7 mV.

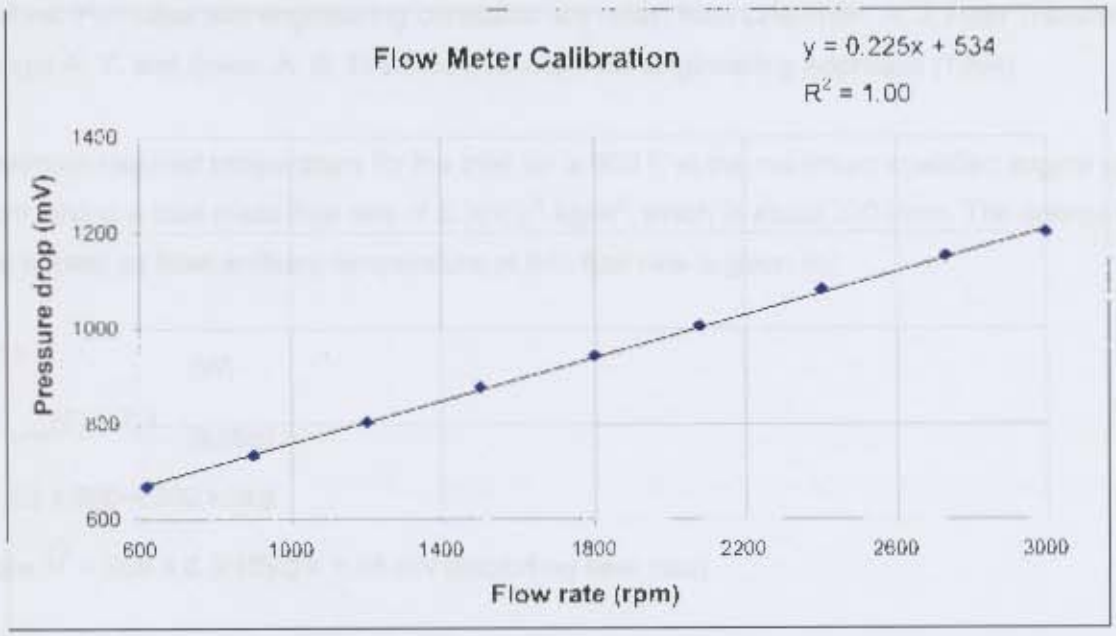

Figure B-5: Laminar flow element calibration curve

B.3 Throttling device

A ½" stainless steel ball valve was used to adjust the inlet pressure from 1 to 0.4 bar. The experimental method used during autoignition testing was to choke the inlet airflow while motoring the engine, then inject the test fuel under heated inlet conditions and then finally, slowly adjust the inlet pressure until autoignition occurred. The inlet pressure was measured using an absolute pressure sensor mounted in the air plenum; the operating range for the transducer was 0 – 1 bar and the output 0 – 5 V. Due to interference noise from the inverter drive, the signal had to be calibrated according to its normal output in addition to an offset voltage. Details of transducers and signal processing are discussed in Appendix D.

Table B-2: Ball valve specifications

Hardware	Stainless steel ball valve
Type	1" stainless, nylon ball
Company	Cape Valve

B.4 Inline air heater

The design temperature range for the inlet air was from 300 – 600 K. For this purpose a convection heater was sourced from Leister, a company specialising in process heat and plastic welding applications. Formulae and engineering constants are taken from Chapman, A. J; Heat Transfer (1967) and Cengal A. Y. and Boles, A. B; Thermodynamics – An Engineering Approach (1994).

The maximum required temperature for the inlet air is 600 K at the maximum specified engine speed 3000 rpm, giving a total mass flow rate of $6.3(10)^{-3}$ kg/m^3, which is about 320 l/min. The energy rate required to heat air from ambient temperature at this flow rate is given as:

$$\dot{Q} = \dot{m}\Delta h \quad \text{(W)}$$

$$\Delta h = C_{p,ave}(T_2 - T_1) \quad \text{(kJ/kg)}$$

Δh = 1.03 x 300 = 309 kJ/kg

Therefore $\dot{Q}$ = 309 x 6.3(10)-3 = 1.95 kW (excluding heat loss)

Taking heat loss into account, forced convection heat loss calculations are required.

Thermal conductivity constants (k, in W/m.K) of the following substances were used: air (0.026), steel (80.2) and glass fibre (0.043) (Thermodynamics – An Engineering Approach, pg 95).

Heat loss from a multilayered cylinder by conduction and convection is given as:

$$\frac{q}{L} = \frac{2\pi(T_1 - T_5)}{\frac{1}{r_2 h_{12}} + \frac{\ln\left(\frac{r_3}{r_2}\right)}{k_{23}} + \frac{\ln\left(\frac{r_4}{r_3}\right)}{k_{34}} + \frac{1}{r_4 h_{45}}}$$

(Heat Transfer, pg 59)

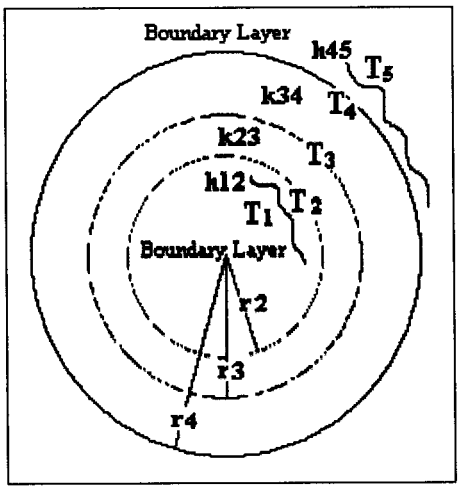

Figure B-6: Schematic for heater calculations

The Reynolds number calculated for air flow within the pipe indicated turbulent flow $(\mathrm{Re} \approx 10000)$. A Nusselt number approximation for forced turbulent convection, with temperature differences greater than 100°F is given as

$$Nu_D = 0.027(\mathrm{Re})^{0.8}(\mathrm{Pr})^{1/3}\left(\frac{\mu}{\mu^s}\right)^{0.14}$$

(Heat Transfer, pg 336)

Using $\mathrm{Pr} = \frac{\mu C_p}{k}$ and convective heat transfer coefficient $h = \frac{Nu.k}{d}$ results in a convective heat transfer coefficient of 26, for inner diameter 25 mm.

For free convection around the outer cylinder the Grashoff-Prantl product is considered with:

$$Gr = \frac{gd^3\rho^2\beta\Delta T}{\mu^2}$$

arriving at constants C = 0.525 and m = ¼ for Nu = C(Gr.Pr)^m (Heat Transfer, pg 361).
The resulting free convective coefficient was calculated as 9. Total heat loss over 300 mm of pipe assuming a minimal lagging instance results in 165 W over the length.

The cartridge heater sourced was 2.2 kW heater, providing an immediate outlet temperature of 600°C at 300 l/min. The minimum flow rate for full constant supply of 220 V is 200 l/min, thus a heater controller was required to prevent overheating of the cartridge. The control thermocouple was placed

50 mm downstream from the heater and other thermocouples for measurement were mounted over the inlet and exhaust ports respectively.

Table B-3: Heater element specifications

Hardware	Cartridge element convection air heater
Model	Typ 32A
Company	Leister
Power rating	2.2 kW
Voltage	230 V
Temperature	600 °C maximum
Flow rate	200 l/min minimum

B.5 Fuel injector

The carburettor system was upgraded to a fuel injection system for the purpose of exacting control of fuelling for experiments with different fuels and inlet air density conditions. In order to prevent heat damage to the fuel injector, a water cooling jacket was machined in the injector mounts.

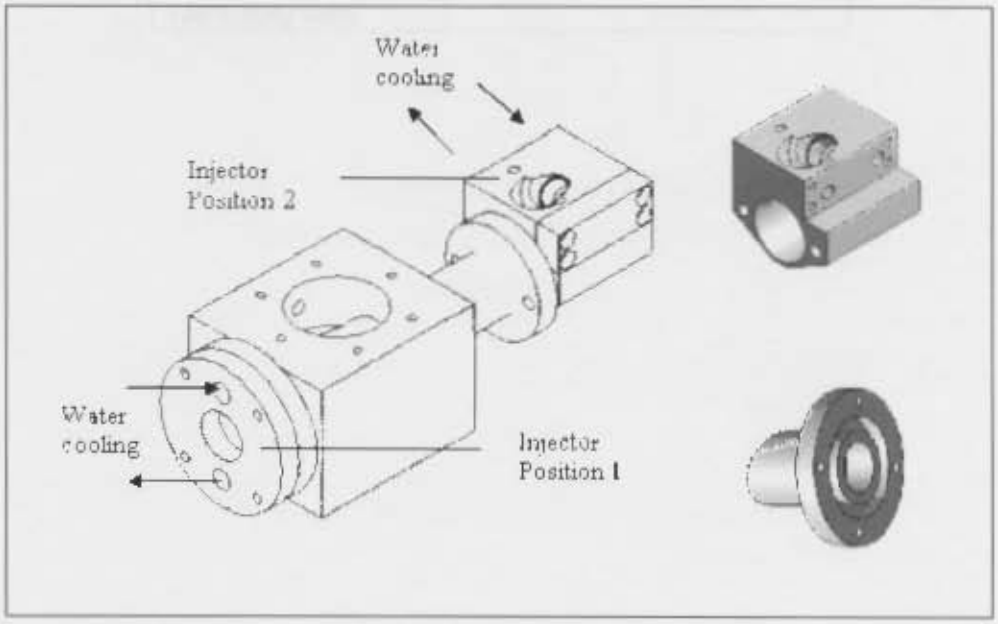

Figure B-7: Injector cooling

Two Bosch injector types were used in the course of the project (0280 150 727, 0280 150 208). The injection system was calibrated using type 0280 150 208 and a commercial 95 octane fuel. It was intended that this injector would serve to meter the test fuel n-heptane in the autoignition experiments.

It was found, however, that after the calibration process n-heptane could not be caused to autoignite in the engine. It was suspected that differences in viscosity between the fuels (which were initially assumed to be negligible in effecting fuel metering) caused the mixture to be too rich for combustion. This injector was then replaced by one with a slighter lower flow rate, type 0280 150 727, which resulted in autoignition of n-heptane under variable inlet conditions as well as in being run constantly for a fixed load under homogenous charge compression ignition (HCCI) conditions. It was hoped that any deviation from a stoichiometric equivalence ratio would not upset the results from modelling the autoignition tests using a stoichiometric autoignition algorithm. Since the deviation in equivalence ratio would be constant, this would result in consistent results and an error that could possibly be corrected through an adjustment factor in the model.

Table B-4: Injector specifications

Hardware	Fuel injectors
Model	0280 150 727, 0280 150 208
Company	Bosch
Power supply	12 VDC
Injection duration at 100% duty ratio	146 ml/min, 156 ml/min

Appendix C Fuel Delivery System

C.1 Mechanical fuel delivery system

The fuel delivery system consisted of a fuel tank, low pressure filter (GUD), fuel pump (Bosch), high pressure filter (Fram), pressure gauge, fuel injector (Bosch), vacuum adjusted pressure gauge (the vacuum adjustment tube of which was connected to the air plenum) and return pipe. The system was pressurised from 3 – 3.5 bars by the fuel pump.

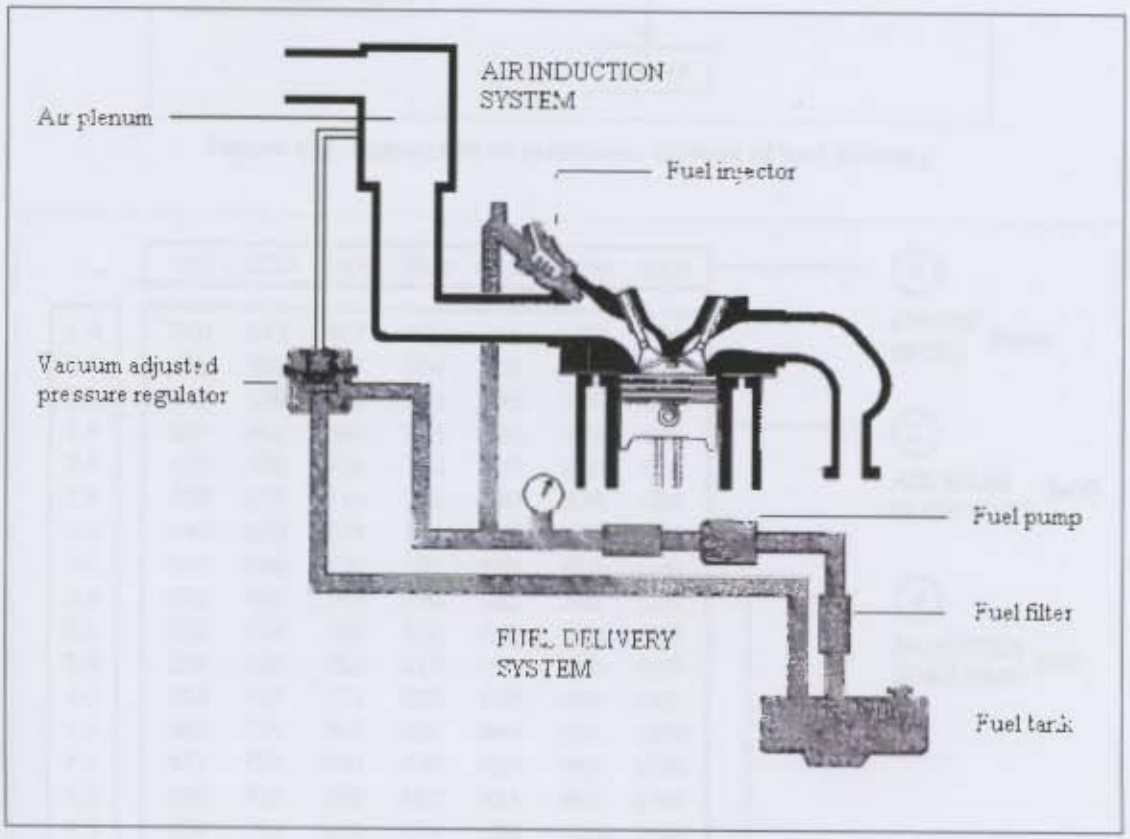

Figure C-1: Mechanical fuel delivery system

C.2 Electronic control

An electronic control unit consisting of a Motorola JK1 8-bit flash memory microcontroller with onboard ADC regulated the fuel injector pulse width and frequency according to the input signal values. The inputs, consisting of the revolution counter and laminar flow element air mass flow, were compared with values arranged in a lookup table stored on the chip. The lookup table contains values which may be

altered by values uploaded to the ECU memory through a RS 423 serial port connection. Linear interpolation between the values results in an output pulse width signal which controls the length of time that the injector solenoid remains open, and therefore the amount of fuel injected. The frequency of injection is regulated by the engine speed and occurs once every two revolutions.

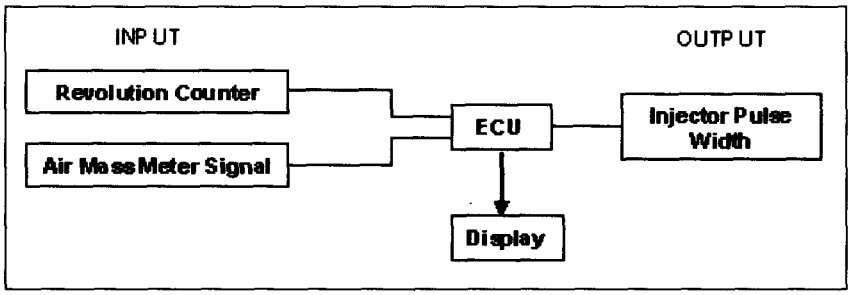

Figure C-2: Schematic of electronic control of fuel delivery

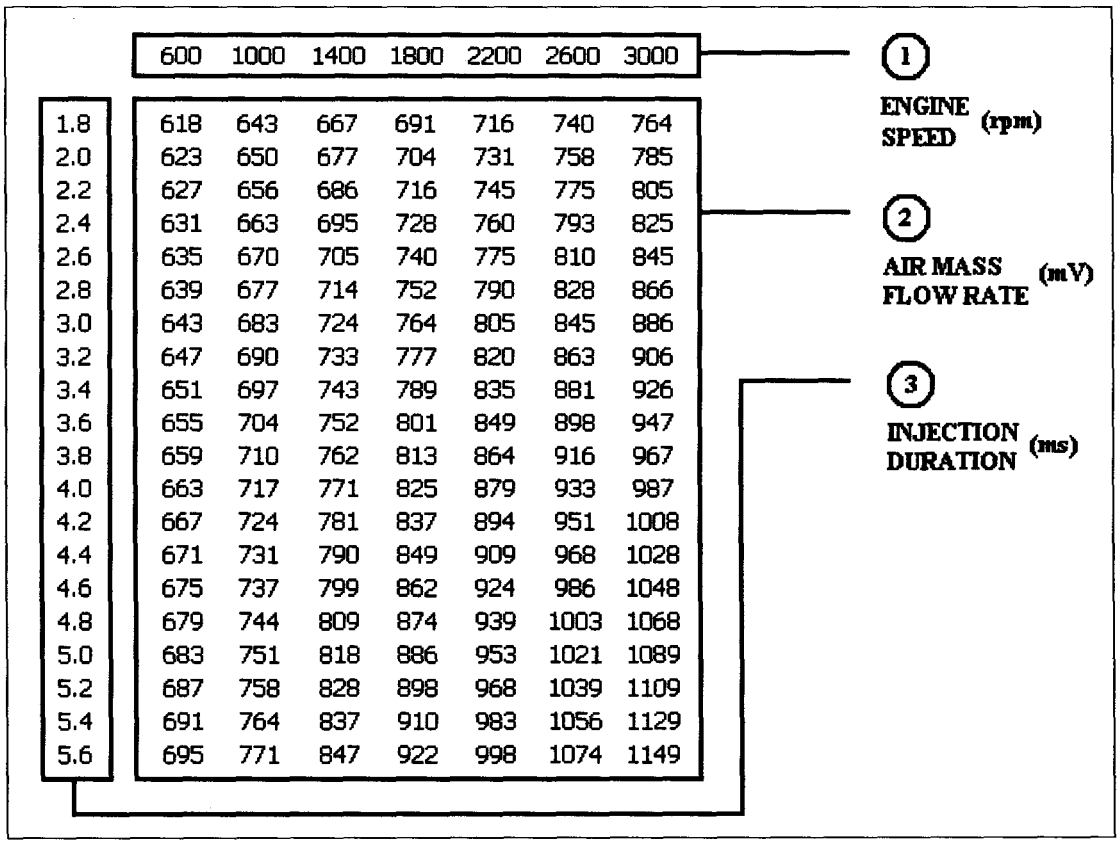

Figure C-3: Lookup table explanation

An engine speed of 2000 rpm and an air mass flow reading of 830 mV is given as an example.

The chip reads the speed and produces the interpolated air flow matrix:
[704 717 731 744 758 771 785 798 812 **825 839** 852 866 879 893 906 920 933 947 960]
The mass flow signal lies between the values 825 – 839 in the air flow matrix, resulting in the linear interpolation of the corresponding values 3.6 – 3.8 of the injection duration matrix and finally sending the output pulse width as 3.67 ms to the injector solenoid.

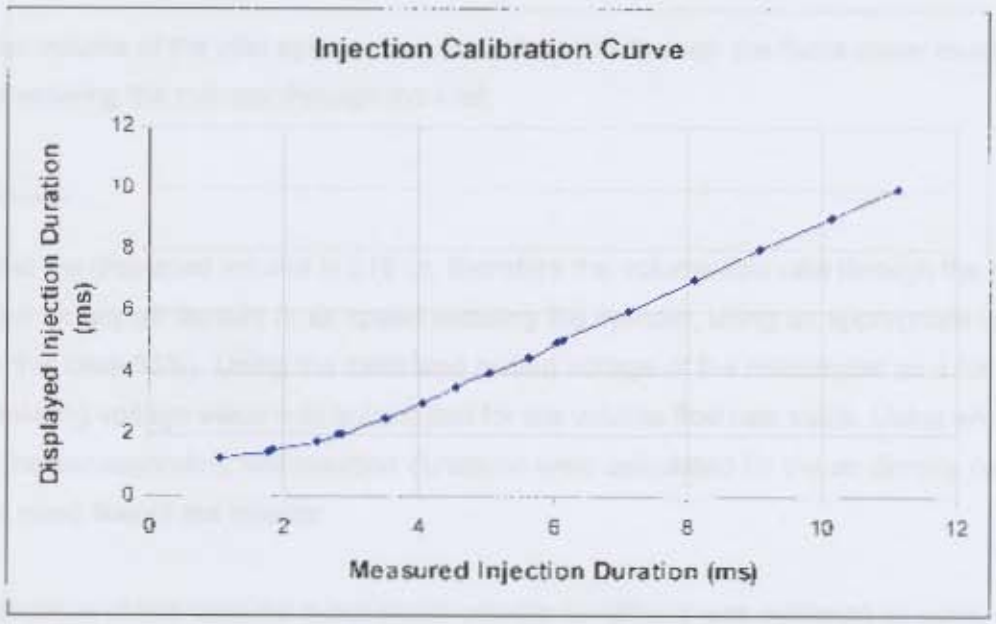

Figure C-4: Calibration of displayed injection duration values to actual injection duration for injector type 0280 150 727

The control unit, including a display of engine speed, air mass signal and injection duration, was designed and built by a 4th year electrical engineering student, Aaron Wetzler. The design and coding specifications are not included in this thesis appendix.

C.3 Calibrating the lookup table for a constant equivalence ratio

For the purposes of commissioning the device, a lookup table was designed for a stoichiometric air/fuel ratio using a commercial 95 octane fuel. This table was then used in the autoignition tests using n-heptane.

A theoretically based lookup table was initially generated using simple airflow calculations. The table represented the air density limiting conditions at designed inlet air heating and choking, as well as engine speed limits.

Table C-1: Experimental design parameters

Inlet pressure range	0.2 – 1 bar
Inlet temperature range	300 – 600 K
Engine speed range	600 – 3000 rpm

For the control volume of the inlet system, the mass flow rate through the mass meter must be the same as that entering the cylinder through the inlet.

$$\dot{m}_{cylinder} = \dot{m}_{massmeter}$$

It is known that the displaced volume is 215 cc, therefore the volume flow rate through the massmeter was calculated for any air density or air speed entering the cylinder, using an appropriate volumetric efficiency (in this case 85%). Using the calibrated output voltage of the massmeter as a function of flow rate, the correlating voltage value was substituted for the volume flow rate value. Using an appropriate air-fuel ratio the corresponding fuel injection durations were calculated for the air density conditions, based on the rated flow of the injector.

Further modification of this table for exact stoichiometric conditions was achieved by using empirical data from fired engine tests. Under varying engine speeds, inlet temperature and pressure conditions, the air fuel ratio was adjusted manually by overriding the air mass signal using a variable DC voltage source. The tests were performed under firing conditions using a spark plug to initiate burning. The speed of the engine was controlled using the load control system. Fuelling was adjusted to stoichiometric conditions using negative feedback from a lamda sensor mounted in the exhaust stream. The data collected from the tests were used to develop an empirically derived volumetric function in order to adjust the values in the lookup table. The correlation was derived using the following method. By definition:

$$\ell_v = \frac{\dot{m}_a}{\rho V_d N / 2}$$

where: $\dot{m}_a$ is mass flow rate of air

ρ is the air density

V_d is the displaced volume

N is engine speed.

$$\frac{\dot{m}_f}{\dot{m}_a} = F / A$$

where F/A is the mass based fuel to air ratio

Therefore... $m_f = {}^{F}\!/_{A} \ell_v \rho V_d$ (per cycle)

Assuming that:

1. Injection duration (ID) α m_f + offset (based on fuel injector calibration tests)
2. $\frac{F}{A} = const$
3. $\ell_v = f(N, N^2, N^3, T_i, P_i)$

where N is engine speed (rpm)

T_i is inlet temperature (^{0}C)

P_i is inlet pressure (remaining as V)

The injection duration function that best correlated the experimental to calculated values was discovered to be that of the form:

$$ID = A_0 + \rho(A_1 N + A_2 N^2 + A_3 N^3)(1 + A_4 T_i)(1 - \frac{A_5}{P_{atm} - P_i}) \text{ (ms)}$$

The air mass flow values were then filled into the table by correlating experimental and calculated values with an equation of the form:

$$\dot{m}_{air} = A_0 + A_1(ID.N) \text{ (mV)}$$

Table C-2: Numerically solved constants for lookup table value calculation

Injection duration correlation (ms)		Air mass flow correlation (mV)	
A_0	-0.744	A_0	582.024
A_1	14.418	A_1	33.770
A_2	-11.984		
A_3	4.649		
A_4	-0.584		
A_5	0.002		
A_6	0.005		

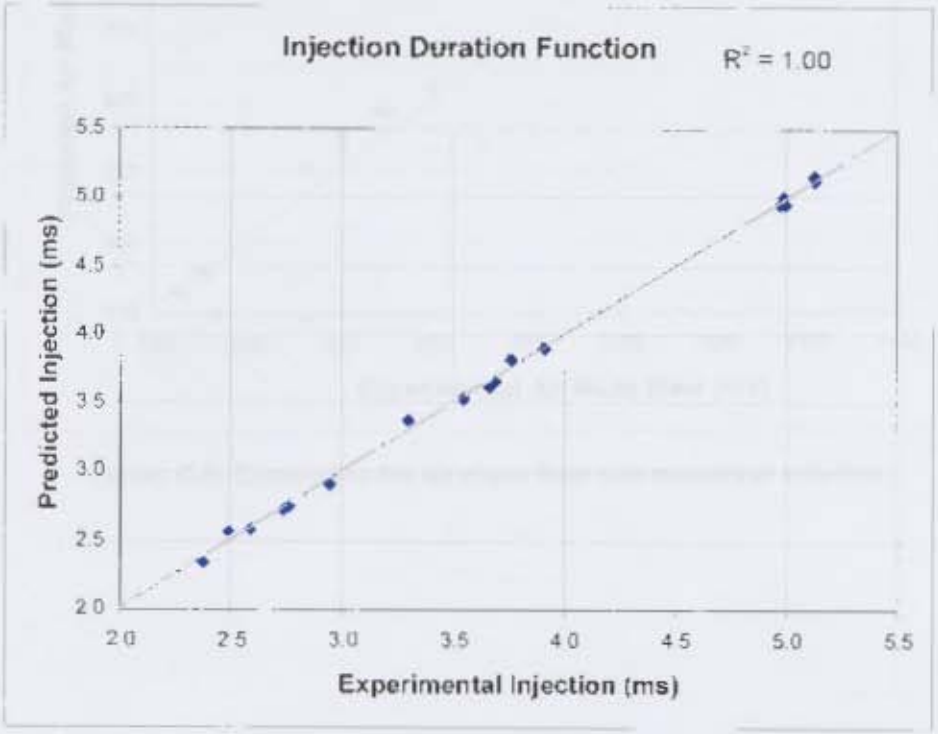

Figure C-5: Correlation for injection duration numerical solution

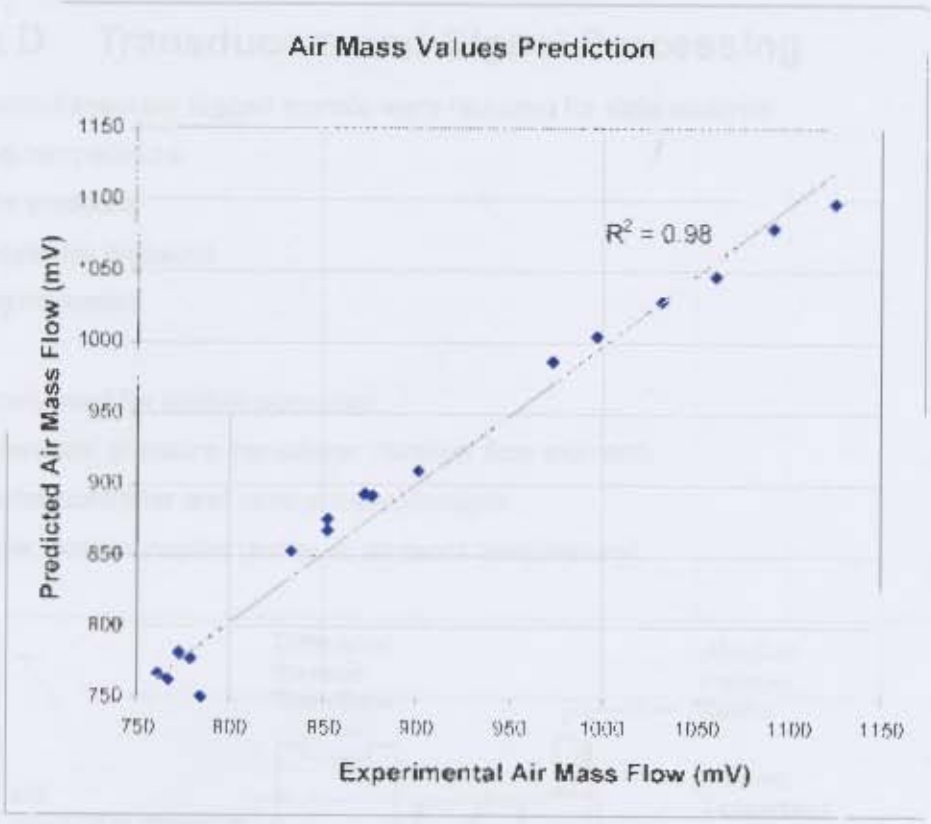

Figure C-6: Correlation for air mass flow rate numerical solution

Appendix D Transducers and Signal Processing

The following simultaneously logged signals were required for data analysis:

1. Inlet temperature
2. Inlet pressure
3. In-cylinder pressure
4. Engine speed

Other transducers used for control purposes:

1. Differential pressure transducer (laminar flow element)
2. Heater controller and control thermocouple
3. Other thermocouples (exhaust, ambient temperature)

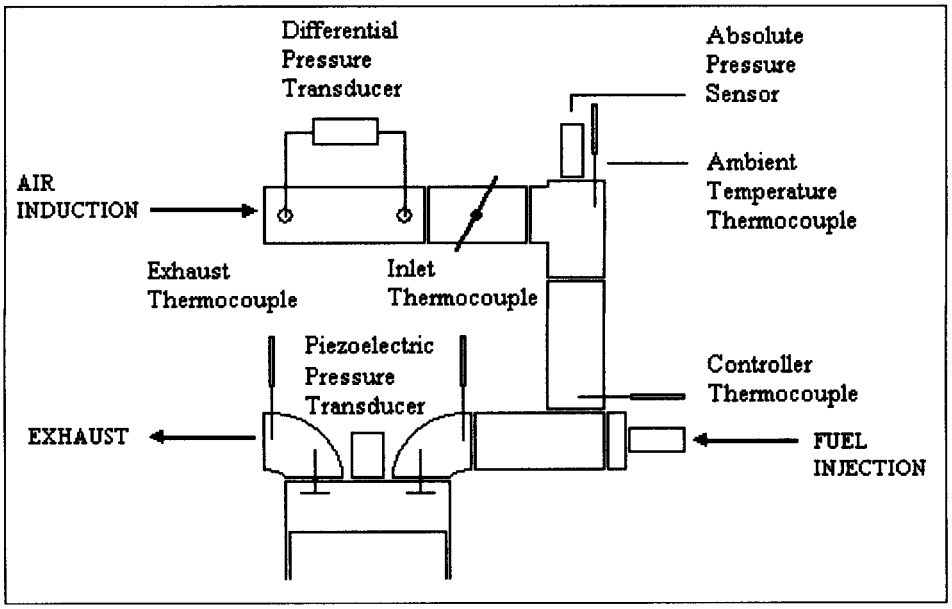

Figure D-1: Schematic of transducers used on the experimental rig

D.1 Signal noise

Signal traces were initially disrupted by high frequency electronic noise generated by the inverter motor controller. Electronic noise was induced in the signal wires despite attempts to prevent emission by using screened cable on signal wires; and motor and controller cables. Finally the problem was

diminished through the installation of low pass filters on the transducer output signals, the design cut off frequency for the filters being around 100 Hz.

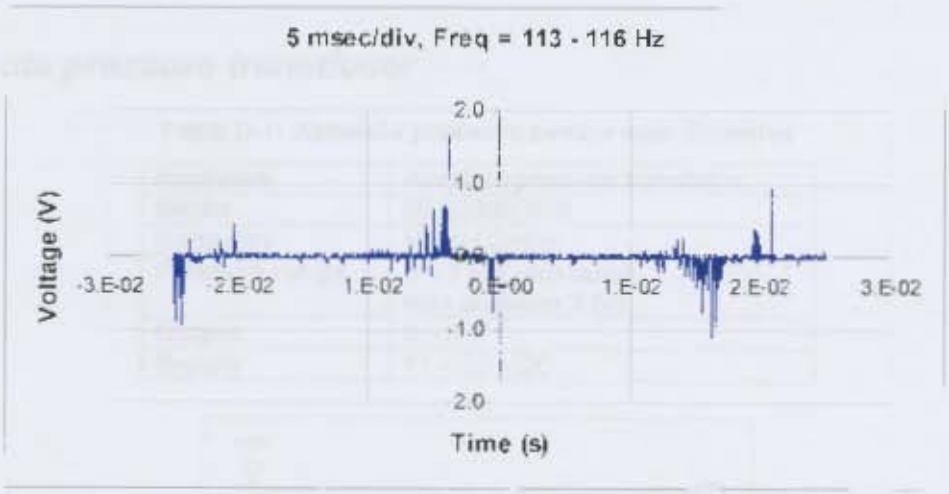

Figure D-2: Signal noise measured at 5 ms/division

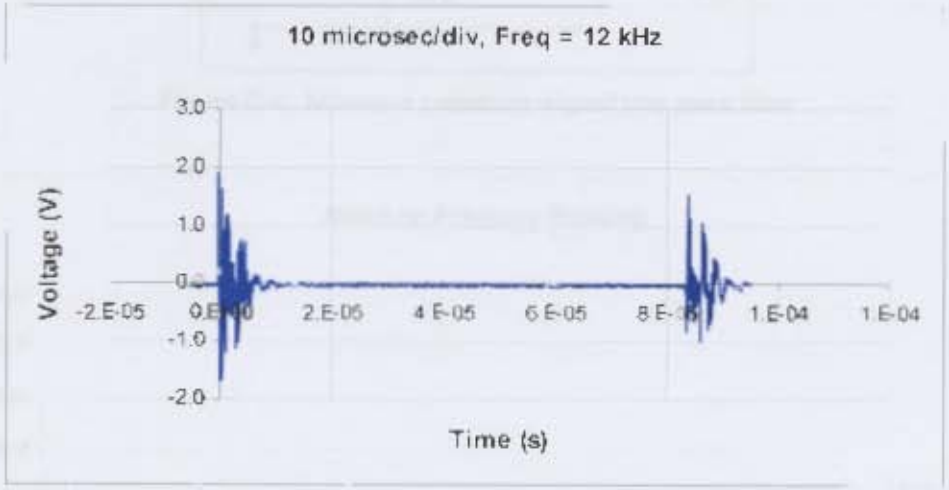

Figure D-3: Signal noise measured at 10 μs/division

The circuits were designed according electronic precepts and equations in (pg 526-530, Hughes. E., Hughes – Electrical Technology). For low pass filter design:

$$C = \frac{1}{2\pi Rf}$$

Therefore, using a resistor of 1 kΩ for a cut off frequency of 100 Hz, gives a capacitance of 1.6 μF. It was found, however, that larger capacitors provided better eradication of noise on the signal.

D.2 Absolute pressure transducer

Table D-1: Absolute pressure sensor specifications

Hardware	Absolute pressure transducer
Model	691.90000005
Company	Huba Control
Pressure range	0 – 1 bar (absolute); max pressure 2 bar
Output	0 – 5 V
Supply	11 – 33 VDC

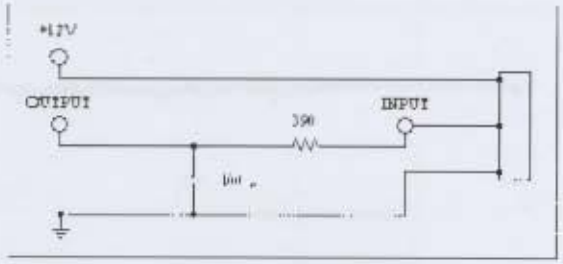

Figure D-4: Absolute pressure signal low pass filter

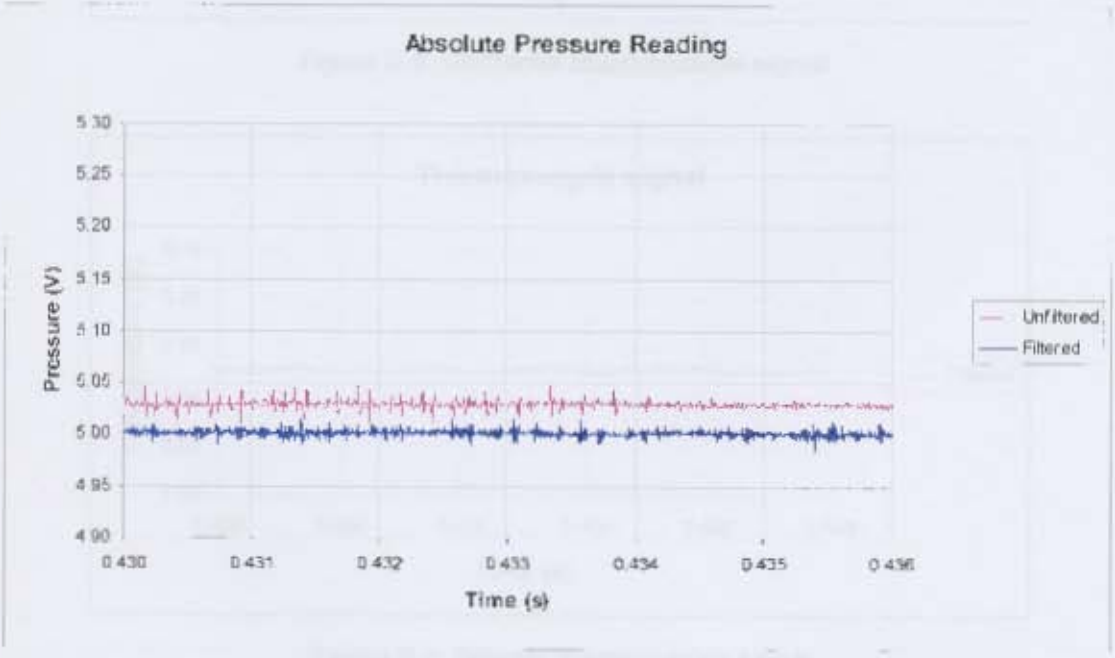

Figure D-5: Filtered and unfiltered signals of absolute pressure sensor

D.3 Inlet temperature measurement

The inlet temperature signal was logged using the oscilloscope. Due to the presence of electronic noise, the signal required filtering. High amplification of the EMF generated by the thermocouple and an intended high sampling rate for logging purposes required the construction of a more complex filtering device. Graeme McPhillips designed and built the filter on the output of the AD 595 operational amplifier for the K-type thermocouple used.

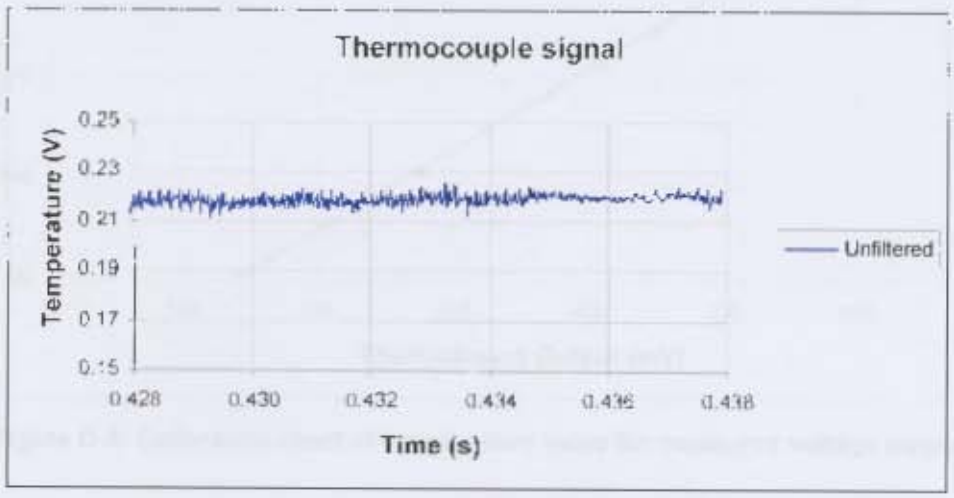

Figure D-6: Unfiltered thermocouple signal

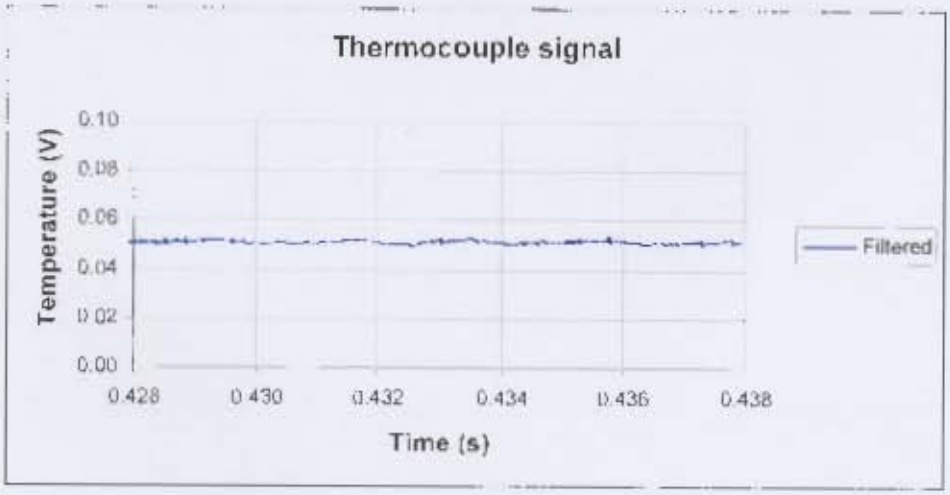

Figure D-7: Filtered thermocouple signal

The heater system was tested and the circuit thermocouple signal was calibrated using data from motored engine experiments. The results of the calibration tests are in Figure D-8.

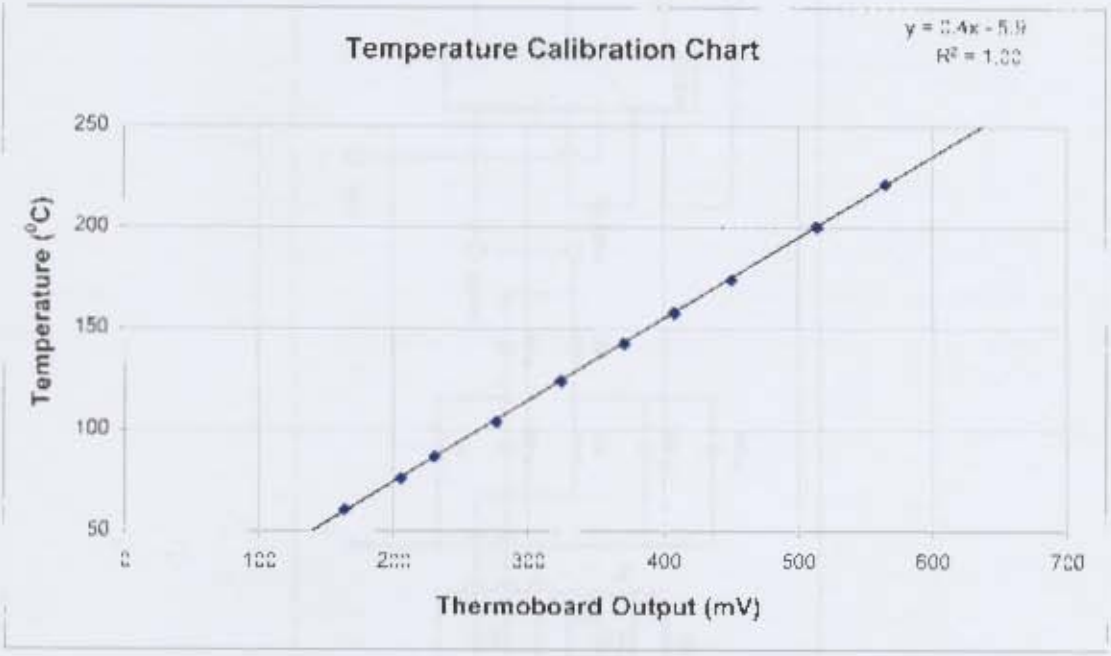

Figure D-8: Calibration chart of temperature value for measured voltage output

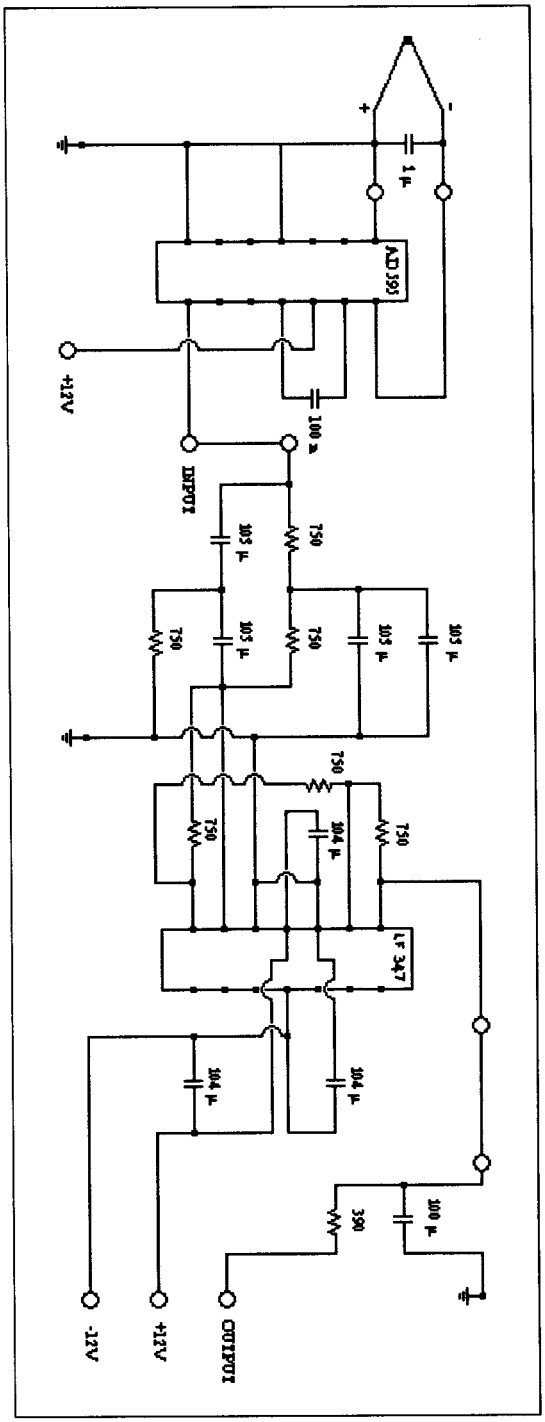

Figure D-9: Processing circuit of thermocouple signal for data acquisition

D.4 In-cylinder pressure

A piezoelectric differential pressure transducer was used to measure in-cylinder pressures. The pressure transducer was calibrated using a dead weight tester.

Table D-2: In-cylinder pressure transducer specifications

Hardware	Piezoelectric pressure transducer
Model	
Company	Kistler
Pressure range	120 bar
Output	44.88 pC/bar

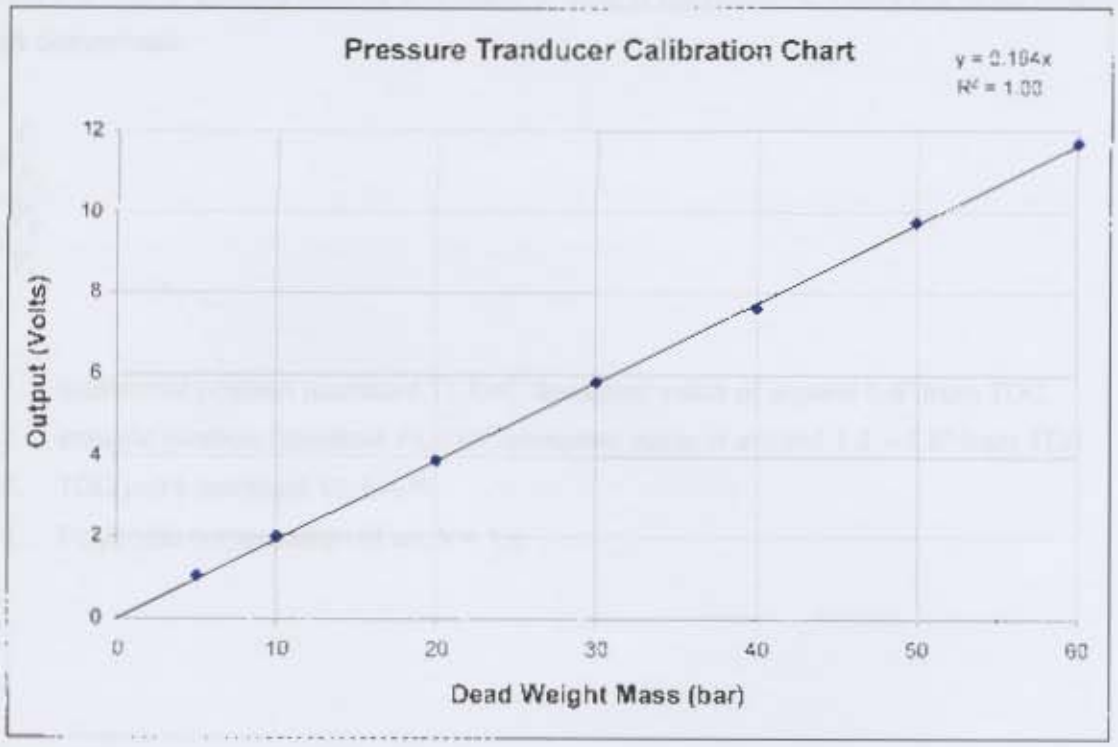

Figure D-10: Calibration of pressure transducer using a dead weight tester, charge amplifier setting 44.88 pC/bar input sensitivity and 5 bar/volt

D.5 Engine speed measurement

Initially, an inductive pickup was used to measure engine speed from a cut out on a steel disk attached to the flywheel. When the engine was run in spark ignition mode for air-fuel ratio calibration, it was found that the signal was disturbed by the electromagnetic pulse generated by the magneto as a result

of sparking. This resulted in the ECU not being able to process the engine speed correctly. This led to the use of an optical pickup based measuring system; the disk with reflective tape being the stimulus. The circuit with required filtering was designed and built by Graeme McPhillips.

D.6 CAD encoder

The signal produced by the optical sensor every cycle was used to calibrate the position of the test data according to top dead centre. Using motored engine traces at 2000 rpm, the offset from the signal marker to TDC was determined. The TDC point is not simply the position of peak pressure in a motored engine, but due to heat loss the TDC point occurs slightly after the point of maximum pressure. By calculating the ratio of specific heat as a function of time in the motoring traces the exact location of TDC was determined.

$$k = \frac{\log \frac{P_1}{P_2}}{\log \frac{V_2}{V_1}}$$

For:

1. isothermal position (constant T), k=0, accepted value of around 0.6^0 from TDC.
2. isobaric position (constant P), k=1, accepted value of around $1.2 - 1.6^0$ from TDC.
3. TDC point (constant V), $k \rightarrow \infty$
4. Polytropic compression of air, k = 1.4

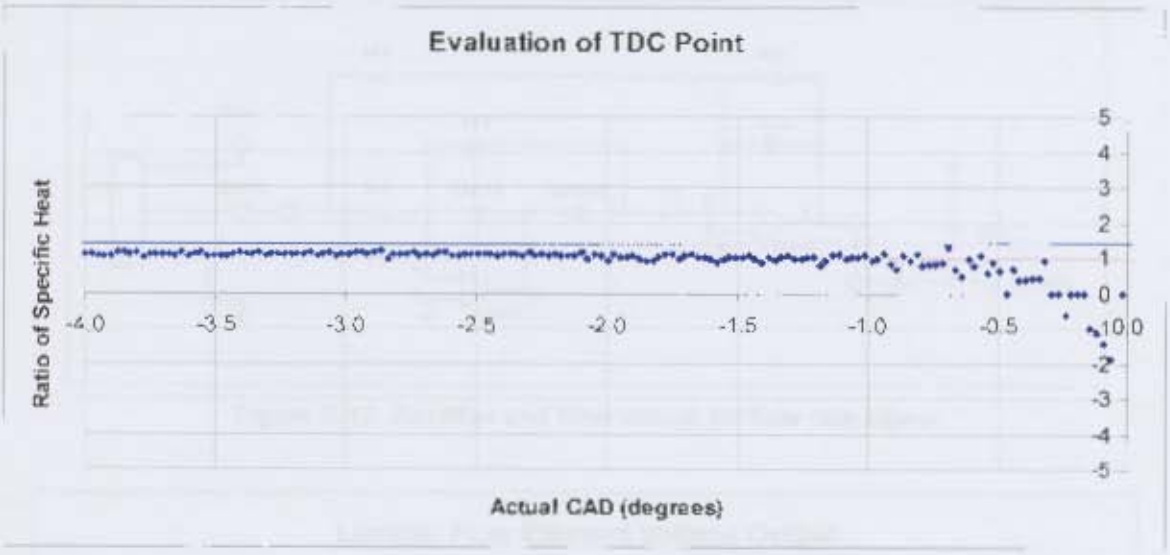

Figure D-11: Investigation of TDC point

Thus the offset from the position of TDC to the signal marker was determined as 41.2°, which is about 0.3° from peak pressure in the motored cycle at that speed.

D.7 Differential pressure transducer

Table D-3: Specifications of differential pressure transducer of laminar flow element

Hardware	Signal conditioned differential pressure transducer
Model	142 PC01D
Company	Honeywell Products
Pressure range	0 – 1 psi (0 – 6.9 kPa)
Output	0 – 5 V

The fluctuating pressure drop signal from the differential pressure transducer for the laminar flow element was averaged with a rectifier circuit.

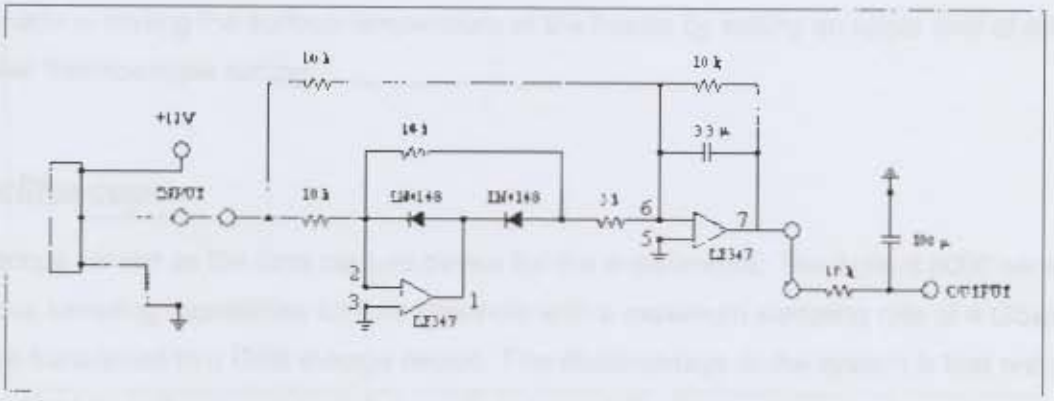

Figure D-12: Rectifier and filter circuit for flow rate signal

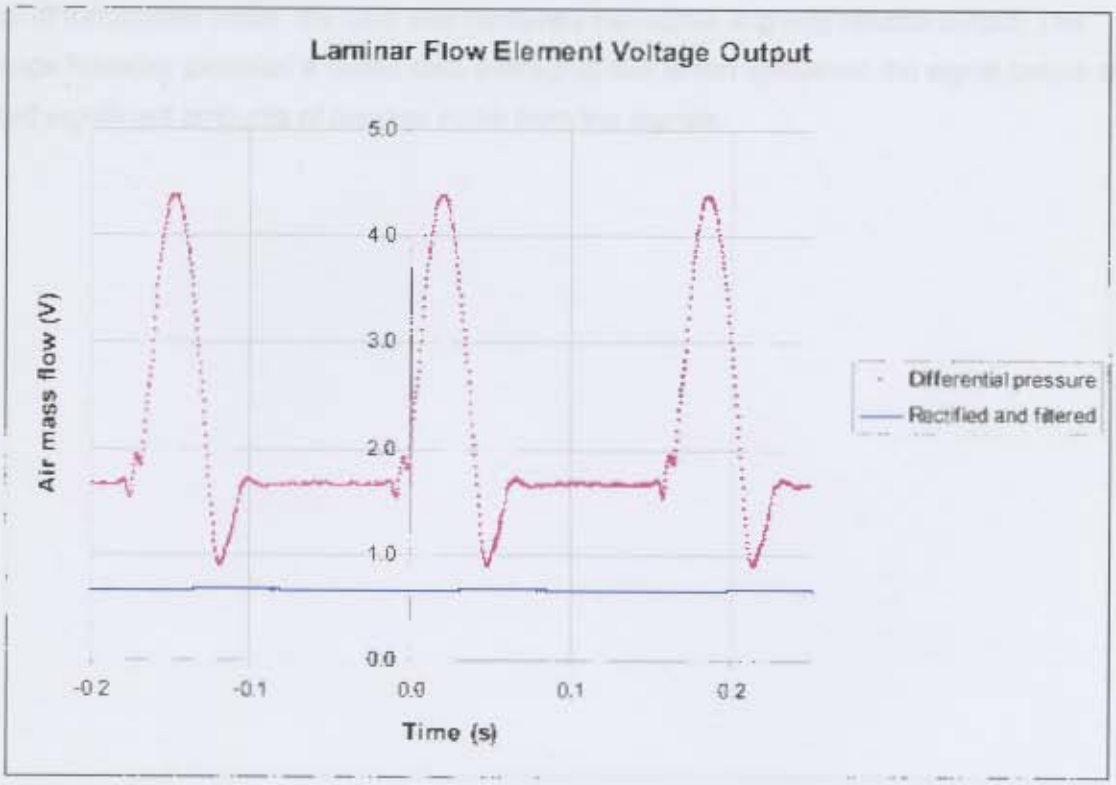

Figure D-13: Actual to rectified flow rate signal

D.8 Heater controller

A solid state relay and REX 100 k-type thermocouple controller were used to control the air heater temperature. The temperature of the heater needed to be kept below around 650°C to prevent melting of the ceramic, thus the design flow rate of the device is 200 l/min. The engine, however, was required to be motored with resulting flow rates lower than this (the minimum being 120 l/min). Precautions were

therefore made in limiting the surface temperature of the heater by setting an upper limit of 400^{0}C on the controller thermocouple setting.

D.9 Oscilloscope

An oscilloscope served as the data capture device for the experiments. The Agilent 6000 series has simultaneous sampling capabilities for four channels with a maximum sampling rate of 4 GSa/s. Data files may be transferred to a USB storage device. The disadvantage of the system is that only 1000 points are stored from the screen to disk, providing some difficulty in capturing and reorganising the data in a single stream. A data capture card was previously tried (and is preferred), but with the presence of transmitted noise, the card was rendered ineffective in giving reliable output. The oscilloscope however provided a useful data averaging tool which smoothed the signal output and eradicated significant amounts of residual noise from the signals.

Appendix E Drawings

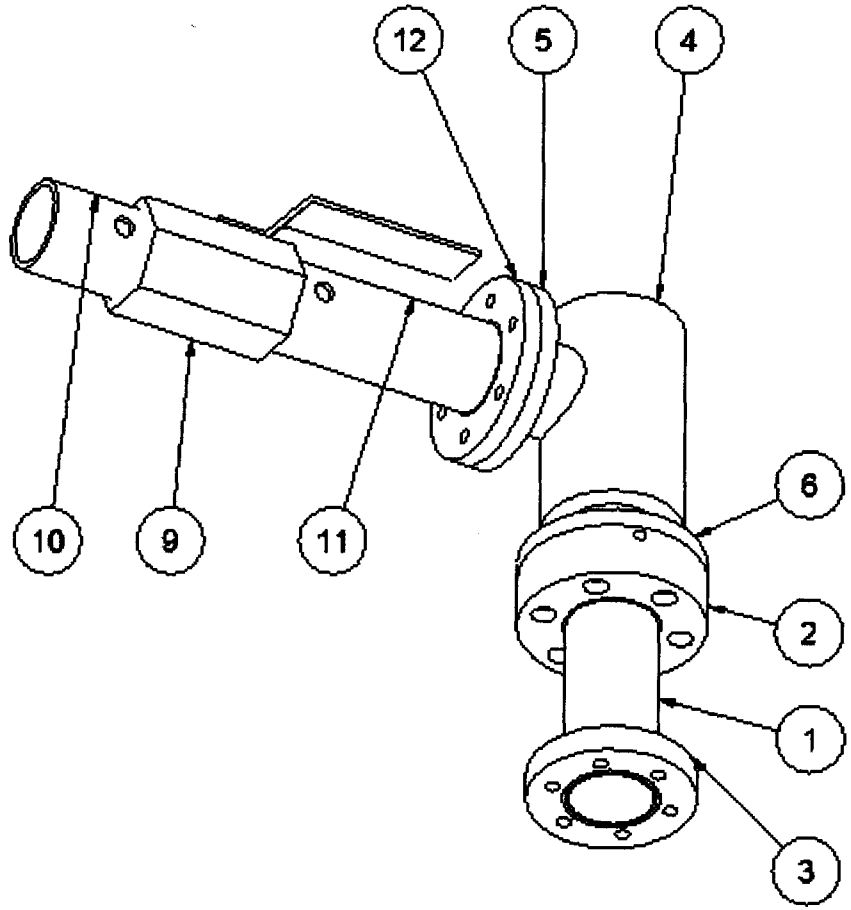

Parts List			
ITEM	QTY	PART NUMBER	DESCRIPTION
1	1	Heater Tube	Stainless steel
2	1	Heater Tube Inlet	Stainless Steel
3	1	Heater Tube Outlet	Stainless Steel
4	1	Air Plenum	Mild Steel
5	1	Air Plenum Inlet	Mild Steel
6	1	Air Plenum Outlet	Mild Steel
9	1	Ball Valve	Stainless Steel
10	1	Ball Valve Inlet Tube	Stainless Steel
11	1	Ball Valve Outlet Tube	Stainless Steel
12	1	Ball Valve Outlet	Stainless Steel

Designed by	Checked by	Approved by - date		Date	
Simon Demnitz				02/02/2005	

Sasol Oil

Heater, Throttle Assembly

Edition

Sheet 1 / 1

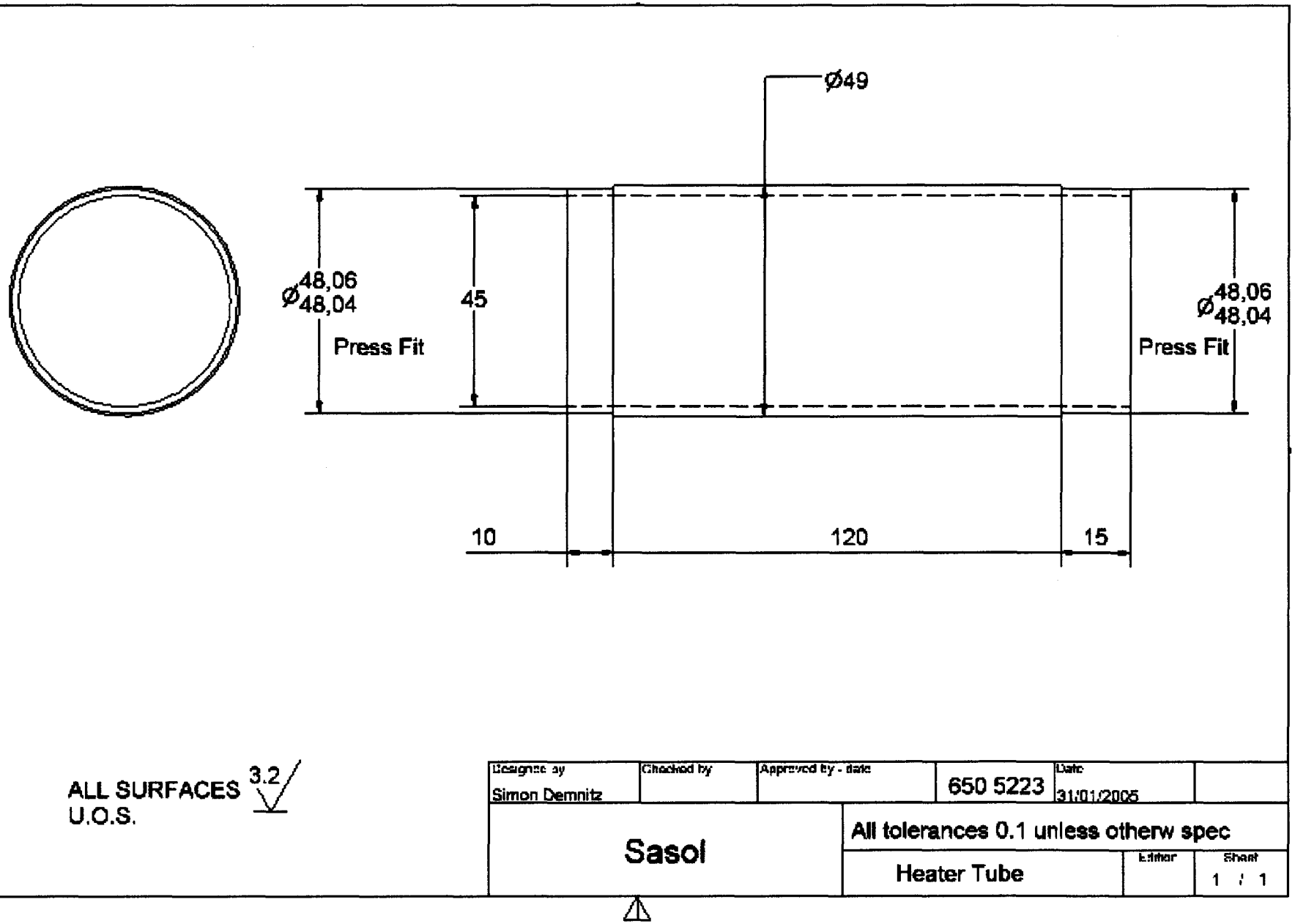
Ø49
Ø48,06
Ø48,04
Press Fit
45
Ø48,06
Ø48,04
Press Fit
10
120
15
ALL SURFACES
U.O.S.
3.2
Designed by
Simon Demnitz
Checked by
Approved by - date
650 5223
Date
31/01/2005
Sasol
All tolerances 0.1 unless otherw spec
Heater Tube
Edition
Sheet
1 / 1

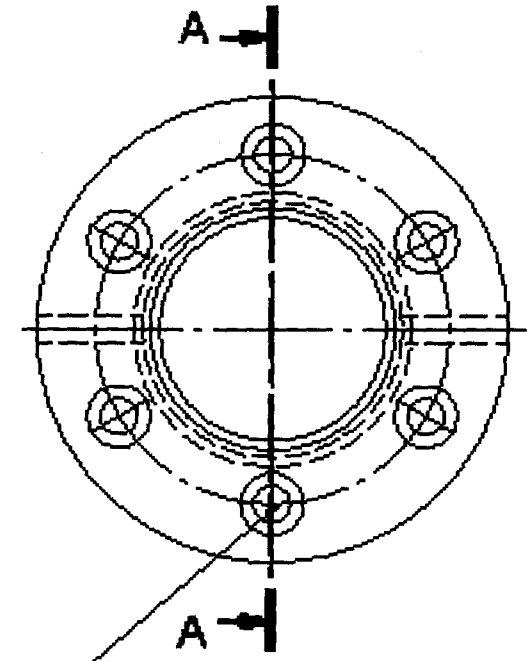

A-A (3 : 4)

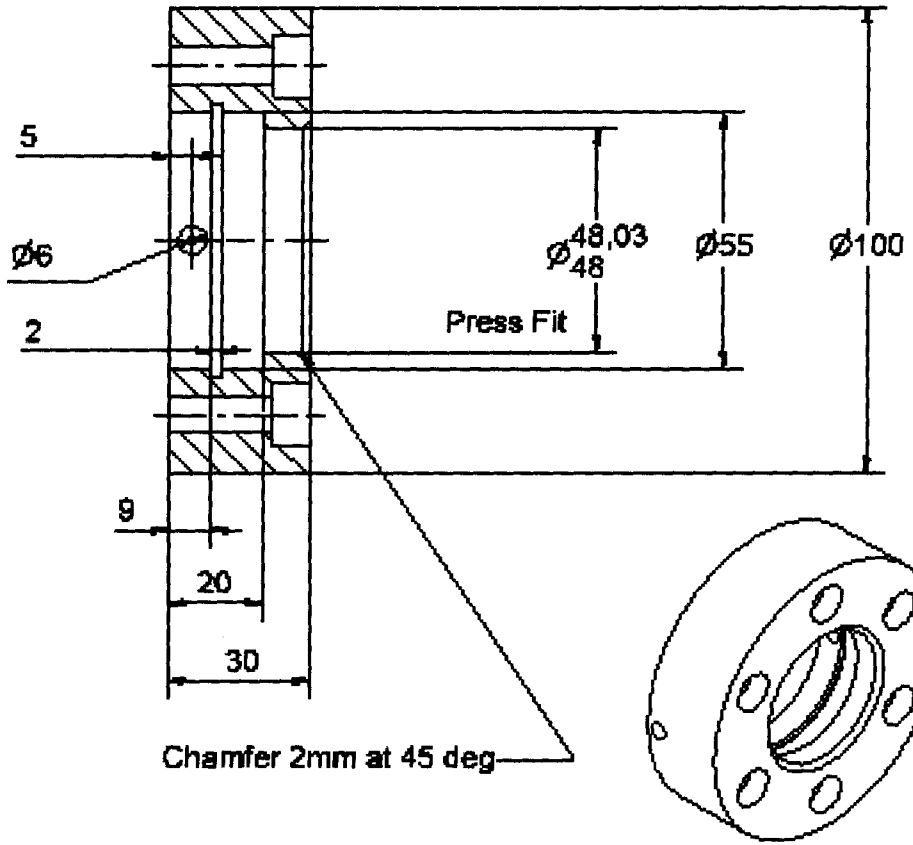

ALL SURFACES 3.2
U.O.S.

Designed by	Checked by	Approved by - date	650 5223	Date
Elmer Bernz				2:10:2005
Sasol	All tolerances 0.1 unless otherw spec			
	Heater Tube Inlet	Edition	Sheet 1 : 1	

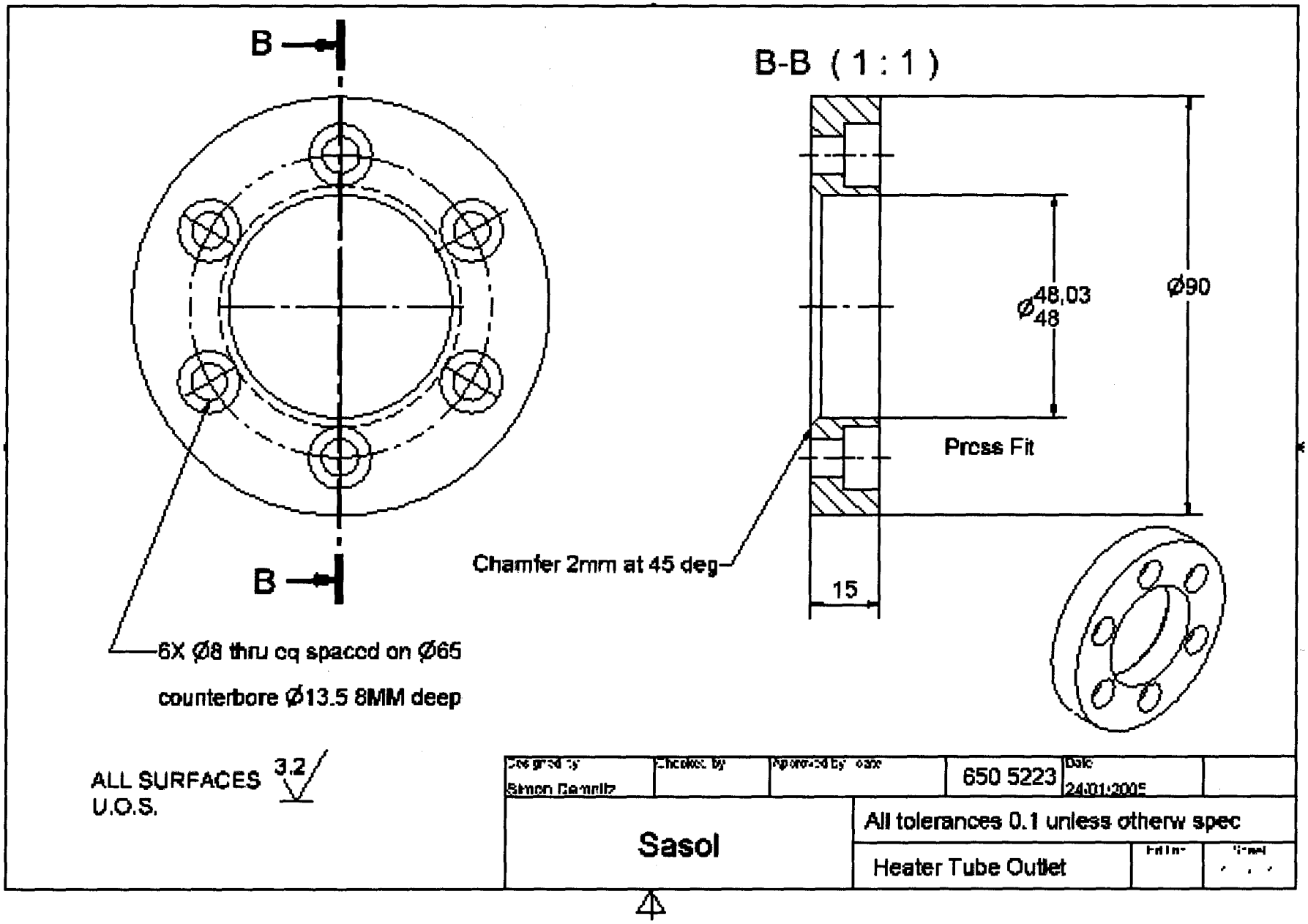
B
B
B-B (1 : 1)
Ø90
Press Fit
15
Chamfer 2mm at 45 deg
6X Ø8 thru cq spaced on Ø65
counterbore Ø13.5 8MM deep
ALL SURFACES
U.O.S.
3.2
650 5223
Date
24/01/2005
Sasol
All tolerances 0.1 unless otherw spec
Heater Tube Outlet

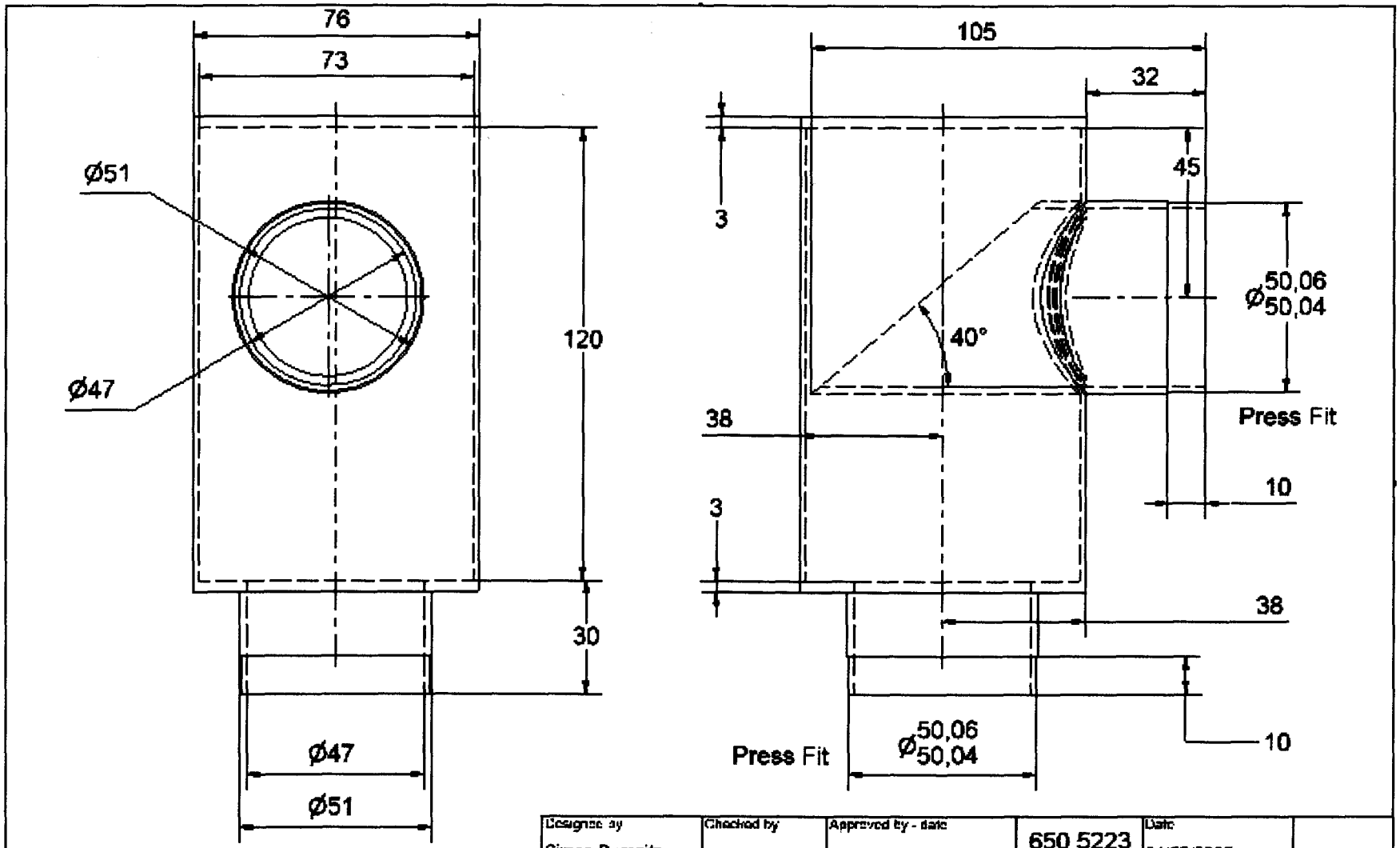
76
73
Ø51
Ø47
120
30
Ø47
Ø51
105
32
45
3
40°
Ø50,06
Ø50,04
Press Fit
38
10
3
38
10
Press Fit
Ø50,06
Ø50,04
Designed by
Simon Demnitz
Checked by
Approved by - date
650 5223
Date
01/02/2005
Sasol
All tolerances 0.1 unless otherw spec
Air Plenum
Sheet
1 / 1

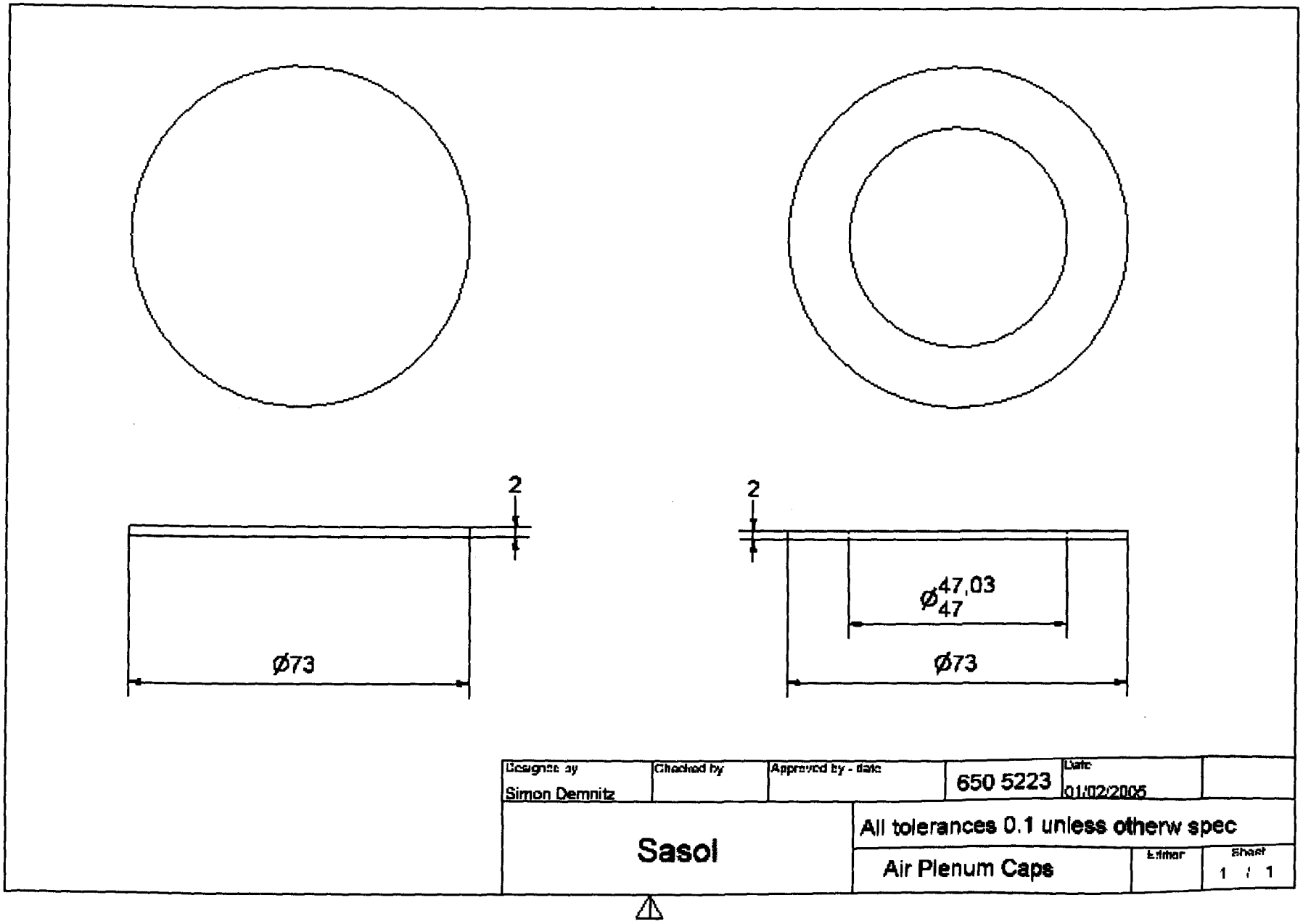

Designed by	Checked by	Approved by - date		Date
Simon Demnitz			650 5223	01/02/2005

Sasol	All tolerances 0.1 unless otherw spec		
	Air Plenum Caps	Either	Sheet 1 / 1

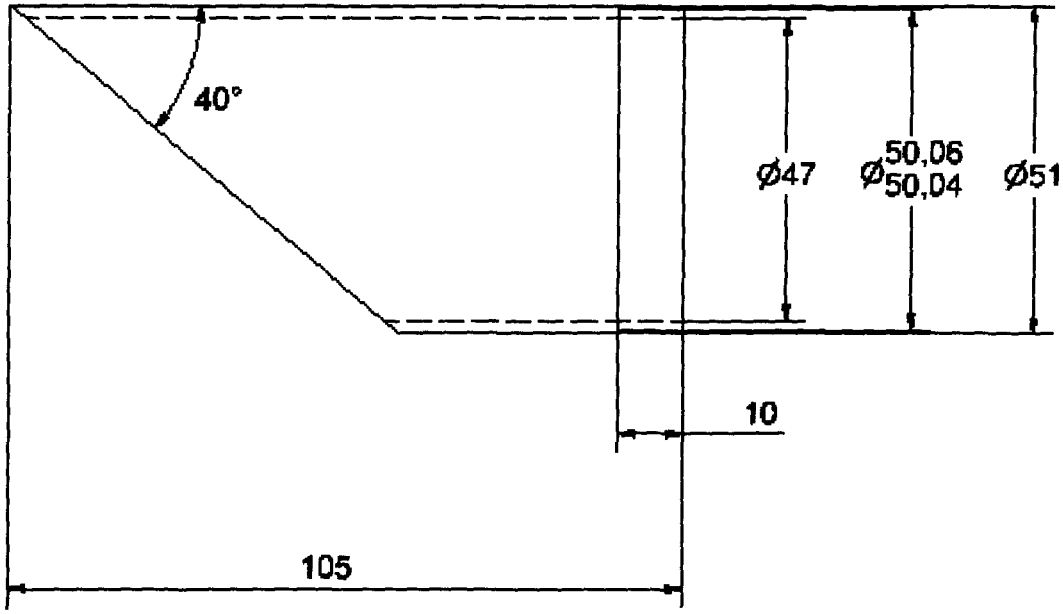

Air Plenum Inlet Pipe
MILD STEEL
1 OFF

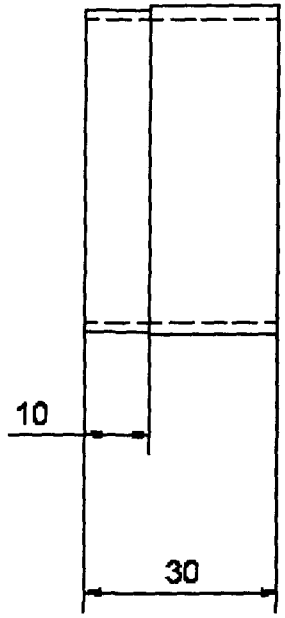

Air Plenum Outlet Pipe
MILD STEEL
1 OFF

Designed by	Checked by	Approved by - date		Date
Simon Demnitz			650 5223	01/02/2005

Sasol	All tolerances 0.1 unless otherw spec		
	Air Plenum Inlet Pipe	Edition	Sheet 1 / 1

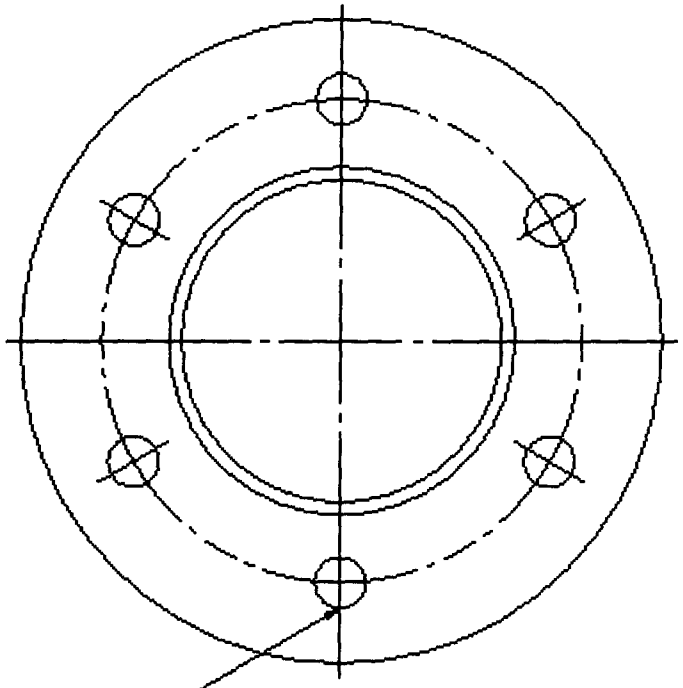

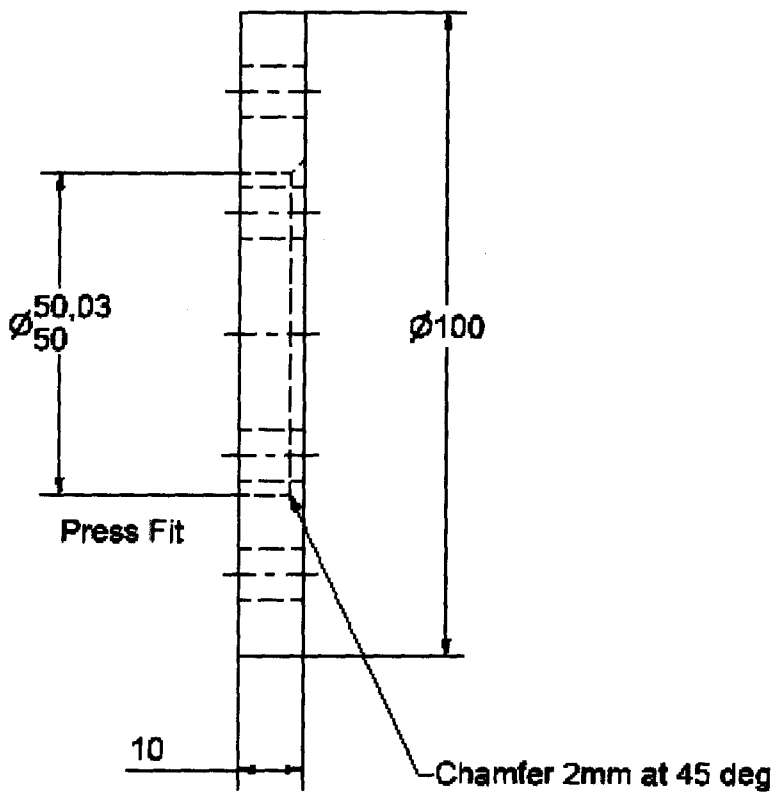

ALL SURFACES 3.2
U.O.S.

Designed by	Checked by	Approved by - date		Date
Simon Demnitz			650 5223	31/01/2005

Sasol	All tolerances 0.1 unless otherw spec		
	Air Plenum Inlet	Edition	Sheet 1 / 1

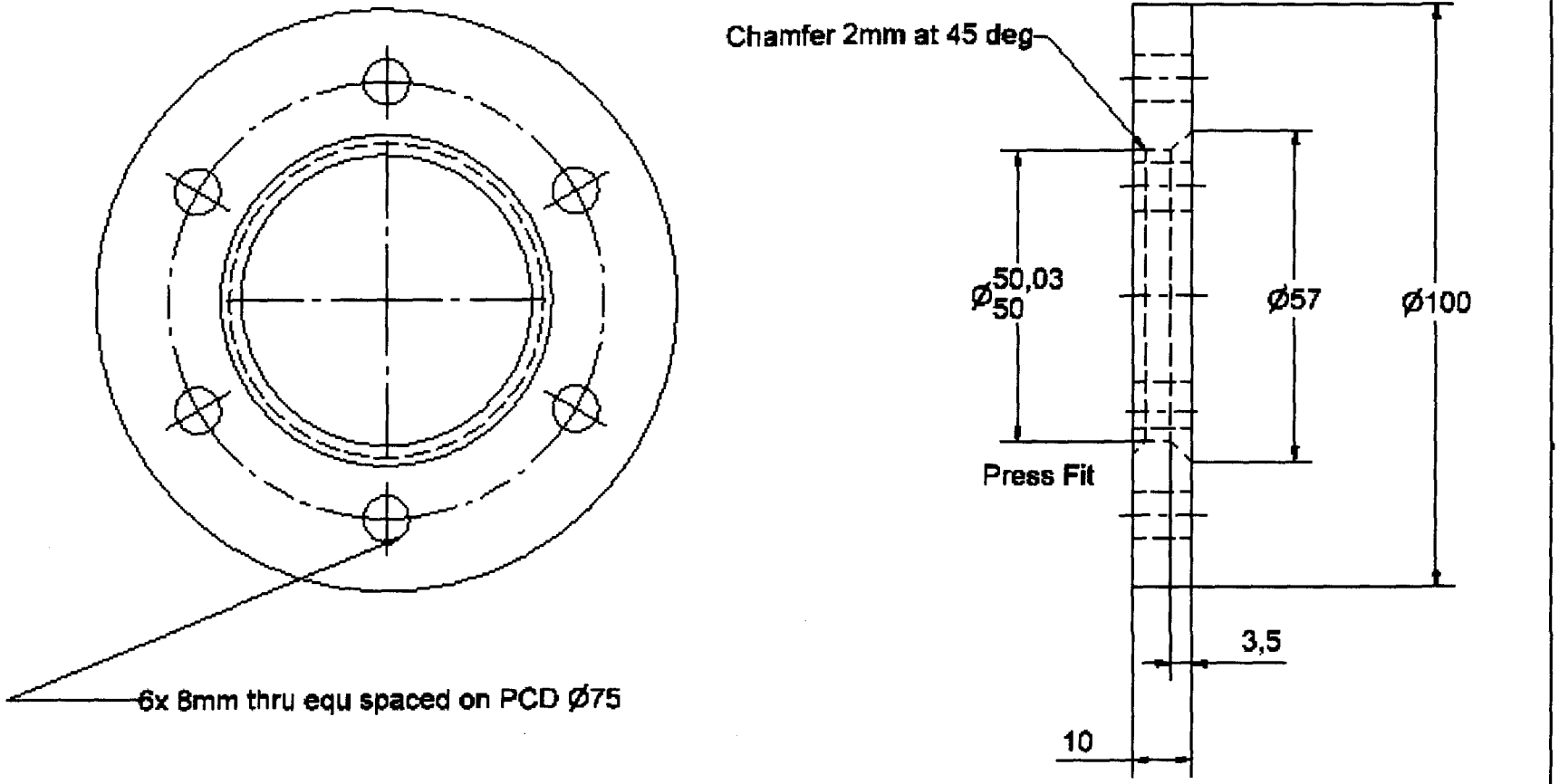

ALL SURFACES 3.2
U.O.S.

Designed by	Checked by	Approved by - date		Date	
Simon Demnitz			650 5223	31/01/2005	
Sasol		All tolerances 0.1 unless otherw spec			
		Air Plenum Outlet	Edition	Sheet 1 / 1	

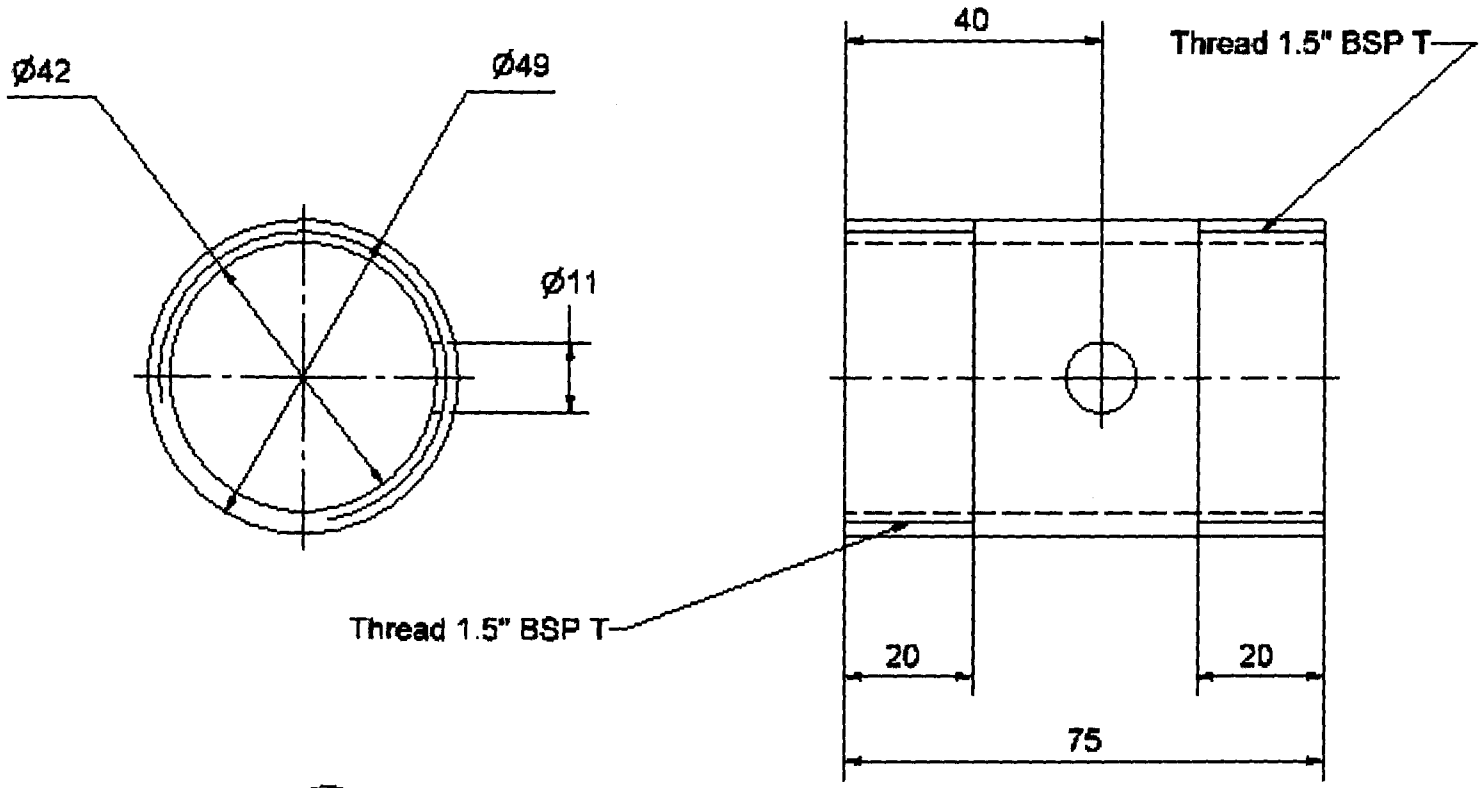

Designed by	Checked by	Approved by - date		Date	
Simon Demnitz			650 5223	01/02/2005	

Sasol	All tolerances 0.1 unless otherw spec		
	Ball Valve Inlet Tube	Edition	Sheet 1 : 1

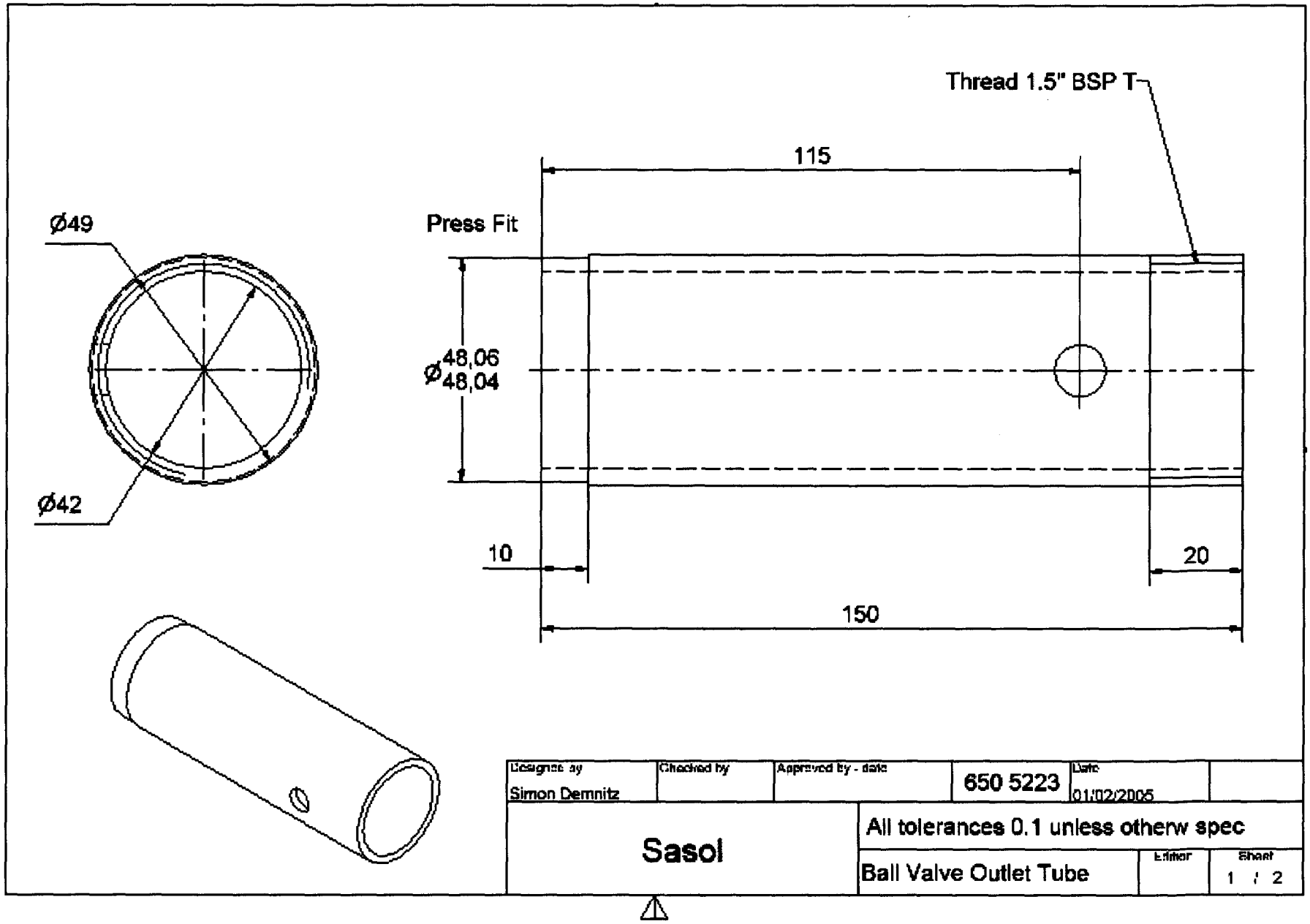

Designed by	Checked by	Approved by - date		Date
Simon Demnitz			650 5223	01/02/2005

Sasol	All tolerances 0.1 unless otherw spec		
	Ball Valve Outlet Tube	Editor	Sheet 1 / 2

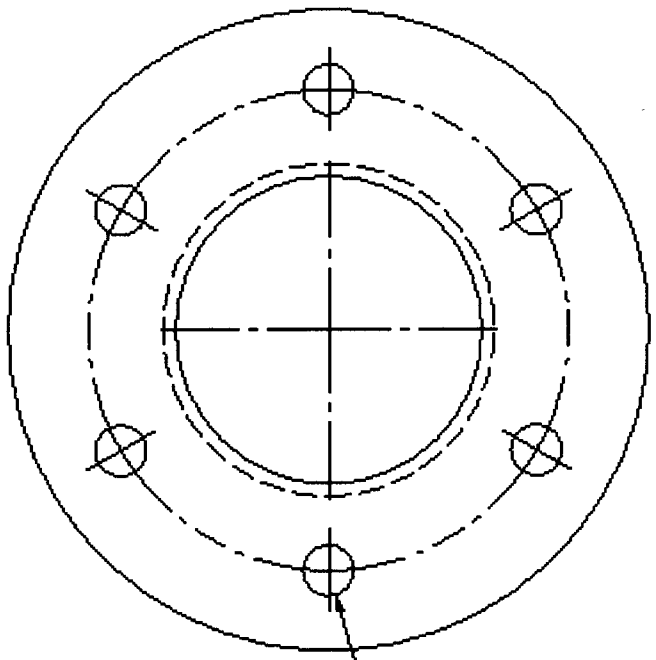

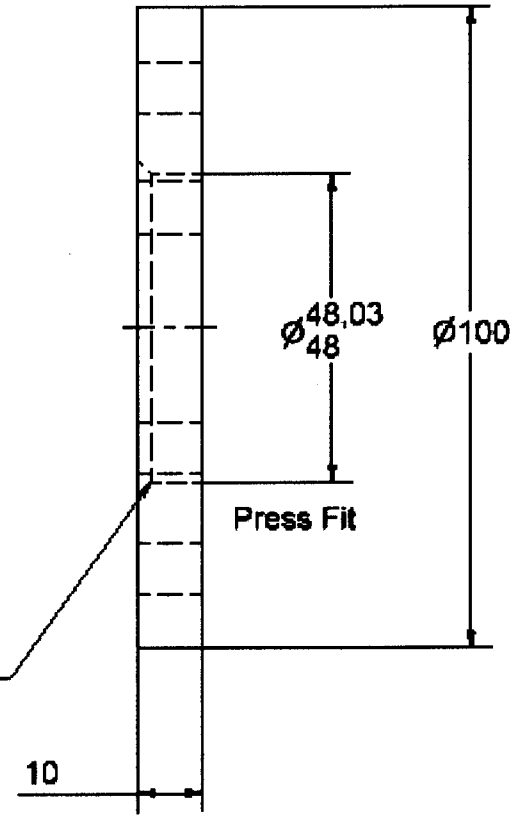

6xØ8 THRU on PCD Ø75

ALL SURFACES 3.2
U.O.S.

Designed by	Checked by	Approved by - date		Date	
Simon Demnitz			650 5223	31/01/2005	

Sasol	All tolerances 0.1 unless otherw spec		
	Ball Valve Outlet	Edition	Sheet 1 / 1

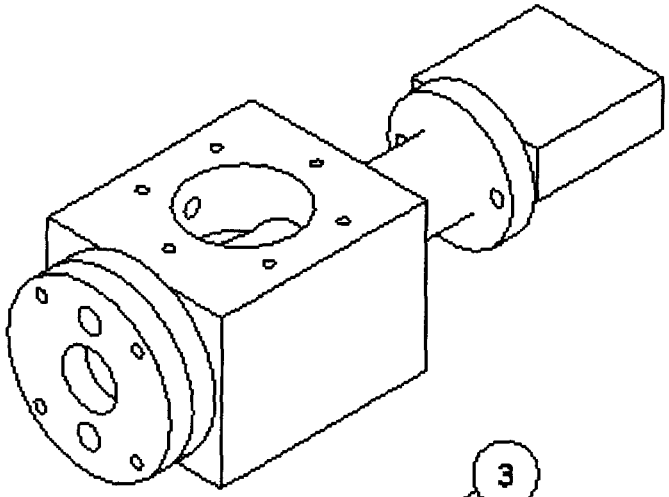

Parts List			
ITEM	QTY	PART NUMBER	DESCRIPTION
1	1	Inlet Holder Blank	Mild Steel
2	1	Injector Tube	Mild Steel
3	1	Injector Plug1	Mild Steel
4	1	Injector Plug Cap	Mild Steel

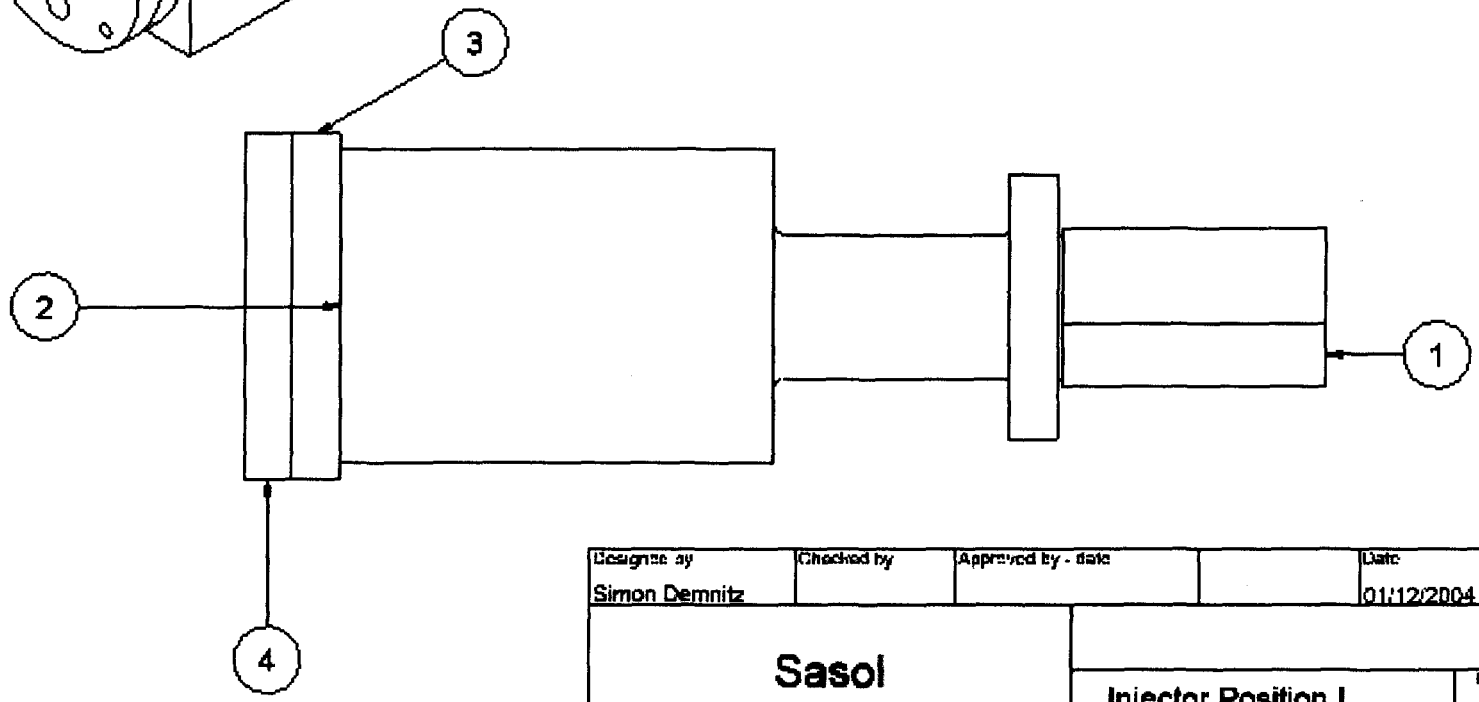

Designed by	Checked by	Approved by - date		Date	
Simon Demnitz				01/12/2004	

Sasol

Injector Position I

Sheet 1 : 2

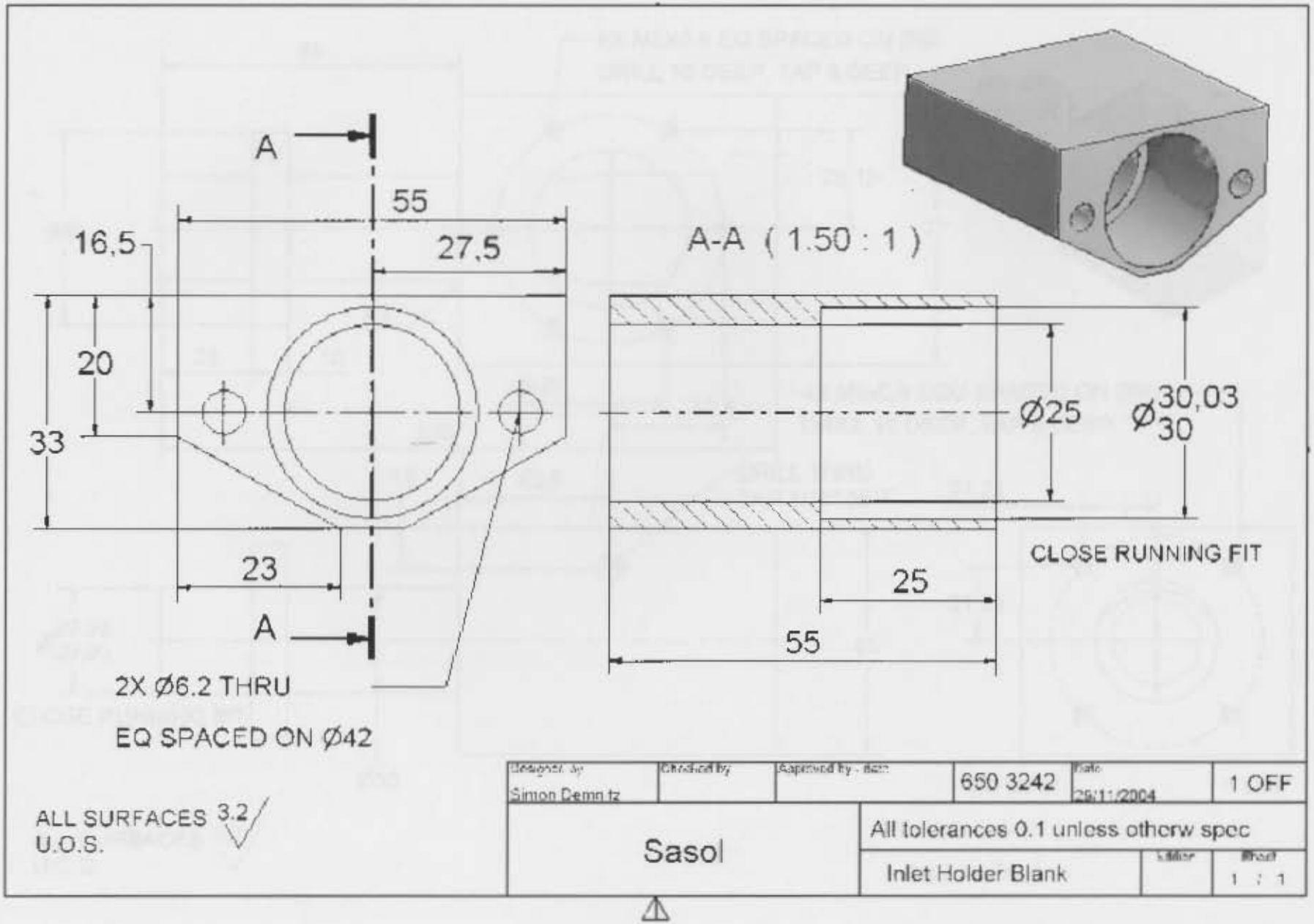
A
55
27,5
16,5
20
33
23
A
2X Ø6.2 THRU
EQ SPACED ON Ø42
A-A (1.50 : 1)
Ø25
Ø30,03
30
25
55
CLOSE RUNNING FIT
ALL SURFACES 3.2
U.O.S.
Designed by
Simon Demnitz
Checked by
Approved by - date
650 3242
Date
29/11/2004
1 OFF
Sasol
All tolerances 0.1 unless otherw spec
Inlet Holder Blank
Sheet
1 : 1

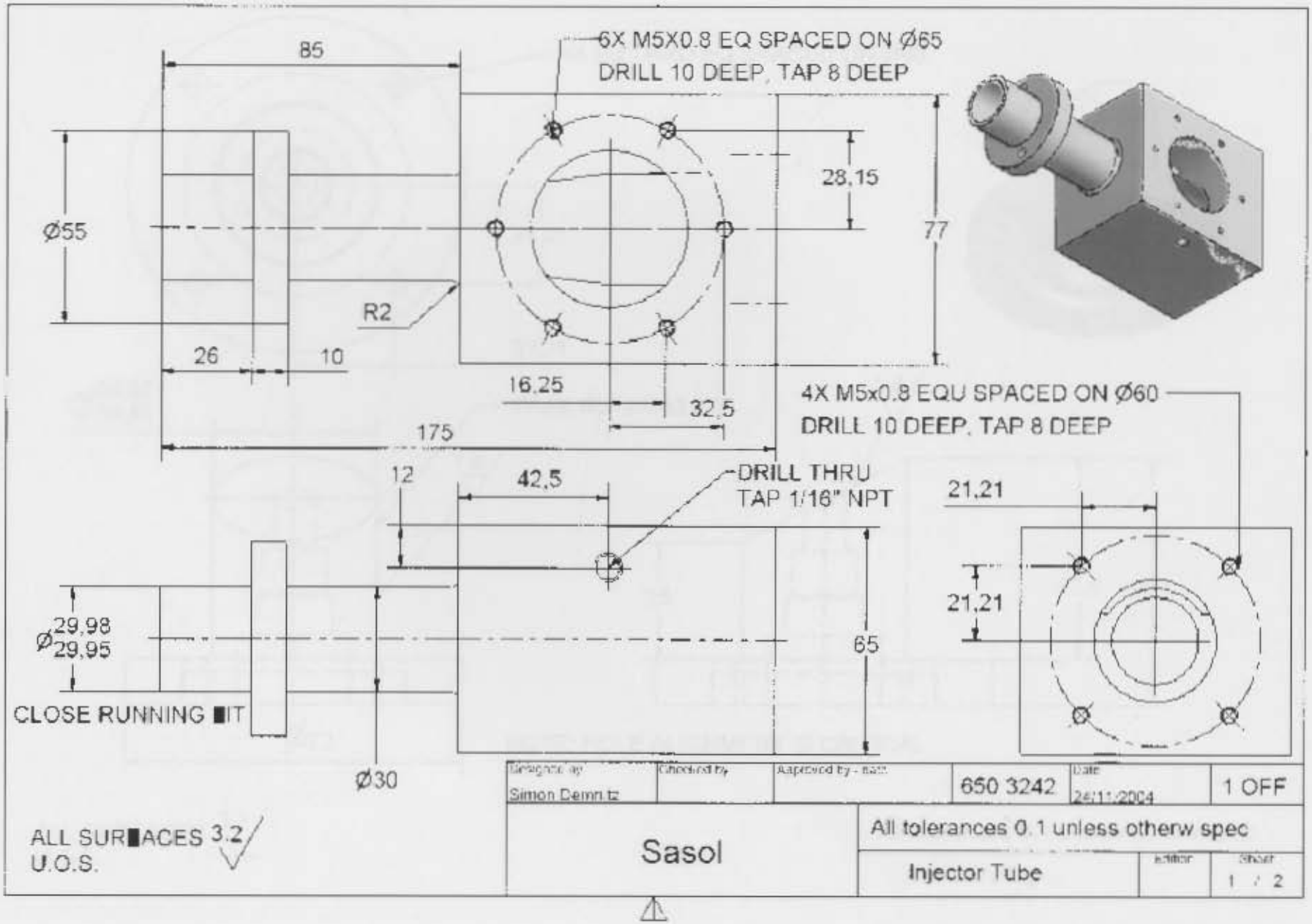
6X M5X0.8 EQ SPACED ON Ø65
DRILL 10 DEEP, TAP 8 DEEP
85
28,15
77
Ø55
R2
26
10
16,25
32,5
175
4X M5x0.8 EQU SPACED ON Ø60
DRILL 10 DEEP, TAP 8 DEEP
12
42,5
DRILL THRU
TAP 1/16" NPT
21,21
21,21
29,98
Ø29,95
65
CLOSE RUNNING FIT
Ø30
ALL SURFACES 3.2
U.O.S.
Designed by
Simon Dennitz
Checked by
Approved by - each
650 3242
Date
24/11/2004
1 OFF
Sasol
All tolerances 0.1 unless otherw spec
Injector Tube
Sheet
1 / 2

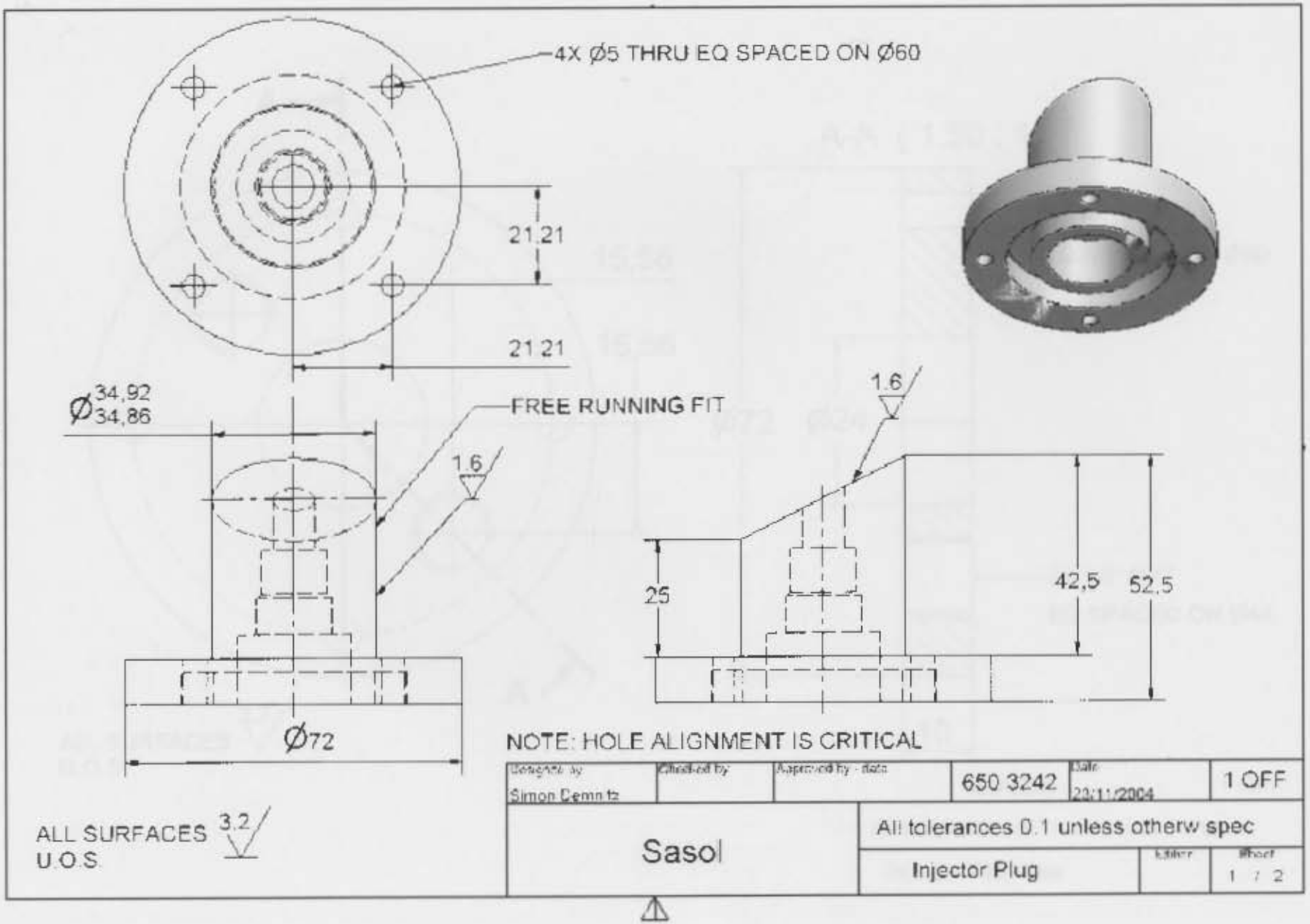
4X Ø5 THRU EQ SPACED ON Ø60
21.21
21.21
Ø34,92
Ø34,86
FREE RUNNING FIT
1.6
Ø72
1.6
25
42,5
52.5
NOTE: HOLE ALIGNMENT IS CRITICAL
ALL SURFACES 3.2
U.O.S.
Designed by
Simon Demnitz
Checked by
Approved by - date
650 3242
Date
23/11/2004
1 OFF
Sasol
All tolerances 0.1 unless otherw spec
Injector Plug
Sheet
1 / 2

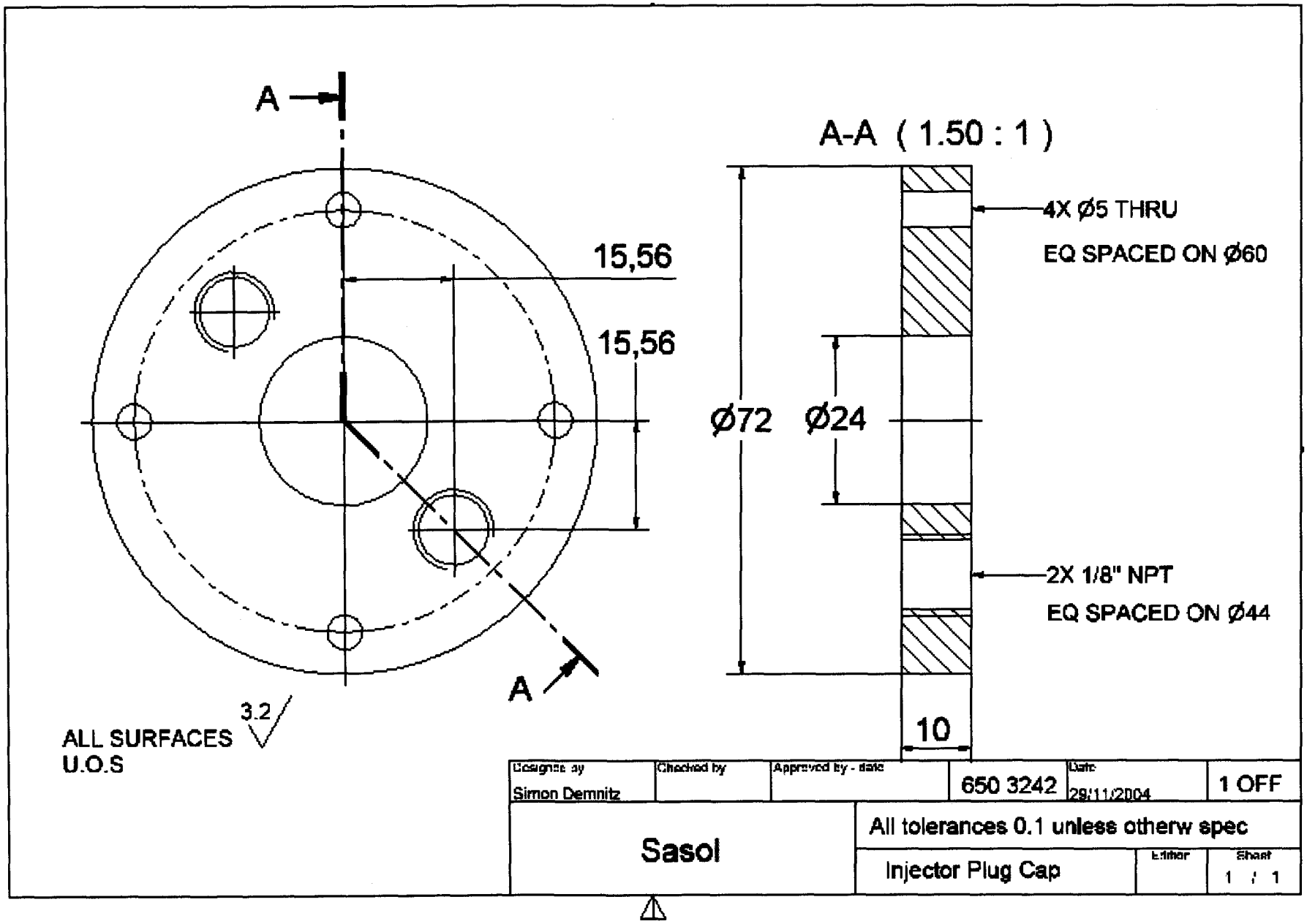
A
A
15,56
15,56
A-A (1.50 : 1)
4X Ø5 THRU
EQ SPACED ON Ø60
Ø72
Ø24
2X 1/8" NPT
EQ SPACED ON Ø44
10
3.2
ALL SURFACES
U.O.S
Designed by
Simon Demnitz
Checked by
Approved by - date
650 3242
Date
29/11/2004
1 OFF
Sasol
All tolerances 0.1 unless otherw spec
Injector Plug Cap
Sheet
1 / 1

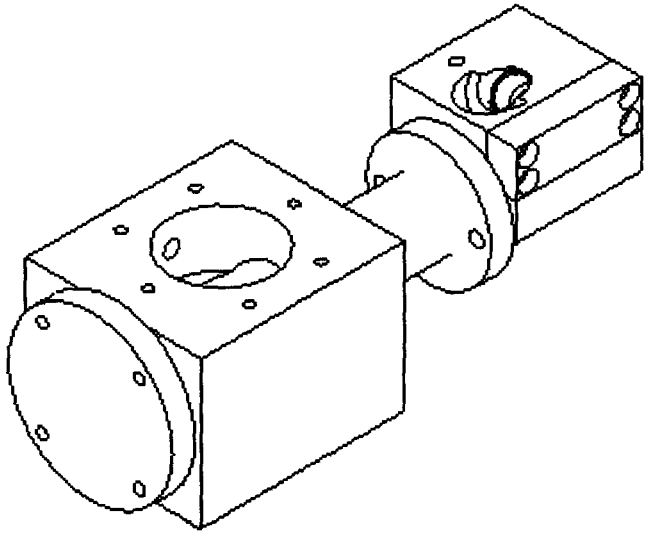

Parts List			
ITEM	QTY	PART NUMBER	DESCRIPTION
1	1	Inlet Holder Injector	Mild Steel
2	1	Injector Tube	Mild Steel
3	1	Inlet Holder Injector Cap	Mild Steel
4	1	Injector Plug	Mild Steel

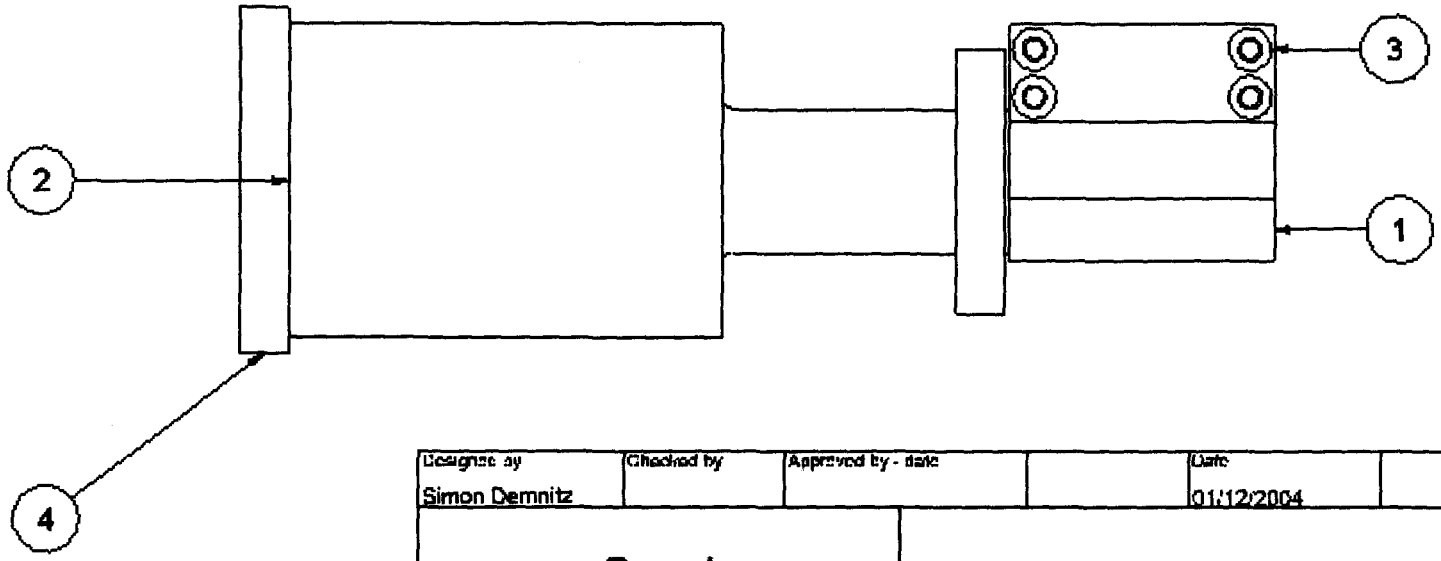

Designed by	Checked by	Approved by - date		Date	
Simon Demnitz				01/12/2004	

Sasol

Injector Position II

Sheet 1 : 2

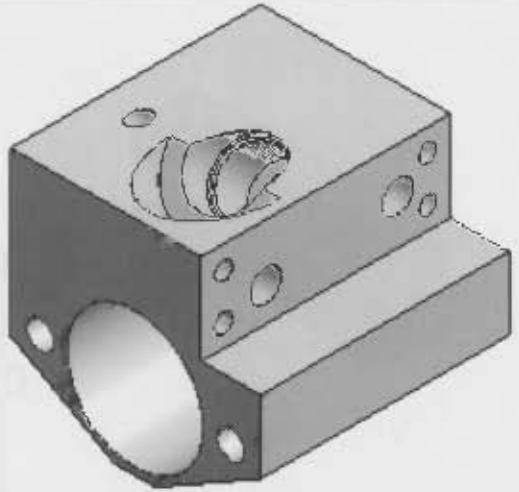

55
19
55
M5X0.8 ANGLED 45 DEG TO SURFACE, TAP 10 MM DEEP
2X Ø7 THRU
27,5
13
12,5
5
14,3
10
10
20
49
36
32,5
5
4X M5X0.8
DRILL 10MM DEEP
TAP 8MM DEEP
29,2
45
23
ALL SURFACES 3.2
U.O.S.
2X Ø6.2 DRILL
THRU ON Ø42
Designed by
Simon Demnitz
Checked by
Approved by - date
650 3242
Date
22/1/2004
1 OFF
Sasol
All tolerances 0.1 unless otherw spec
Inlet Holder Injector
Sheet
1 : 2

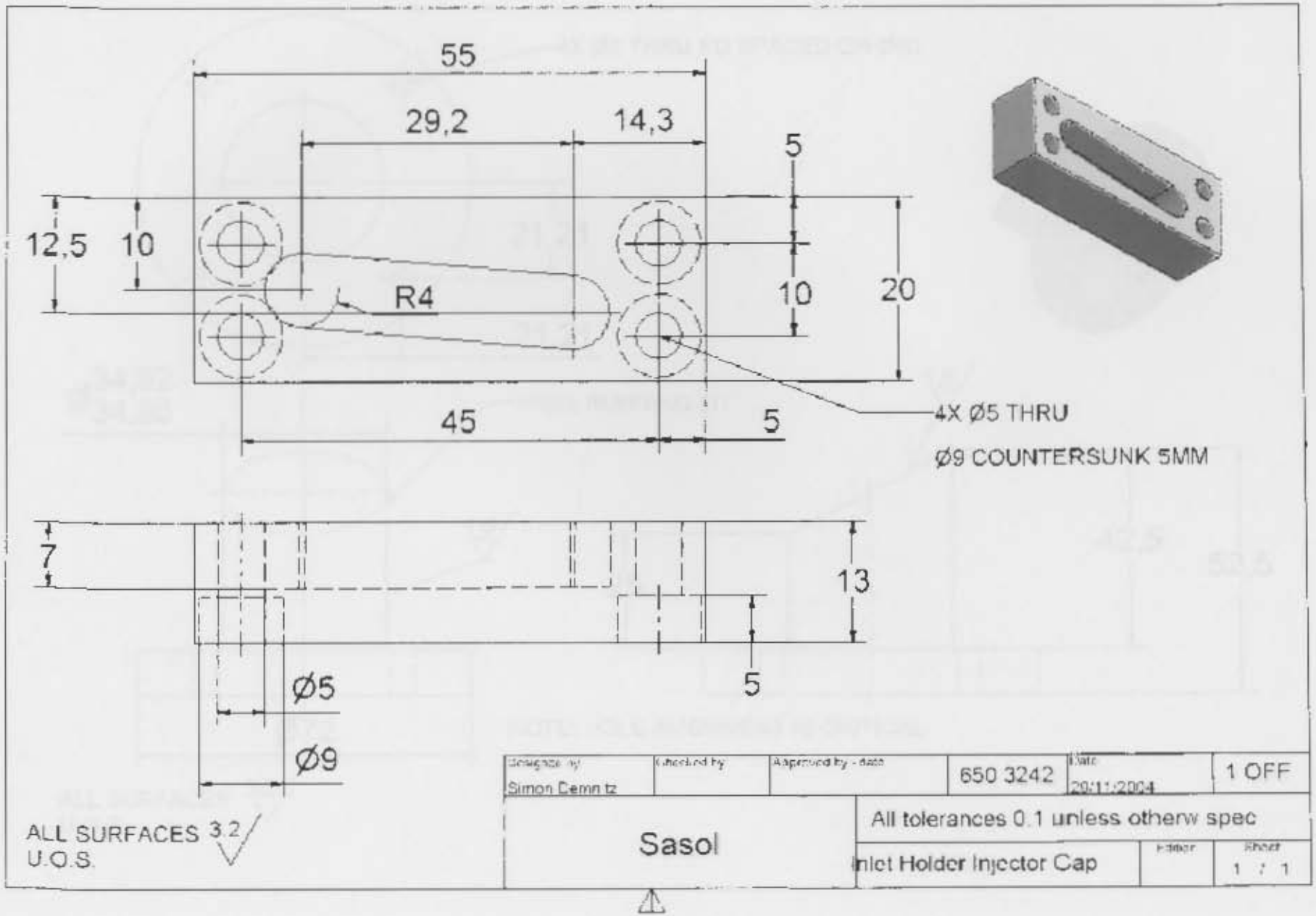
55
29,2
14,3
5
12,5
10
R4
10
20
45
5
4X Ø5 THRU
Ø9 COUNTERSUNK 5MM
7
13
5
Ø5
Ø9
ALL SURFACES 3.2
U.O.S.
Designed by
Simon Demmitz
Checked by
Approved by - date
650 3242
Date
20/11/2004
1 OFF
Sasol
All tolerances 0.1 unless otherw spec
Inlet Holder Injector Cap
Sheet
1 / 1

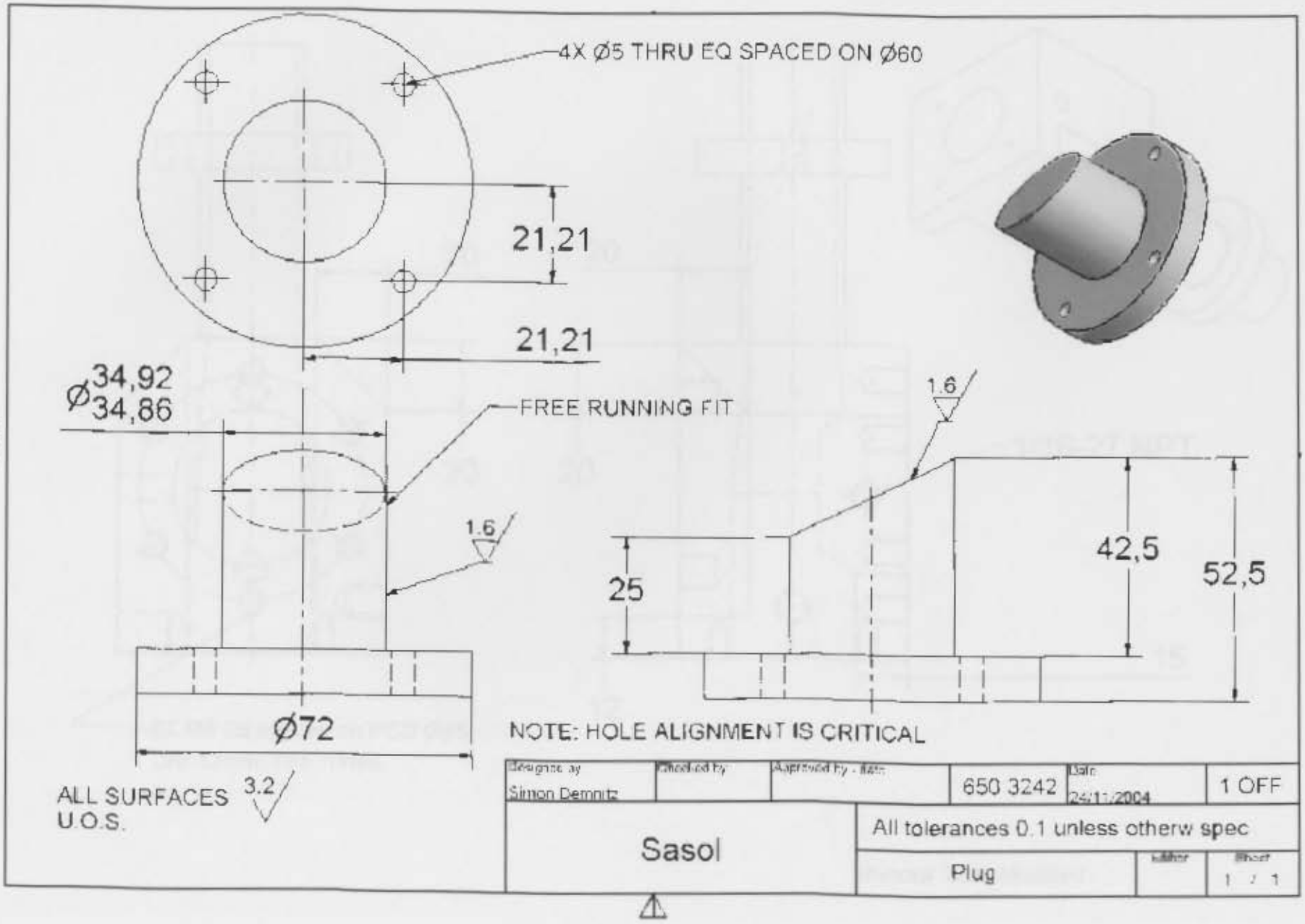
4X Ø5 THRU EQ SPACED ON Ø60
21,21
21,21
Ø34,92
Ø34,86
FREE RUNNING FIT
1.6
1.6
25
42,5
52,5
Ø72
NOTE: HOLE ALIGNMENT IS CRITICAL
ALL SURFACES
U.O.S.
3.2
Designed by
Simon Demnitz
Checked By
Approved By - Date
650 3242
Date
24/11/2004
1 OFF
Sasol
All tolerances 0.1 unless otherw spec
Plug
Sheet
1 / 1

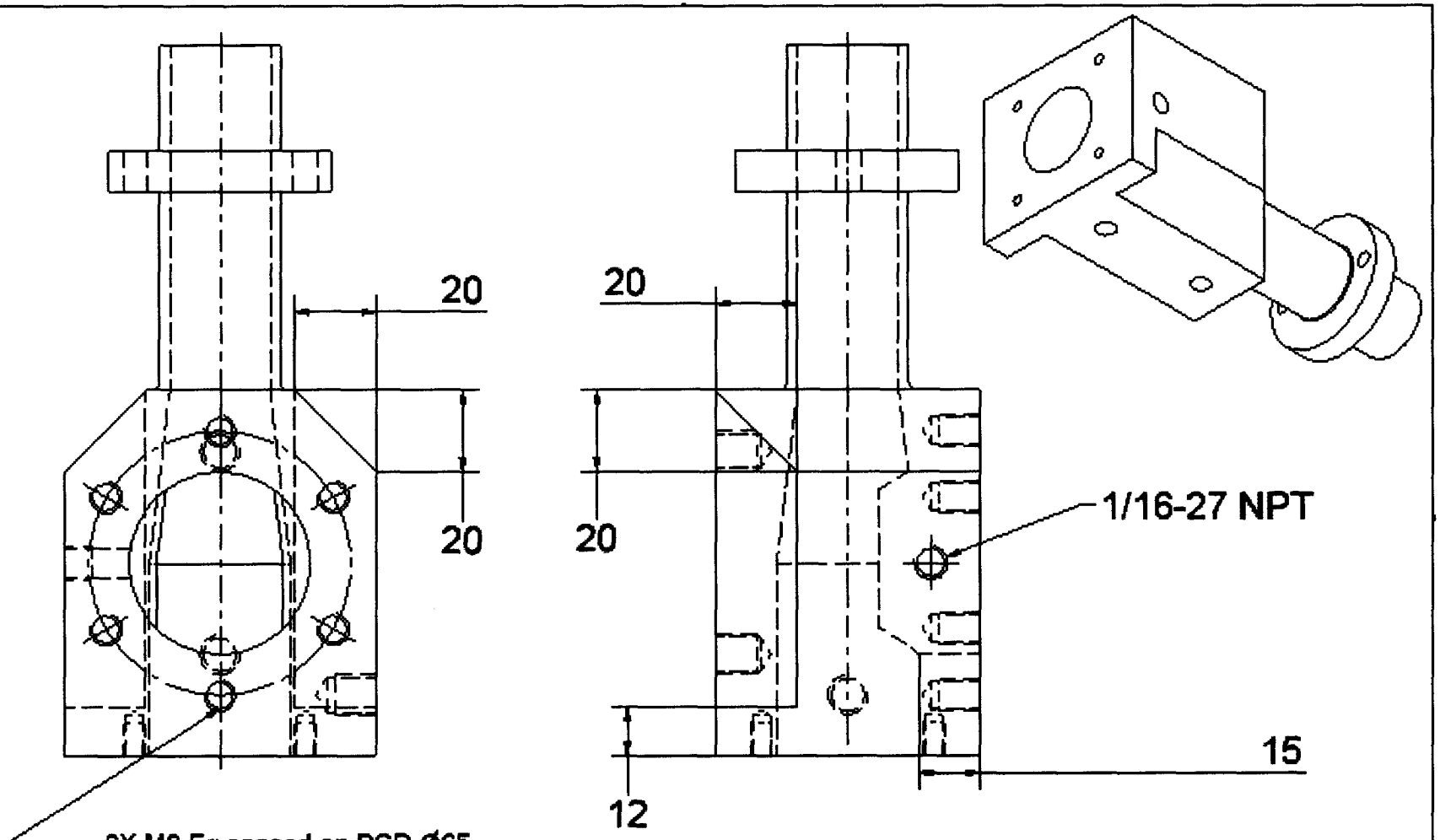

Designed by	Checked by	Approved by - date		Date	
Simon Demnitz				31/01/2005	

Sasol	Injector Tube Modified	Editor	Sheet
			1 / 1

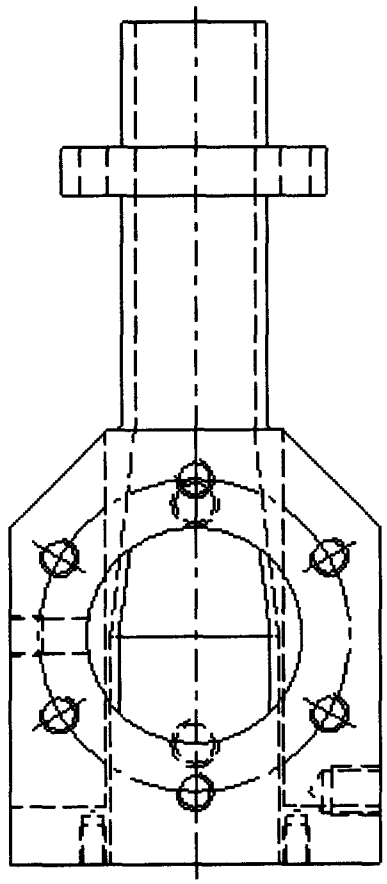

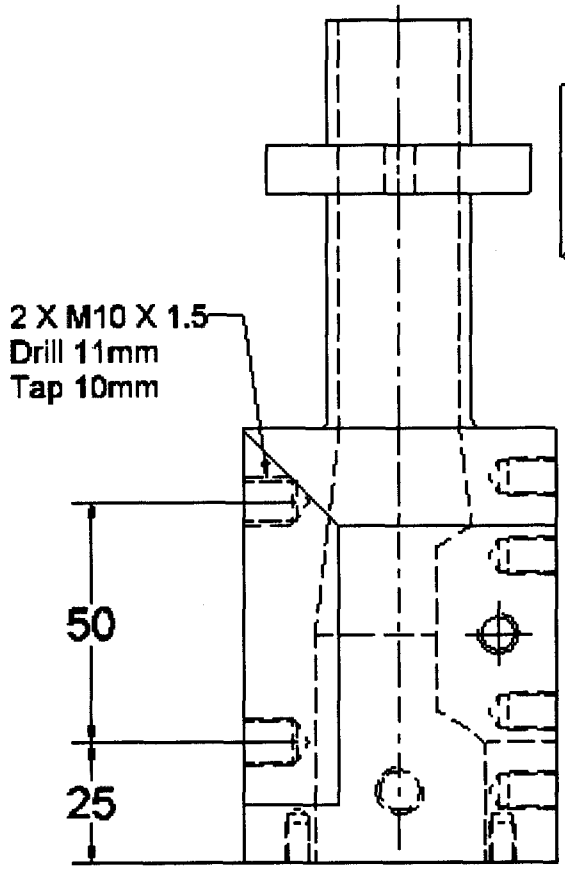

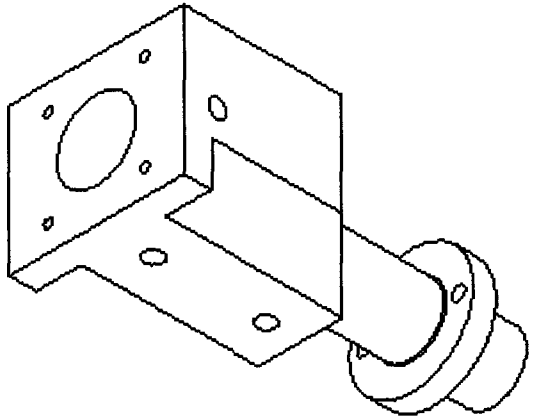

Designed by	Checked by	Approved by - date		Date	
Simon Demnitz				31/01/2005	

Sasol	Injector Tube Modified (Again)	Letter	Sheet
			1 / 1

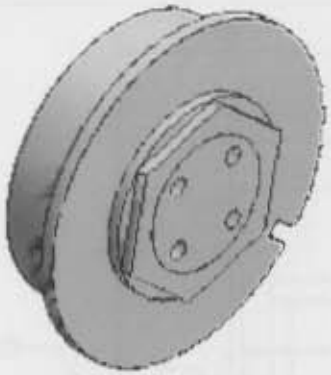

Parts List			
ITEM	QTY	PART NUMBER	DESCRIPTION
A	1	Flange Transmission	Mild Steel
B	1	Reference Disk	Mild Steel
C	1	Lock Nut	Mild Steel

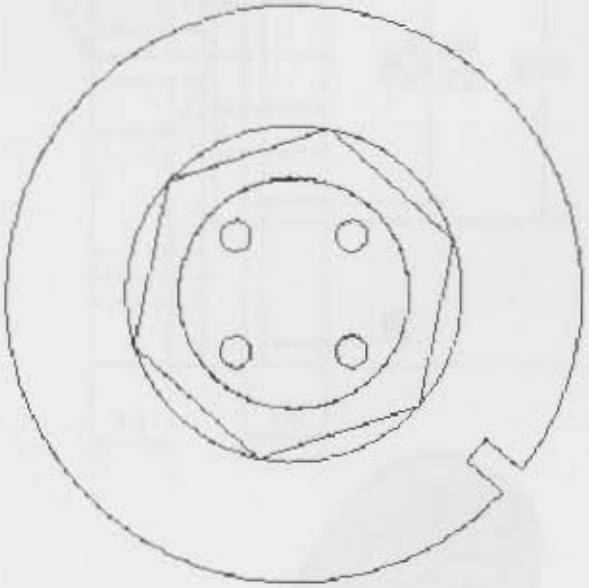

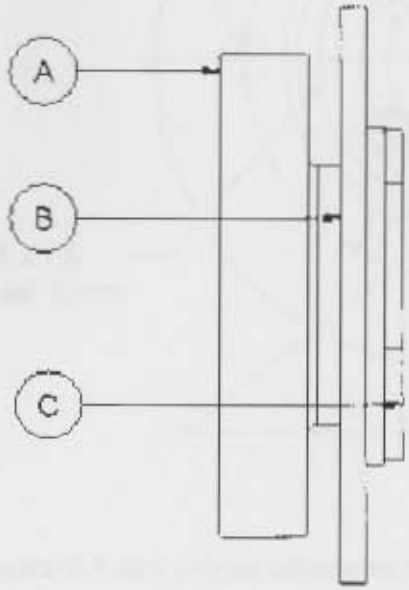

Drawn by: Simon Demnitz	Checked By	Approved By - date		Date: 08:11:2004	
Sasol		Transmission Assembly			
		Transmission	Edition	Sheet 1 / 1	

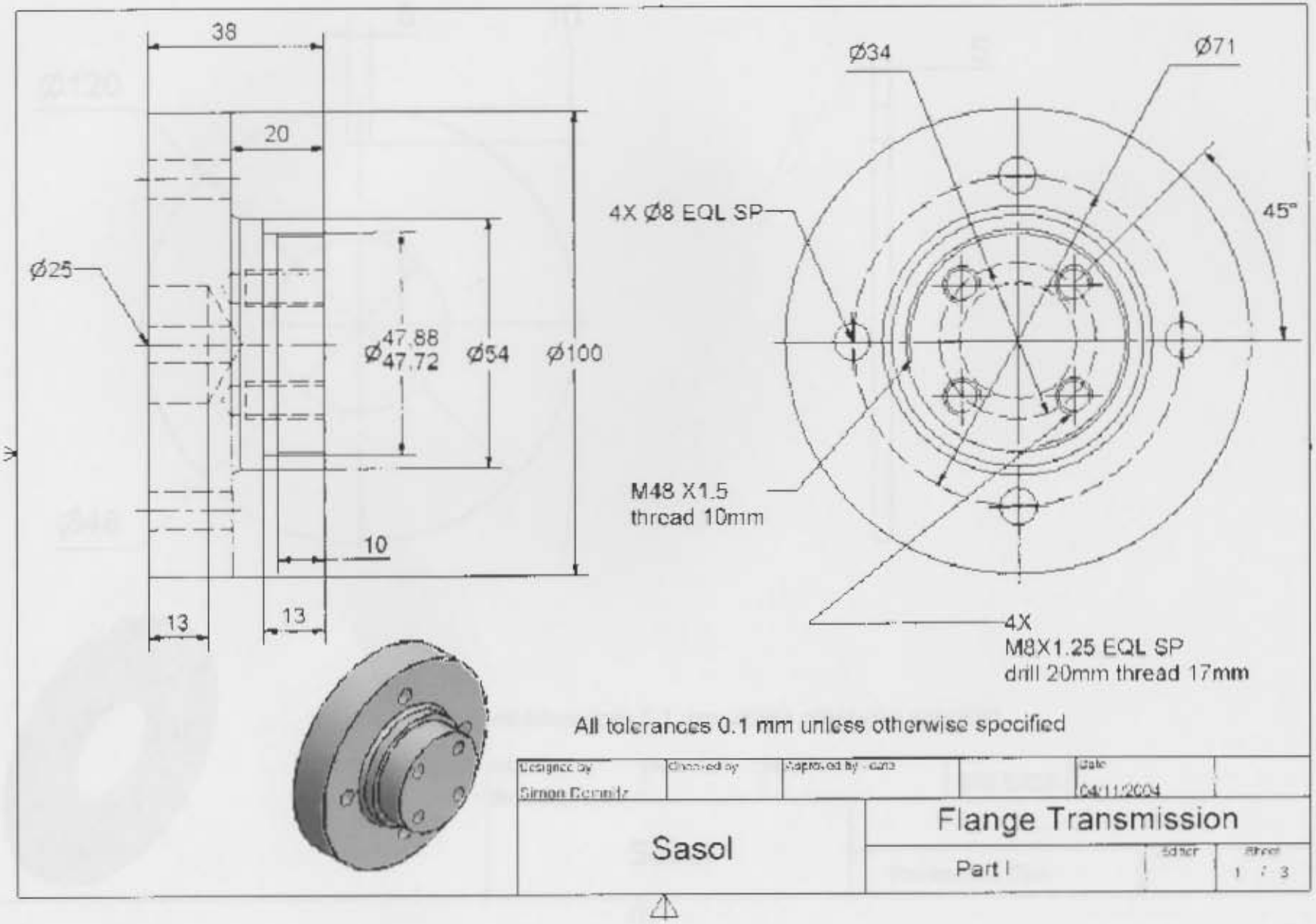
38
20
Ø25
47.88
Ø47.72
Ø54
Ø100
10
13
13
Ø34
Ø71
4X Ø8 EQL SP
45°
M48 X1.5
thread 10mm
4X
M8X1.25 EQL SP
drill 20mm thread 17mm
All tolerances 0.1 mm unless otherwise specified
Designed by
Simon Benadiz
Checked by
Approved by - date
Date
04/11/2004
Sasol
Flange Transmission
Part I
Sheet
1 / 3

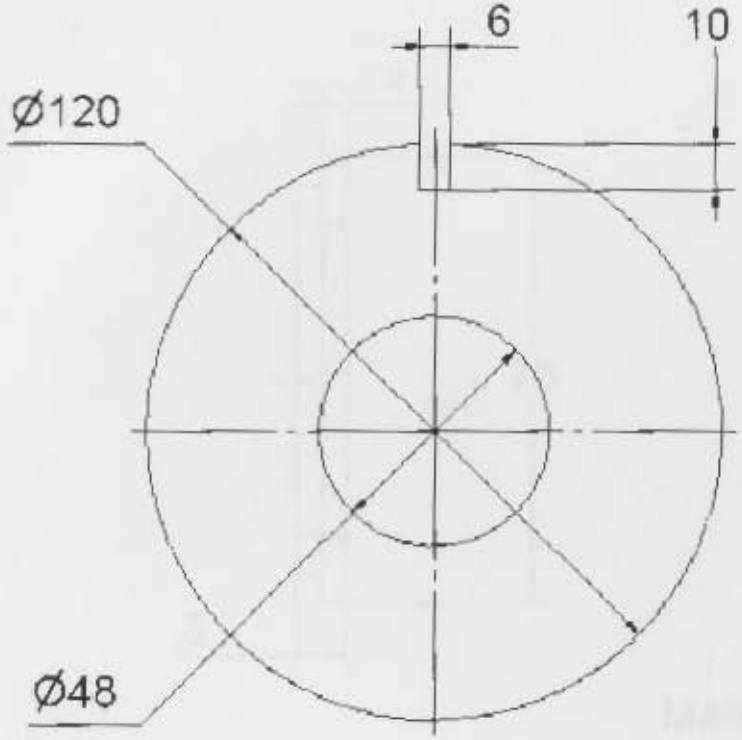

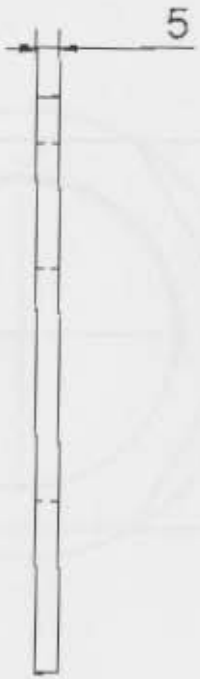

All tolerances 0.1 mm unless otherwise specified

Designed by	Checked by	Approved by - date	650 5223	Date	
Simon Demnitz				Dec1*/2004	
Sasol			Reference Disk	edition	Sheet 1 / 2

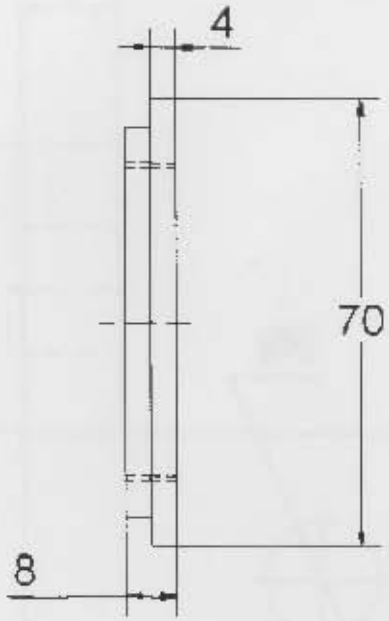

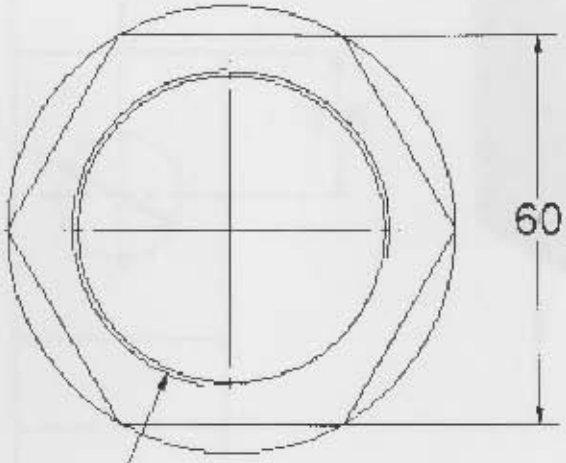

M48x1.5 - 6H

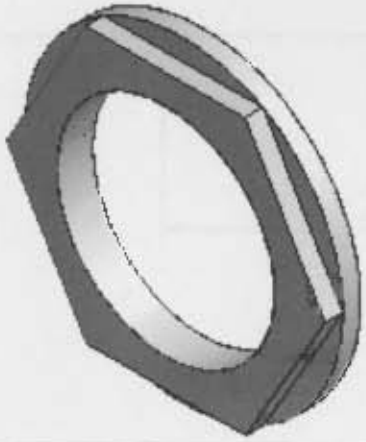

All tolerances 0.1 mm unless otherwise specified

Designed by	Checked by	Approved by - date		Date	
Simon Demnitz				04/11/2004	

Sasol	Lock Nut		
	Part II	Edition	Sheet 1 / 1

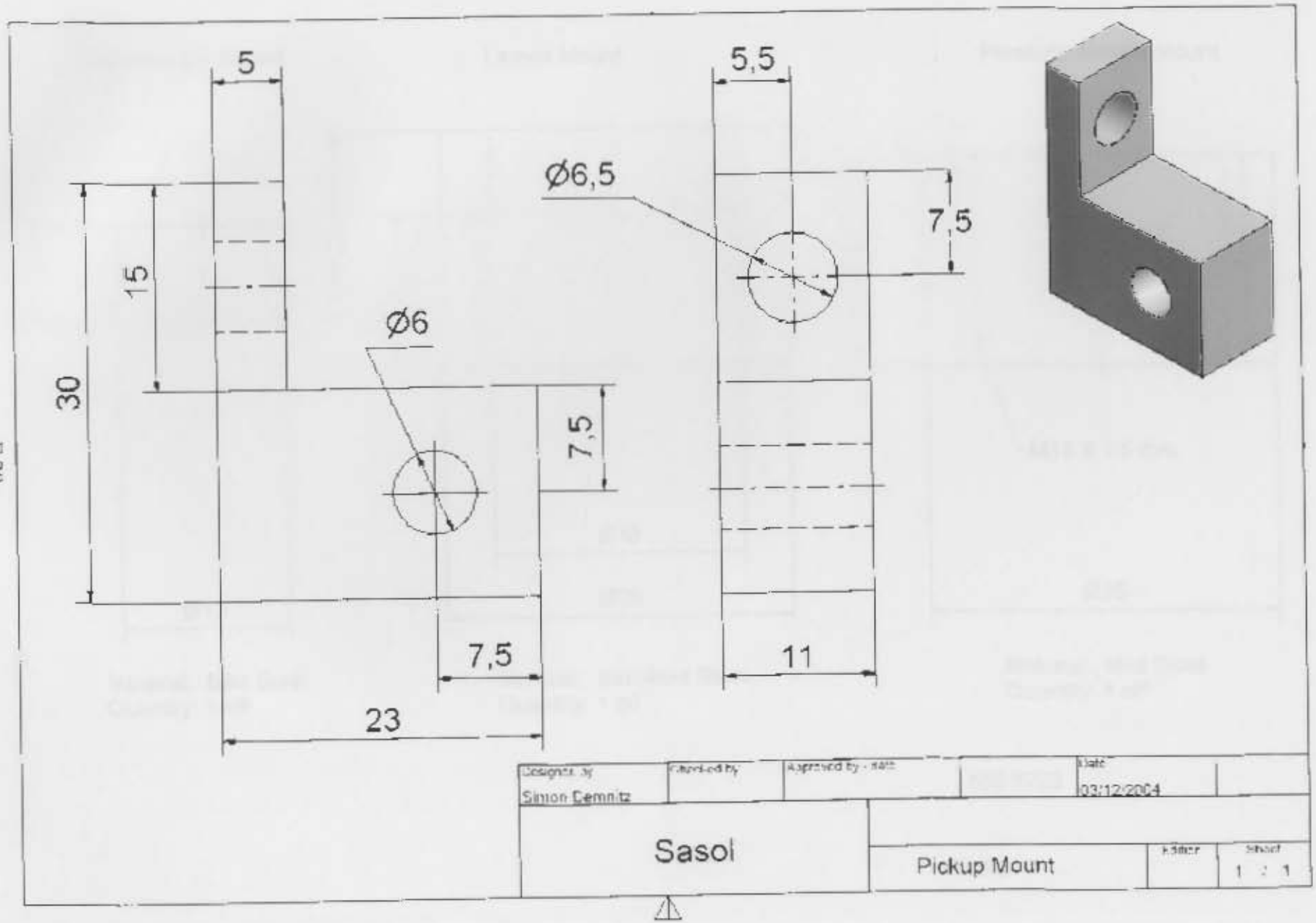
5
5,5
Ø6,5
7,5
15
30
Ø6
7,5
7,5
11
23
Designed by
Simon Demnitz
Checked by
Approved by - date
Date
03/12/2004
Sasol
Pickup Mount
Number
Sheet
1 : 1

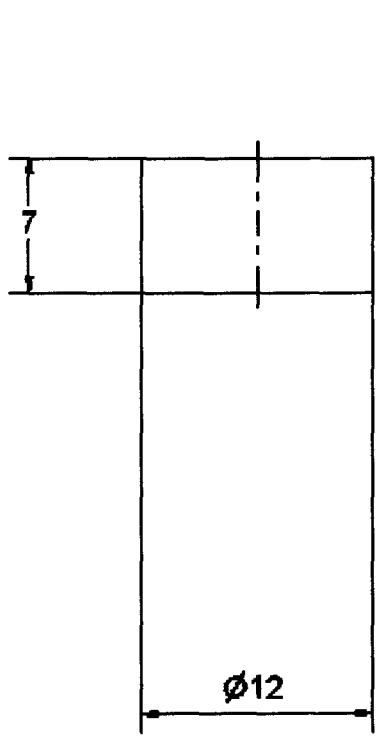

Material: Mild Steel
Quantity: 1 off

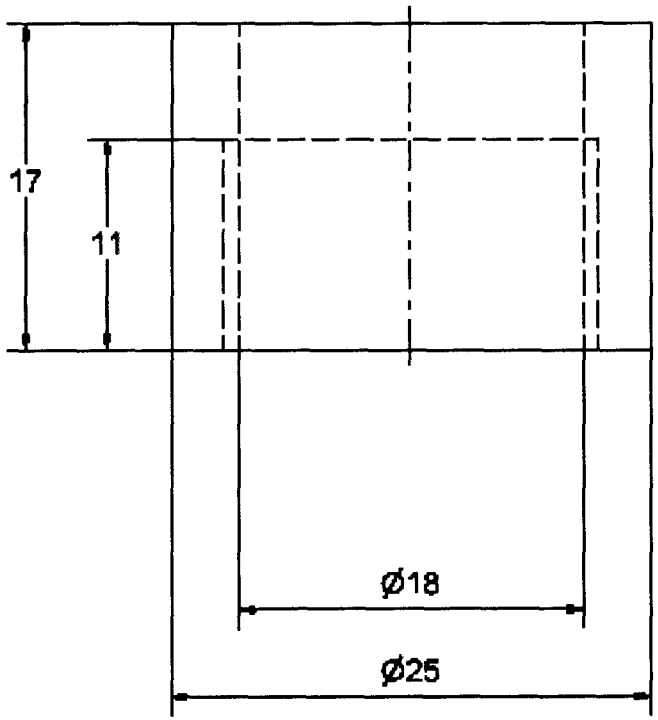

Material: Stainless Steel
Quantity: 1 off

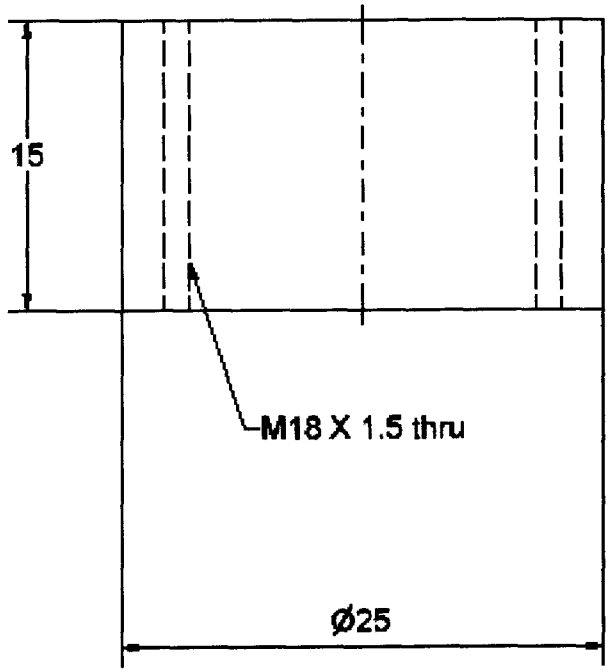

Material: Mild Steel
Quantity: 1 off

Designed by	Checked by	Approved by - date		Date
Simon Demnitz			650 5223	26/04/2005

Sasol

Fittings

Letter

Sheet 1 : 1

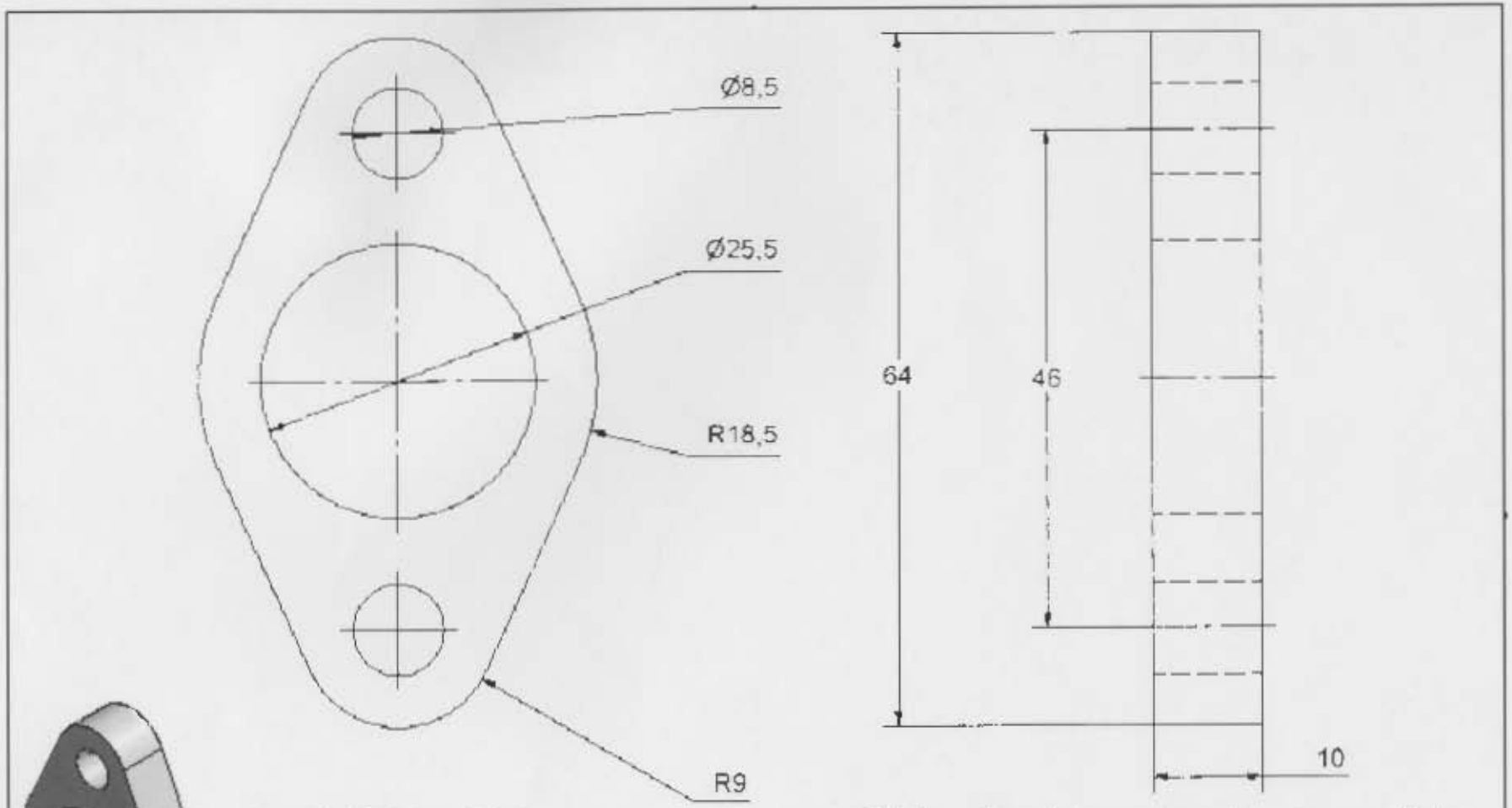

Material: Stainless Steel
Quantity: 1 off

All dimensions 0.1mm unless otherwise specified

Designed by	Checked By	Approved by - Date	650 5223	Date
Simon Demnitz				26/04/2005

Sasol

Exhaust Flange

Sheet 1 / 1